NIST
National Institute of Standards and Technology
Technology Administration, U.S. Department of Commerce

NIST Technical Note 1541

Propagation and Detection of Radio Signals Before, During, and After the Implosion of a Large Sports Stadium (Veterans' Stadium in Philadelphia)

Christopher L. Holloway
Galen Koepke
Dennis Camell
Kate A. Remley
Dylan F. Williams
Susan A. Schima
Seturnino Canales

NIST Technical Note 1541

Propagation and Detection of Radio Signals Before, During and After the Implosion of a Large Sports Stadium (Veterans' Stadium in Philadelphia)

Christopher L. Holloway
Galen Koepke
Dennis Camell
Kate A. Remley
Dylan F. Williams
Susan A. Schima
Seturnino Canales

Electromagnetics Division
National Institute of Standards and Technology
325 Broadway
Boulder, CO 80305

October 2005

U.S. Department of Commerce
Carlos M. Gutierrez, Secretary

Technology Administration
Michelle O'Neill, Acting Under Secretary of Commerce for Technology

National Institute of Standards and Technology
William Jeffrey, Director

Certain commercial entities, equipment, or materials may be identified in this document in order to describe an experimental procedure or concept adequately. Such identification is not intended to imply recommendation or endorsement by the National Institute of Standards and Technology, nor is it intended to imply that the entities, materials, or equipment are necessarily the best available for the purpose.

National Institute of Standards and Technology Technical Note 1541
Natl. Inst. Stand. Technol. Tech. Note 1541, 122 pages (October 2005)
CODEN: NTNOEF

U.S. Government Printing Office
Washington: 2005

For sale by the Superintendent of Documents, U.S. Government Printing Office
Internet bookstore: gpo.gov Phone: 202-512-1800 Fax: 202-512-2250
Mail: Stop SSOP, Washington, DC 20402-0001

Contents

Executive Summary

This is the second in a series of NIST technical notes (TN) on propagation and detection of radio signals in large buildings before, during, and after implosion. The first NIST TN (NIST TN 1540) described a similar experiment carried out on a 13-story apartment building in New Orleans, LA. These data will give first responders a better understanding of what to expect from the radio-propagation environment in disaster situations. The goals of this work are two-fold: (1) to create a large, public-domain data set describing the attenuation in various building types of radio signals in public safety and cellular telephone bands and (2) to investigate various schemes for detecting signals from first responders with radios or from civilians with cell phones who are trapped in voids in a collapsed or partially collapsed building.

With the above goals in mind, measurements were carried out on a large sports stadium (the Veteran's Stadium) in Philadelphia, PA. Frequencies near public safety and cell phone bands (approximately 50 MHz, 150 MHz, 225 MHz, 450 MHz, 900 MHz, and 1.8 GHz) were chosen for these experiments. Radio transmitters similar to those used by first responders were used. An automated system to measure signal strength was developed. Three different types of signal-strength experiments were performed.

First, we carried out a "radio-mapping" experiment that provided data on how well radio signals at the different frequencies coupled into the stadium. From this we determined the field strength variability throughout the stadium. This experiment involved carrying a set of transmitters tuned to the various frequencies throughout the stadium, while recording the received signal at a fixed receive site located outside the building. Transmitters were also carried around the perimeter of the stadium with a fixed receiving site on the outside. These measurements were carried out a few days before the stadium was imploded. Results show that:

- Maximum signal attenuation for the perimeter mapping of the stadium was on the order of 75 dB.
- The mean interior to exterior signal attenuation ranged from 25 to 50 dB.
- The standard deviation for interior to exterior signal attenuation ranged from 6 to 14 dB, depending on frequency.

These results indicate the variability in signal level that a communication-system user might expect throughout a structure of this type.

Second, radios in protective cases were placed in fixed sites throughout the stadium. Received signals were collected external to the structure before, during, and after the implosion. Our receiving sites in this case were both fixed and mobile. A mobile cart was pulled around the perimeter of the stadium both before and after the implosion, enabling direct comparison of signal strength as a function of azimuth angle through the standing stadium and the resulting pile of rubble. Results show that:

- Some transmitter signals experienced large amounts of attenuation (some greater than 100 dB, at the noise floor of our receivers), while other transmitter signals increased during the implosion, depending on the receiving site and location of the transmitter cache.

- Large amounts of building rubble caused at least 30 to 50 dB of signal attenuation. The true attenuation was not established in several cases since we measured only noise.

Thus, if someone was trapped under such a rubble pile and tried to communicate with an emergency responder with a two-way radio or cell phone, their communication link would have to overcome at least 30 to 50 dB of attenuation. It is interesting to note that the increase in signal attenuation after the collapse of the stadium was not as large as we expected based on results observed during the apartment building implosion (60 to 80 dB). We attribute this to massive amounts of concrete and steel in the standing stadium that heavily attenuated signals propagating through the interior of the stadium. While the implosion certainly moved and compacted these massive beams, there were still large voids remaining in the rubble pile, leaving us with a propagation environment similar to that of the stadium's standing state. The apartment building, however, went from a relatively open structure to a very dense pile of rubble that had a more pronounced effect on the signals.

The third set of experiments used metallic "debris radiators" to attempt to detect signals from transmitters buried underneath the rubble pile. The goal was to investigate whether radio signals from transmitter(s) under rubble might couple onto metallic construction material such as pipes or conduit, and radiate signals to the edges of the rubble pile. Results show that:

- Signals could be received from all buried transmitters using either a direct connection to the metallic debris through a matching network or a directional receive antenna placed in close proximity to the debris radiator.

- Directional receive antennas in close proximity to a debris radiator generally had higher received signal levels than did signals acquired using direct connection to the metallic debris.

The results given in this NIST TN are the second in a series of reports detailing implosion experiments performed by NIST in order to better understand the first responder's radio propagation environment and to investigate new methods for weak-signal detection. The first set of implosion experiments was performed in an apartment building in New Orleans. The results of that experiment and implosion experiments performed in the Washington D.C. Convention Center are the subject of separate NIST TNs. Besides implosion experiments, NIST has also performed radio-mapping experiments in various other large structures, including apartment and office buildings, sports stadiums, stores, malls, hotels, a convention center, and warehouses. The results of the signal-strength measurements and statistical distribution for these radio-mapping experiments will also be published separately.

Propagation and Detection of Radio Signals Before, During and After the Implosion of a Large Sports Stadium (Veterans' Stadium in Philadelphia)

Christopher L. Holloway, Galen Koepke, Dennis Camell,
Kate A. Remley, Dylan F. Williams, Susan A. Schima, and Seturnino Canales

Electromagnetics Division
National Institute of Standards and Technology
325 Broadway, Boulder, CO 80305

In this report, we investigate radio communications problems faced by emergency responders (firefighters and police) in disaster situation such as collapsed buildings. A fundamental challenge to communications into and out of large buildings is the strong attenuation of radio signals caused by losses and scattering in the building materials and structure. We designed experiments that take advantage of building demolitions in an effort to quantify radio-signal attenuation through standing and collapsed structures. We also investigated various schemes for detecting signals from firefighters and civilians with portable radios or cell phones who are trapped in voids in these collapsed building. We placed RF transmitters, similar to those used by first responders, in various locations in these buildings and performed measurements before, during, and after the building was imploded. The transmitters were tuned to frequencies near public safety and cell phone bands. Once the building was down, we measured the signals from the buried transmitters in the building to investigate weak-signal detection schemes that involved searching with directional antennas and connecting instruments to some of the metal debris located on the perimeter of the collapsed building. This report summarizes the second in a series of such experiments, performed in Veterans' Stadium in Philadelphia, PA. In this report, we describe the experiments, detail the measurement system, show primary results of the data we collected, and discuss some of the interesting propagation effects we observed.

Key words: building implosion; building shielding and coupling; collapsed buildings; emergency responders; radio communications; radio propagation experiments; weak-signal detection

1. Introduction

When emergency (or first) responders enter large structures (e.g., apartment and office buildings, sports stadiums, stores, malls, hotels, convention centers, and warehouses) communication to individuals on the outside is often impaired. Cell phone and mobile-radio signal strength is reduced due to attenuation caused by propagation through the building materials and scattering by the building geometry [1-5].

We report on a National Institute of Standards and Technology (NIST) project to investigate the communications problems faced by first responders (firefighters and police) in disaster situations such as collapsed buildings. As part of this effort, we are investigating the propagation and coupling of radio-waves into large structures. We are also investigating various schemes for

detecting first responders and civilians with portable radios or cell phones who are trapped in voids of a collapsed or partially collapsed building.

Buildings scheduled for implosion provide the ideal research environment for investigating radio-wave propagation conditions in fully or partially collapsed structures. The rapid change in the building structure during an implosion was also favorable to our experimental time frame. We could perform one set of experiments within about a two-week period as opposed to several months during a conventional demolition. Working in cooperation with demolition and implosion contractors, we identified a high-rise apartment building in New Orleans as the site of our first set of experiments. A summary of this work appears in References [5] and [6]. This current report summarizes the second in a series of implosion experiments. The data discussed here were collected during the implosion of the Veteran Stadium in Philadelphia, PA, in March 2004.

The experiments reported here were performed before, during, and after the implosion of the building and are essentially measurements of the reduction in radio signal strength caused by propagation through the structure. In order to study the radio characteristics of the building at the various frequencies of interest to first responders, frequencies near public safety and cell phone bands (approximately 50 MHz, 150 MHz, 225 MHz, 450 MHz, 900 MHz, and 1.8 GHz) were chosen. A detailed description of the transmitters we used is given in Section 4.

Three types of data were collected in the experiment. The first set of data, which we refer to as a "radio mapping," was collected a few days before the building was imploded. This involved carrying transmitters (or radios) tuned to various frequencies throughout the stadium while recording the received signal at a site located outside the stadium. The reference for these data was a direct, unobstructed line-of-sight signal-strength measurement with the transmitters external to the stadium and in front of the receiving antennas. The purpose of the radio-mapping measurements was to investigate how the signals at the different frequencies couple into the stadium, and to determine the field strength variability throughout the stadium.

The second set of data was gathered from radios placed at fixed sites throughout the stadium. Received signals were collected before, during, and after the implosion. The receiving systems in this case were both at fixed sites and mobile. The mobile receiving system consisted of measurement instruments and antennas mounted on a modified garden cart. A detailed description of the measurement system and antennas is given in Section 5. The cart was pulled around the perimeter of the stadium both before and after the implosion, enabling direct comparison of signal strength as a function of (a) azimuth angle through the standing stadium and (b) the resulting pile of rubble after the collapse.

The third set of data consisted of monitoring signals coupled to metallic debris located in the proximity of transmitters buried in the collapsed stadium. These metallic "debris radiators" (a set of cables laid to investigate the concept) ran through the rubble and were exposed at the perimeter of the collapsed stadium. The idea is that when a large structure collapses, metal objects (electrical wires, metal piping, re-bar, venting pipe, etc.) protrude from the rubble. These objects may improve radio reception by coupling radio signals to searchers on the outside. When first responders approach a collapsed structure, one of their first priorities is to determine

whether survivors are present in the debris. Reception of signals from handheld radios or cell phones may let searchers know of survivors' presence and their condition. We measured the signals from the buried transmitters using instruments physically connected to the metallic debris through impedance tuners. Antennas were also used to investigate signal detection from these metallic debris radiators.

This report summarizes a set of experiments in a large sports stadium in Philadelphia, PA, formally known as Veterans' Stadium (see Figure 1). Details of the stadium layout are presented in Section 2. Section 3 describes the frequencies used in these experiments. Section 4 discusses the transmitters and Section 5 describes the automated measurement system used in the radio-mapping and propagation measurements. In Section 6, our experimental procedures are discussed. In Section 7 we present the data collected at various stages of the experiment. Section 8 briefly discusses the recovery of the transmitters after the implosion. Finally, in Section 9, we summarize the results of these experiments and discuss some of the interesting propagation effects observed.

2. Stadium Description

The structure for the radio propagation experiments discussed in this report was Veterans' Stadium, a large sports arena in Philadelphia, PA (see Figure 1). The nearly circular stadium was constructed of reinforced concrete, steel, and standard interior finish materials. Figures 1-3 show details of the original stadium and some of the preparations and partial demolition of the different sections of the stadium. As shown in these figures, the stadium had multiple levels with large open areas. The exterior perimeter of the stadium was approximately 805 m (1/2 mile). Significant demolition was already completed when we arrived two weeks before the implosion; all plumbing fixtures, most glass windows and doors, and other contents had been removed. Material had been judiciously removed from certain structural parts of the lower levels including stairwells and elevator shafts to facilitate a proper collapse during the implosion. Figure 4 shows a plan of the structure and approximate locations of the transmitter and receive instruments.

3. Frequency Bands

An overview of the frequencies used by the public safety community nationwide (federal, state, and local) is given in Table 1. From this table, we see that there is a broad range of frequencies ranging from 30 MHz to 4.9 GHz. The modulation scheme has historically been analog FM, but this is slowly changing to digital as Project 25 radios come online [7]. The modulation bandwidth in the VHF and UHF bands has been 25 kHz, but due to the need for additional communications channels in already crowded spectrum, all new bandwidth allocations are 12.5 kHz. The older wide-bandwidth allocations will gradually be required to move to narrow bandwidths to increase the user density even further. The crowded spectrum and limited bandwidth are also pushing the move to higher frequency bands in order to use new data-intensive technologies. The cellular phone bands are summarized in Table 2.

As shown in Table 1, frequencies currently used by public safety and other emergency responders and cellular telephones are typically below 2 GHz, for current technology. New frequency allocations and systems including higher frequencies (e.g., around 4.9 GHz) will become increasingly important in the future, but in these studies, we concentrated on the major communications bands in use today. We chose six frequency bands below 2 GHz, from about 50 MHz to just above 1800 MHz. These include four VHF bands typically used for analog FM voice, one band used for multiple technologies (analog FM voice, digital trunked FM, and cellular telephone), and one band near the digital cellular telephone band.

Table 1. Public safety community frequencies.

Frequency band	Description
30-50 MHz	Used mainly by highway patrol for long-distance propagation. This is currently being phased out of use.
150-174 MHz	Local police and fire. Lower frequency again used because of its better long distance propagation quality.
406-470 MHz	Used by federal officers and others.
700-800 MHz	Used in urban areas.
800-869 MHz	Primarily urban usage.
4.9 GHz	A newly allocated band with 50 MHz bandwidth just coming on line for sending images and data.

Table 2. Cellular phone frequencies.

Frequency band (MHz)	Description
800	AMPS or analog systems
1900	PCS or digital system

In designing an experiment to investigate the propagation characteristics into large buildings at these different frequency bands, we chose frequencies very close, but not identical, to the above bands. If frequencies were chosen in the public safety or commercial land-mobile bands, interference to the public safety and cellular systems could possibly occur. Conversely, these existing systems could interfere with our experimental setup. In addition, obtaining frequency authorizations in these bands for our experiments would have been problematic due to the intense crowding of the spectrum. To circumvent these issues we were able to receive temporary authorization to use frequencies in the U.S. government frequency bands adjacent to these public safety bands. Table 3 lists the frequency bands that were used in the experiments. The lower four bands correspond to the frequencies used by the public-safety community; 902 MHz can be associated with several services including public safety and cellular phone; and the highest frequency is near the digital cellular phone band.

Table 3. Frequency bands used in the experiments.

Frequency band (MHz)	Description
49	Simulate a public safety band
162	Simulate a public safety band
226	Simulate a public safety band
448	Simulate a public safety band
902	Simulate a public safety or cellular phone band
1830	Simulate a cellular phone band

Table 4. Frequency sets and grouping used in the experiments

Band (MHz)	Location A (MHz)	Location B (MHz)	Location C (MHz)	Location D (MHz)
49	49.78	49.66	49.72	49.60
162	162.20	163.3	165.54	162.90
226	226.50	225.4	226.4	225.30
448	448.80	448.60	448.70	448.50
902	902.45	902.60	--	--
1830	1830.0	1831.00	--	--

For the fixed transmitter experiments, where signals were monitored before during and after the implosion, twenty transmitters operating at different frequencies within the above six bands were placed at four different locations in the stadium (refer to Fig. 4). The 20 different frequencies used in this experiment are listed in Table 4. The first two locations had frequencies in all six bands, while the last two locations had transmitters tuned to only four different frequency bands. A detailed description of the transmitters is given in the next section.

4. Transmitters

The design requirements for the transmitters used in this experiment were to (1) transmit at the frequencies listed in the tables above, (2) operate continuously for 12 h, (3) be sufficiently robust to have a high probability of surviving the building collapse, and (4) be relatively inexpensive in the event that they did not survive the building collapse.

To accomplish this, two different types of transmitters were chosen. For the four lower frequency bands (the VHF/UHF public-safety bands), off-the-shelf amateur radios were modified. The modifications included (a) reprogramming the frequency synthesizer to permit transmitting at government frequencies, (b) disabling the transmitter time-out-timer mode in order to allow for a continuous transmission, and (c) connecting a large external battery pack. The specifications of

these modified radios then had to be reported to the National Telecommunications and Information Administration (NTIA) frequency coordinator in order to gain approval for use in government frequency bands. With the larger battery packs, the modified radios could transmit continuously for 12 to 18 h. The extended transmitting time required us to provide additional cooling since the radios were designed for typical communications, that is, to transmit intermittently with cooling time between transmissions.

The stability and radiated power from these inexpensive radios was measured over a 24-hour period. This measurement was performed in the NIST reverberation chamber, and is discussed below. The modified radios and battery packs were placed in durable orange plastic cases to provide some protection from debris during the implosion. These cases obviously could not withstand a crushing load of debris, so careful placement in the building was key to survival. Figure 5 shows the final arrangement of modified transmitters used for the lower four frequency bands.

Commercial transmitters were available for the two higher frequency bands (900 and 1800 MHz). These off-the-shelf transmitters were already in plastic protective cases and could transmit continuously for 12 h. Figure 6 shows these transmitters. Note that the higher-frequency transmitters were grey in color and not orange.

To ensure that the plastic protective cases did not affect the total radiated power and radiation pattern of the transmitters, measurements of these two quantities were taken in the NIST reverberation and fully anechoic chambers. Measurements of the total radiated power both with and without the plastic cases indicated that the cases had minimal effect on the total radiated power. Radiated power patterns of the transmitters in the protective cases were also measured to ensure that the cases did not have dramatic effects on the radiation patterns. The transmitters were placed in the NIST anechoic chamber (see Figure 7) for these pattern measurements. Figures 8-10 illustrate the results for 164 MHz, 225 MHz, and 448 MHz. These figures show that the radiation patterns of the transmitters in the protective cases were very similar to the dipole type pattern that the radio would produce in free space.

5. Receiving Antenna and Measurement System

The receiving system is sketched in Figure 11. We assembled four antennas on a 4-meter mast as illustrated. The radio-frequency output from each antenna was fed through a 4:1 broadband power combiner. This arrangement gave us a single input to the portable spectrum analyzer, which could then scan over all the frequencies of interest without switching antennas. The four antennas were chosen to be optimal (or at least practical) for each of the frequency bands we were measuring. The selected antennas were an end-fed vertical omnidirectional antenna for 50 MHz, a log-periodic-dipole-array (LPDA) used for the 160, 225, and 450 MHz bands, and Yagi-Uda arrays for 900 and 1830 MHz. This assembly could then be mounted on a fixed tripod at one of the listening sites, or it could be inserted into the modified garden cart for portable measurements. The receiving sites contained, in addition to the antenna system, a generator, uninterruptible power supply (UPS), spectrum analyzer, global positioning system (GPS)

receiver, computer, and associated cabling. Photos of the antenna assembly mounted on a tripod and mounted on the mobile cart are shown in Figure 12.

As shown in Figure 11, the measurement system consists of a portable spectrum analyzer, GPS receiver, and a laptop computer. The data collection process was automated using a graphical programming language. This software was designed to control the analyzer, collect, process, and save data at the maximum throughput of the equipment. The software controlled the spectrum analyzer via an IEEE-488 interface bus and the GPS receiver via a serial interface. The GPS information was recorded to track the position of the mobile cart during the perimeter measurements around the building.

The software was written to maximize throughput of the data collection process and to run for an undefined time interval. This was achieved by running parallel processes of collecting, processing, and saving the data for post-collection processing. The data were continuously read from the spectrum analyzer at its optimal settings and stored in data buffers. These buffers were read and processed for each signal and displayed for operator viewing. The processed data were then stored in additional buffers to be re-sorted and saved to a file on disk.

The initial setup of the parameters for the spectrum analyzer determined the quality of optimization for this process. There were several instrument parameters that were critical during the setup, including the analyzer sweep time, resolution bandwidth and frequency span of the spectrum analyzer trace. The number and spread of the test frequencies in a particular band influenced the allowed range of adjustment for these parameters. These two factors also influenced the number of traces necessary to cover all the test frequencies. Interference from signals in the adjacent spectrum influenced the instrument setup and data collection speed by forcing smaller resolution bandwidths. The reference level for each trace was also checked and adjusted during the measurement to improve the resolution and accuracy of the power level reading. All of these factors had some effect on the sampling rate.

The sampling rate of a complete measurement sequence was the major factor in how much spatial resolution we had during walk-through or field-mapping experiments (we also had some flexibility in our walking speed) and the time resolution for recording the signals during the implosion. The time resolution of the measured data determined how much detail we could record for the rapid changes in signal strength as the building collapsed. Even though we were concerned primarily with the before and after values, we hoped to record the signals with enough detail to correlate the movement of the structure during the event to our received signals.

We used three different models of spectrum analyzers, each having a different sampling rate, ranging from about 2 to 7 s, to measure all 20 frequencies in the six frequency bands. The frequencies were spaced such that we could utilize one spectrum analyzer trace for each band. These rates were achieved only after optimizing the instrument control and data transfer processes mentioned above. The data from the spectrum analyzer trace were saved in binary format to disk (to allow us to reprocess the raw data at a later time if needed); they were then processed to extract the signals at each particular frequency. These results were then put into a spreadsheet file and saved with other measurement information. The sampling rates were

sufficient for the field-mapping experiments (if we did not walk too fast) but very few samples could be recorded during the implosion.

6. Experimental Set-up

Three types of data were collected in the experiment. The first set of data, which is here referred to as a "radio mapping," was collected a few days before the building was imploded. This involved carrying transmitters (or radios) tuned to various frequencies through the interior and exterior of the stadium while recording the received signal from a site located outside the stadium. The purpose of these measurements was to investigate how signals at the different frequencies couple into the stadium and to determine the variability in field strength throughout the stadium. Also, by carrying the transmitters around the exterior perimeter of the stadium the amount of signal blockage caused by the stadium from one side to the other could be investigated. For the radio mapping experiments, one fixed receiving site (as described above) was assembled on the southwest perimeter of the stadium (see Figure 13), approximately 53 m from Column #10. During this experiment, the transmitters were carried (and at times, driven aboard an all-terrain-vehicle or ATV) throughout the stadium (see Figure 14) and the received signal levels were recorded. Measurements were performed with the receiving antennas polarized in both the horizontal and vertical direction (with respect to the ground). As the received signal was recorded, the location of the transmitters in the buildings was also recorded.

For the second data set, radios were placed at four different fixed locations in the stadium where they would have a high likelihood of surviving the implosion. These four sites are labeled as "TX A", "TX B", "TX C", and "TX D" in Figure 4. Received signals were collected before, during, and after the implosion. After a careful analysis of the building, the following four sites were chosen: (1) against a concrete wall on the west side of the stadium in a sublevel (Site TX A: see Figure 15); (2) on the playing field against a concrete retaining wall (Site TX B, see Figure 16); (3) against a concrete wall on the south side of the stadium in a sublevel (Site TX C, see Figure 17); and (4) in a turnstile on the third level of the stadium (Site TX D, see Figure 18).

A few comments are in order about the transmitters against concrete walls on the west and south side of the stadium. This building had no basement, however, these two walls were below ground level and the walls were backed by dirt. These walls were part of a large open area that opened onto the playing field (see Figures 15 and 17). During the implosion these walls would not collapse, because the implosion was designed to have the upper levels roll over these walls. However, these walls would be covered with a significant amount of debris. Placing the transmitters against these concrete walls ensured that these two sets of transmitters would have some protection from the impact of the collapse and the majority of the concrete rubble would be on top of the transmitters after the implosion. In a similar manner, the transmitters on the playing field were first placed against a retaining wall and a large concrete column was then laid on top of transmitters (see Figure 16). Because the stadium was designed to roll onto the playing field during the implosion, this concrete column ensured that this set of transmitters would have some protection from the impact of the collapse and the majority of the concrete rubble would be on top of the transmitters after the implosion. Finally, the transmitters on the third level were tied to a metal turnstile to provide protection from the impact as the stadium levels collapsed and fell onto the playing field.

To protect all the transmitters from implosion dust, they were all wrapped in blast cloth, a fabric used to contain shrapnel from the explosions (see Figure 19). Notice that plywood was placed near the transmitters located at the south and west walls. This was done to give added protection to the transmitters from flying shrapnel.

The receiving sites in this second mode of data collection were both fixed and mobile. Three fixed receiving sites were used to collect data before, during, and after the implosion. These three sites were placed around the perimeter of the stadium (see Figures 4 and 20). Receiving site RX 1 was placed approximate 53 m (173 ft) from the south west perimeter of the stadium. The measurement equipment at this site was placed in a yellow metal construction container (see Figure 20a) for protection during the implosion. Receiving site RX 2 was placed 37 m (120 ft) from the south east perimeter of the stadium. The measurement equipment at this site was placed in a small guard building (see Figure 20b) for protection during the implosion. A piece of plywood was placed over the front window of this building for additional protection (Figure 20b). This precaution was actually necessary because the plywood took direct hits from flying concrete. Receiving site RX 3 was placed 53 m (173 ft) from the north west perimeter of the stadium. The measurement equipment at this site was placed in the NIST van (see Figure 20b) for protection during the implosion. Since these three sites were very close to the stadium, there were no personnel present in them during the implosion. During the implosion the receiving antennas at receiving site RX 1 and RX 2 were polarized in the vertical direction, while the three high-band antennas at receiving site RX 3 were polarized in the horizontal direction. These different polarizations were chosen in order to investigate whether polarization effects would be significant during the implosion. The idea was to see if the stadium rubble would have the effect of depolarizing the transmitter signals.

The mobile receiving system consisted of measurement instruments placed on a cart (see Figure 21) as described above. The cart was pulled around the perimeter of the building both before and after the implosion, enabling direct comparison of signal strength through the standing building and later through the rubble.

We collected a third set of data to investigate the use of so-called "debris radiators." This set of data was collected by first using antennas and then connecting instruments through tunable impedance matching network to metal in the building rubble. This experiment was designed to investigate the possibility of detecting radio signals from a buried transmitter that might couple onto metal objects such as electrical wires, metal pipes, re-bar, venting ducts, etc., and carry signals to the edges of the rubble pile.

To simulate the best-case scenario, the experiment was designed to ensure that there was an unbroken metallic object placed near two of the transmitter sets. Steel cables were used as the metal object and were placed near the transmitters at sites TX A and TX B (labeled as Cables 1 and 2 in Figure 4). The cables were then run 15 m from the stadium perimeter (see Figures 22 and 23). The 15 m distance was anticipated to be beyond the point where the building debris would lie after the implosion so that we could connect instruments to the ends of the cable.

7. Experimental Results

In this section the measured data are presented. This section is divided into several subsections, with each subsection covering the different types of experiments performed in the effort.

7.1 Radio Mapping of Stadium: Measured Signal Strengths

The six different frequencies listed in Table 5 are the ones used in the radio mapping, or "walk-through", experiments. The receiving site for this set of experiments was outside the stadium at a location approximately 53 m (173 ft) on the south side straight out from Column #10 (see Figures 4). To calibrate the system, the transmitting units were turned on at a location outside the stadium, which was at a line-of-sight (LOS) location between the receiving antennas and the stadium. After all six transmitters were turned on, the units were carried either around the perimeter or through the interior of the stadium. At various points both inside and outside the stadium, the transmitter locations were noted in the data file.

Table 5. Frequencies used in the stadium walk-through experiments.

Frequency band (MHz)	Description
49.60	Simulates a public safety band
162.09	Simulates a public safety band
225.30	Simulates a public safety band
448.50	Simulates a public safety band
902.45	Simulates a public safety or cellular phone band
1832.00	Simulates a cellular phone band

7.1.1 External Stadium Measurements

Figures 24 and 25 show the received signal strengths as the transmitters were carried around the perimeter of the stadium. Each figure shows the six frequencies listed in Table 5 and the two different figures correspond to the vertical or horizontal polarization of the receiving antenna The results in these figures have been normalized to the peak received signal at their respective frequencies. The peak values occurred at the line-of-sight reference location. From these graphs we can see that as the transmitters are carried around the perimeter of the stadium the signal strength steadily decreases, reaching a minimum of –70 to –75 dB on the backside, then steadily increases again. Part of this decrease is due to the distance fall-off proportional to $1/r$, which for the diameter of the stadium (~256 m) could be on the order of 20 dB. The data are not corrected for this $1/r$ effect since we are interested in the net effect of the structure and its physical size on communications. The net effect indicates that, since the stadium is such a large structure, communication problems can occur when simply trying to communicate external to external (i.e., from one side of the stadium to the other). This was also observed in our personal communication equipment used during this test. Personnel at the receiving site were in

communication with the personnel carrying the transmitters via two-way 160 MHz radios. This communication link allowed us to mark the location of the transmitter recorded on the dataset at the receiving site. When the transmitters were located on the back side of the stadium, communication using our two-way radios was very difficult.

7.1.2 Internal Stadium Measurements

Figures 26-28 show the received signal strengths for the data collected during the building walk-throughs. Each figure shows the six frequencies used in this test. The results in these figures have been normalized to the peak received signal at their respective frequencies. The peak values occurred at the line-of-sight reference location. Figures 26 and 28 correspond to horizontally polarized receiving antennas, while Figure 27 corresponds to vertically polarized antennas. The stadium was actively being demolished with heavy machinery as these experiments were being performed and our access to the stadium was limited. As a result, our time inside the structure was limited to safe periods when the equipment was idle, usually only during the operators' lunch break or quiet periods when the machines required maintenance. Thus, the data in the experiment were obtained in the following manner such that our time in the stadium was minimized. First, an all-terrain-vehicle (ATV) was used to haul the transmitters through the stadium. The receiving antennas were initially aligned in a horizontally polarized direction. The transmitters were placed in the ATV and powered on at a light-of-sight reference location outside the stadium. Once a baseline of data was recorded, the ATV was driven in and throughout the upper levels of the stadium. Once the ATV was at the highest level in the stadium (called Level 700) we stopped the ATV at a location where the receiving antennas could be seen. At that point the transmitters were powered off. The receiving antennas were then rotated to a vertically polarized alignment. The transmitters were then energized and we drove the ATV back, retracing its track to the exterior of the stadium. This sequence was repeated into the lower levels of the stadium and onto the playing field. However, since there was no visible reference to the receivers in the lower levels where we could flip polarizations, we chose to use one of the sites that would be used to cache transmitters during the implosion (Site A) as our turn-around location. As before, the transmitters were powered off, the receiving antennas rotated to a horizontally polarized alignment, and the ATV retraced its track to the exterior of the stadium.

From the graphs in Figures 26-28, we can see a large variability in the received signal as the transmitters were moved throughout the building. These results show that the building induced about 50 to 60 dB of shielding of the signals. This 50 to 60 dB indicates the additional design margins that would be required in a link budget analysis of a communication system in order to achieve communication into a large building of this type.

7.2 Radio Mapping of Stadium: Statistical Distributions of Signal Strength

The results in the previous section illustrate that the field strengths varied by as much as 60 dB throughout the stadium and 75 dB around the outside of the stadium. In communication systems design, the variability of the field strength is as important as the field strength itself. Knowing the variability allows the system designer to develop devices for first responders that must be capable of operating in an environment with large dynamic range in signal strength. In this

section, some statistics of the field strength variability inside and outside the stadium are investigated. The first set of data analyzed was collected when we carried the transmitters around the perimeter of the stadium (data in Figures 24 and 25). The histograms (2 dB bin size) for this dataset are shown in Figure 29 and 30, for vertically and horizontally polarized receiving antennas, respectively. Tables 6 and 7 summarize the mean received signal strength and the standard deviation for each frequency.

The next set of data was collected when the transmitters were driven through the upper levels of the stadium for horizontally polarized receiving antennas (data in Figure 26). The histograms for this dataset are shown in Figure 31. Table 8 summarizes the mean received signal strength and the standard deviation for each frequency.

The next set of data was collected when the transmitters were driven through the upper levels of the stadium to the playing field for vertically polarized receiving antennas (data in Figure 27). The histograms for this dataset are shown in Figure 32. Table 9 summarizes the mean received signal strength and the standard deviation for each frequency.

The final set of data was obtained from driving through the lower levels and playing field for horizontally polarized receiving antennas (data in Figure 28). The histograms for this dataset are shown in Figure 33. Table 10 summarizes the mean received signal strength and the standard deviation for each frequency.

Table 6. Mean and standard deviation of the received signal strengths for the exterior perimeter measurements for vertically polarized receiving antennas.

Frequency (MHz)	Mean (dB)	Standard deviation (dB)
49.60	–37.3	18.1
162.09	–50.0	19.9
225.30	–50.9	20.3
448.50	–45.5	21.1
902.45	–47.9	22.2
1830.00	–42.3	19.7

Table 7. Mean and standard deviation of the received signal strengths for the exterior perimeter measurements for horizontally polarized receiving antennas.

Frequency (MHz)	Mean (dB)	Standard deviation (dB)
49.60	–28.0	15.5
162.09	–29.2	15.1
225.30	–34.2	18.3
448.50	–32.8	16.1
902.45	–36.9	17.3
1830.00	–39.0	17.4

Table 8. Mean and standard deviation of the received signal strengths for the upper level measurements for horizontally polarized receiving antennas.

Frequency (MHz)	Mean (dB)	Standard deviation (dB)
49.60	–30.6	15.0
162.09	–34.4	15.2
225.30	–30.0	13.9
448.50	–33.5	14.4
902.45	–37.2	13.8
1830.00	–43.6	12.0

Table 9. Mean and standard deviation of the received signal strengths throughout the upper levels of the stadium to the playing field for vertically polarized receiving antenna.

Frequency (MHz)	Mean (dB)	Standard deviation (dB)
49.60	–32.9	14.1
162.09	–39.4	15.7
225.30	–34.4	13.5
448.50	–28.7	11.2
902.45	–27.3	11.3
1830.00	–26.6	9.5

Table 10. Mean and standard deviation of the received signal strengths for the lower levels and the playing field for horizontally polarized receiving antenna.

Frequency (MHz)	Mean (dB)	Standard deviation (dB)
49.60	–43.4	8.5
162.09	–36.1	10.6
225.30	–39.7	9.7
448.50	–36.6	8.6
902.45	–52.7	12.8
1830.00	–31.3	7.4

7.3 Pre-implosion Radio Signal Measurements with Transmitters at Fixed Sites

Before the implosion, sets of transmitters were placed at three fixed sites and secured (see Section 6 for details). In order to get an indication of the relative difference in signal strengths for the transmitters at the four different fixed transmit sites, a set of baseline data was collected. The data were collected by placing the transmitters at each of the four fixed transmitter sites and measuring the received signals with the equipment on the mobile cart. The cart was pulled around the perimeter of the stadium.

7.3.1 Signal-Strength Measurements for Fixed Sites

Figures 34 and 35 show the variability in the signal strength around the perimeter of the stadium for all six frequencies for transmitters located at fixed Site A. These two figures are for vertically and horizontally polarized receiving antennas, respectively. It should be noted that as the cart was pulled around the building, the antennas on the cart were always pointed toward the center of the stadium. Figures 36 and 37 show the data in Figure 34 and 35 normalized with respect to the overall (either horizontal or vertical polarization) maximum received signal. That is, each frequency is normalized to its maximum level for all data recorded during both perimeter travels of the receiving cart. We should note that this normalization reference includes a certain unknown amount of attenuation, caused by the structure between the transmit site and the location of best coupling on the exterior perimeter, which we cannot remove. These two plots show the relative variability in the signal strength as the cart is moved around the stadium. From these plots, we see that the presence of the stadium causes the signal to vary by as much as 55 dB around the stadium perimeter.

Figures 38 and 39 show the variability in the signal strength around the perimeter of the stadium for all six frequencies for transmitters located at fixed Site B. These two figures are for vertically and horizontally polarized receiving antennas, respectively. Again, as the cart was pulled around the building, the antennas on the cart were always pointed toward the center of the stadium. Figures 40 and 41 show the data in Figure 38 and 39 normalized with respect to the maximum received signal. That is, each frequency is normalized to its maximum level as described above. Figures 40 and 41 show the relative variability in the signal strength as the cart is moved around the stadium. In these plots, we see that the presence of the stadium construction causes the signal to vary by as much as 40 dB around the stadium perimeter.

Figures 42 and 43 show the variability in the signal strength around the perimeter of the stadium for all six frequencies for transmitters located at fixed Site C. These two figures are for vertical and horizontal polarized receiving antennas, respectively. As above, the antennas on the cart were always pointed toward the center of the stadium. Figures 44 and 45 show the data in Figure 42 and 43 normalized with respect to the maximum received signal. From these plots, we see that the stadium causes the signal to vary by as much as 50 dB around the stadium perimeter.

Figures 46 and 47 show the variability in the signal strength around the perimeter of the stadium for all six frequencies for transmitters located at fixed Site D. These two figures are for vertical and horizontal polarized receiving antennas, respectively. Figures 48 and 49 show the data in Figures 46 and 47 normalized with respect to the maximum received signal. These two plots show the relative variability in the signal strength as the cart is moved around the stadium. We see that the stadium causes the signal to vary by as much as 60 dB around the stadium perimeter.

7.3.2 Statistical Distributions of Signal Strength for Fixed Sites

The results in the previous section illustrate that the field strengths varied by as much as 60 dB around the perimeter of the stadium. In this section, some statistics of the field strength variability around the perimeter are investigated. The first set of data analyzed is for fixed transmitter site A (data in Figures 34 and 35). The histograms (2 dB bin size) for this dataset are shown in Figures 50 and 51, for vertically and horizontally polarized receiving antennas, respectively. Note the histograms were generated from the normalized data. This presents the typical variability that would be seen for a communication system carried around the perimeter. Tables 11 and 12 summarize the mean received signal strength and the standard deviation for each frequency. Once again, this is not the attenuation resulting from coupling into the stadium, but is the variability a communication system would experience.

The next set of data analyzed is for fixed transmitter site B (data in Figures 38 and 39). The histograms (2 dB bin size) for this dataset are shown in Figures 52 and 53, for vertically and horizontally polarized receiving antennas, respectively. Note the histograms were generated from the normalized data. This would be the actual variability that would be seen for a communication systems carried around the perimeter. Tables 13 and 14 summarize the mean received signal strength and the standard deviation for each frequency.

The next set of data analyzed is for fixed transmitter site C (data in Figures 42 and 43). The histograms (2 dB bin size) for this dataset are shown in Figures 54 and 55, for vertically and horizontally receiving antennas, respectively. Note the histograms were generated from the normalized data. Tables 15 and 16 summarize the mean received signal strength and the standard deviation for each frequency.

The next set of data analyzed is for fixed transmitter site D (data in Figures 46 and 47). The histograms (2 dB bin size) for this dataset are shown in Figures 56 and 57, for vertically and horizontally polarized receiving antennas, respectively. Note the histograms were generated from the normalized data. Tables 17 and 18 summarize the mean received signal strength and the standard deviation for each frequency.

Table 11. Mean and standard deviation of the received signal strengths for Fixed Transmitter Site A for vertically polarized receiving antennas.

Frequency (MHz)	Mean (dB)	Standard deviation (dB)
49.60	–31.7	8.0
162.09	–44.4	12.2
225.30	–44.3	13.1
448.50	–37.4	11.1
902.45	–27.4	8.9
1830.00	–25.5	6.7

Table 12. Mean and standard deviation of the received signal strengths for Fixed Transmitter Site A for horizontally polarized receiving antennas.

Frequency (MHz)	Mean (dB)	Standard deviation (dB)
49.60	–32.3	8.4
162.09	–41.7	14.3
225.30	–37.2	12.8
448.50	–37.1	11.1
902.45	–29.0	10.0
1830.00	–27.0	8.2

Table 13. Mean and standard deviation of the received signal strengths for Fixed Transmitter Site B for vertically polarized receiving antennas.

Frequency (MHz)	Mean (dB)	Standard deviation (dB)
49.60	–18.9	5.7
162.09	–17.3	7.8
225.30	–16.9	7.1
448.50	–14.3	6.7
902.45	–28.0	8.8
1830.00	–25.0	8.3

Table 14. Mean and standard deviation of the received signal strengths for Fixed Transmitter Site B for horizontally polarized receiving antennas.

Frequency (MHz)	Mean (dB)	Standard deviation (dB)
49.60	–26.7	6.5
162.09	–24.9	7.5
225.30	–24.9	8.5
448.50	–15.1	5.5
902.45	–17.2	6.4
1830.00	–23.5	6.9

Table 15. Mean and standard deviation of the received signal strengths for Fixed Transmitter Site C for vertically polarized receiving antennas.

Frequency (MHz)	Mean (dB)	Standard deviation (dB)
49.60	–30.4	8.2
162.09	–34.2	9.8
225.30	–42.5	10.8
448.50	–38.1	8.6
902.45	–38.1	8.4
1830.00	–20.8	8.4

Table 16. Mean and standard deviation of the received signal strengths for Fixed Transmitter Site C for horizontally polarized receiving antennas.

Frequency (MHz)	Mean (dB)	Standard deviation (dB)
49.60	–32.1	9.4
162.09	–36.8	11.1
225.30	–36.3	10.8
448.50	–29.7	7.6
902.45	–32.4	8.6
1830.00	–27.3	6.8

Table 17. Mean and standard deviation of the received signal strengths for Fixed Transmitter Site D for vertically polarized receiving antennas.

Frequency (MHz)	Mean (dB)	Standard deviation (dB)
49.60	–43.1	12.4
162.09	–49.3	13.2
225.30	–44.1	13.6
448.50	–34.4	10.5
902.45	–32.6	9.5
1830.00	–31.3	8.8

Table 18. Mean and standard deviation of the received signal strengths for Fixed Transmitter Site D for horizontally polarized receiving antennas.

Frequency (MHz)	Mean (dB)	Standard deviation (dB)
49.60	–45.0	11.0
162.09	–49.6	12.0
225.30	–50.9	10.8
448.50	–42.2	9.2
902.45	–37.7	8.9
1830.00	–42.1	7.7

7.4 Implosion Radio-Signal Measurements with Transmitters at Fixed Sites with Fixed and Mobile Receiving Sites

On the day of the implosion, the fixed receiver sites discussed in Section 6 were assembled and the data collection programs were turned on two hours before the implosion. The transmitters at the four fixed locations in the stadium (see discussion in Section 6) were also turned on two hours before the implosion. Figures 58-61 show the pre- and post implosion data for the fixed receiver located at Receiving Site 1. Each of these four figures corresponds to one of the four fixed transmitter sites. The implosion occurred at around 7 a.m., and this is indicated in the figures by the abrupt change in the signal levels. This receiving site was closest to transmitting Site A. This is seen in the figures by the fact the signal strengths in Figure 58 are higher than those in Figures 59-61. Notice that the signal strengths for the 49.78 MHz transmitter in Figure 58 were very weak even before the implosion.

From Figure 59, it is seen that the 49.66 MHz transmitter was also very weak before the implosion. Also, notice the impulsive nature of the 448.60 MHz transmitter in Figure 59. In this experiment the transmitter was modulated using a Morse code generator as part of the debris radiator tests. This modulated signal showed large variability in measured power on the spectrum analyzer as evidenced by the spikes in Figure 59. The useful part for this experiment is the unmodulated lower baseline which corresponds well to the other frequencies. In Figure 60, we see that the signal strength of all four transmitters from Site C change from the transmitters at Site A by nearly the same amount. The changes in the signals from Site D (Figure 61) are not quite as dramatic as Site C but the event is clearly discernable.

Figures 62-65 show the pre- and post implosion data for the fixed receiver located at Receiving Site 2. Each of these four figures corresponds to one of the four fixed transmitter sites. The implosion occurred at around 7 a.m., and this is indicated in the figures by the dramatic change in the signal levels. This receiving site was farthest from transmitting sites A, B, and C. There is a large portion of the stadium between transmitter sites A, B, and C and the receiver and we see in Figures 62, 63, and 64 that signals from these transmitters are very weak. The spectrum analyzer at this receiving site was a similar model to the one at site 1 and we see a similar response to the modulated Morse code signal in Figure 63. Interesting results are observed in Figure 65. These data are from the transmitters in the upper level and closest to Receiving Site 2.

First, notice that the 49.60 MHz transmitter signal increases for a few moments during the implosion then decreases to a value of –90 dBm. This can be explained by the fact that once part of the stadium fell away the propagation path changed briefly before reaching a final condition. Similar dynamics are seen for the 448.50 MHz transmitter.

Figures 66-69 show the pre- and post implosion data for the fixed receiver located at Receiving Site 3. Each of these four figures corresponds to one of the four fixed transmitter sites. Once again, after the implosion occurred we see a dramatic change in the signal levels. The data in these figures exhibited some interesting variations during the implosion. The implosion was designed to have the stadium collapse in a circular manner, as seen in Figure 70. The implosion lasted over 60 s. During the collapse, half the stadium fell away from the perspective of this receiving site, and as a result this receiving site could see inside the stadium before it totally collapsed. This is illustrated nicely in Figures 66, 67, and 69. This effect is not seen in Figure 68. This is a result of the positioning of the transmitters at Site C. At this transmitting site, the transmitters were below ground level and against a concrete wall backed by soil. This wall was in the general direction of receiving site 3 and did not move during the implosion.

This implosion was designed to obtain a total collapse of the stadium, representing a worst-case scenario for simulating first responder communications, as shown in the photographs in Figures 70-73. Figure 70 shows the stadium collapsing, Figures 71 and 72 show the stadium after the implosion. And Figure 73 shows the change in the landscape as seen from each of the receiving sites before and after the implosion.

After the implosion, the cart was used to move a receiving system around the perimeter of the building to record the transmitted signals. Figure 74 shows the mobile cart being used for the post-implosion measurements. The path used was generally the same path as that used in the cart measurements before the implosion. We collected three sets of measurement data. The first measurements were performed with the receiving antenna for the five higher frequency bands horizontally polarized. Figures 75-78 show the receiver signal strengths for the transmitters at the four different transmitting sites, respectively. By comparing these figures to the results in Figures 35, 39, 43, and 47 (the pre-implosion measurements), the effects of the stadium collapse on the signal strength can be investigated. In order to better compare the pre- and post-implosion measurements, the two datasets are overlaid with respect to the GPS cart location. Figures 79-98 show the comparison of these datasets. In these comparisons, we see an additional 20 to 50 dB of attenuation after the collapse.

The next two sets of measurements were performed with the receiving antenna for the five higher frequency bands vertically polarized. Figures 99-102 show the receiver signal strengths for the transmitters at the four different transmitting sites for the first set of vertical perimeter measurements. While Figures 103-106 show the receiver signal strengths for the transmitters at the four different transmitting sites for the second set of vertical perimeter measurements; the results for the two different vertically polarized measurements are basically the same. By comparing these figures to the results in Figures 34, 38, 42, and 46 (the pre-implosion measurements), the effect of the stadium collapse on the signal strength can be investigated. Once again, in order to better compare the pre- and post-implosion measurements, the two datasets are overlaid with respect to the GPS cart location. Figures 107-126 show the comparison

of these datasets. In these comparisons, we see additional 20 to 40 dB of an attenuation after the collapse.

Thus, if someone were trapped under such a rubble pile and were trying to communicate with an emergency responder with a two-way radio or cell phone, their communication link would have to overcome an additional 20 to 50 dB of attenuation .

7.5 Field Tests of the Debris Radiator Concept

As noted in Reference [5], electric field strength drops off rapidly as one moves away from a transmitter. When line-of-sight conditions exist between transmitter and receiver, use of a standard single-element antenna on a handheld radio or cell phone poses no problem even at distances on the order of miles. However, inside buildings, signal attenuation (loss) and multipath (reflected signals that interfere with the primary received signal) can reduce the usable operating range of these radios to much shorter distances. For collapsed building scenarios, a dense pile of debris can reduce the electric field strength at a receiver by 50 dB or more [5], making standard point-to-point communications difficult.

Our goal in testing the debris radiator concept is to investigate whether the use of metallic debris found at the site of a building collapse or partial collapse can more efficiently guide a radio-frequency signal through the debris pile than a radio or cell phone's built-in antenna. In collapsed building scenarios, a great deal of metallic debris is often present, including long metallic objects such as conduit, wiring, and pipes. The goal of this study was to see whether received signal levels could be improved by placing the existing transmit antenna within the proximity of the metallic object.

Since the opportunity to select a suitable metallic object in an emergency scenario is an uncertain condition, use of debris radiators is envisioned as a tool of last resort for someone trapped in the debris pile. Optimally, one would choose as a debris radiator an object that runs unbroken from the inside to the outside of a building and has suitable transmission properties, including its proximity to earth ground. Close proximity to earth ground can reduce the efficiency of the radiator. Since the choice of debris radiator is quite open-ended and the propagation environment is complicated, use of simulation studies to verify even simple problems would be computationally exhaustive. We have opted for laboratory and field tests to investigate the debris radiator concept. Our studies show that improvement in received signal level can range from zero to several orders of magnitude when debris radiators are used.

To maximize our chances of a useful outcome at the Philadelphia stadium implosion, we simulated the best-case scenario of a metallic object running continuously from a radio to a receive site by laying stranded steel cables from two of the transmit sites (in close proximity to the radios) to the edge of what would be the debris pile after implosion. Use of the pre-placed cables meant that even if post-blast safety considerations kept us from getting close to the collapsed building, we could still acquire useful data. Two cables were run, one from transmit Site A and one from transmit Site B, as shown in Figure 4. Photos of the Cable 1 and Cable 2 receive sites are shown in Figures 22 and 23.

We measured the received signals both before and after the building implosion using a spectrum analyzer. We compared reception using two receiving antenna scenarios. The first consisted of a directional, log-periodic antenna with a gain of approximately ten (that is, the received signal in the direction of the array was ten times stronger than with an omni-directional antenna). For the second scenario, we attached the spectrum analyzer directly to the steel cables through an impedance tuner. These types of impedance tuners are available commercially for use in the amateur radio bands. Connecting our spectrum analyzer to the cable through the tuner maximized the coupling of the signal between the cable and the spectrum analyzer.

We measured signals at receive sites Cable 1 and Cable 2 (see Figure 4) in the 160 MHz, 220 MHz, and 450 MHz frequency bands from all four transmit sites. Figure 127 shows the post-implosion measurements being made at the Cable 1 and Cable 2 receive sites. We were able to receive signals from all four transmit sites at each of the two receive sites, indicating that the attenuation caused by the stadium's debris pile was not as severe as we encountered in the New Orleans implosion [5].

Table 19 shows the results of our measurements. Post-implosion measurements at locations close to the debris pile show signal levels ranging from –55 to –129 dBm (approximately the noise floor of our spectrum analyzer).

Just as we found in the New Orleans implosion experiment [5], Table 19 shows that use of the directional receiving antenna in close proximity to the debris radiator generally resulted in a higher received signal level than that obtained in a direct connection. Cable reception ranged from 9 to 27 dB lower than reception with the antenna. Use of a more highly directional antenna could improve reception even further, but at the expense of having to aim the antenna more precisely, a factor which should be considered during search and rescue operations.

The experiments discussed here demonstrate that the debris radiator concept may provide a "last resort" method for improving wireless communications for someone trapped in a void in a collapsed building. Experiments such as these give us an understanding of what conditions will make debris radiators most effective. Further tests in the field and in the laboratory have been carried out and will be discussed in subsequent publications.

Table 19. Summary of data collected from debris radiator experiments: Cable (C) is the case where the receiver is connected directly to the metallic debris through an impedance tuner, and Antenna (A) is the case where a directional antenna is connected to the receiver.

		Cable 1			Cable 2		
Frequency (MHz)	TX Site	Cable (C) (dBm)	Antenna (A) (dBm)	Diff.(C-A) (dB)	Cable (C) (dBm)	Antenna (A) (dBm)	Diff.(C-A) (dB)
162	A	–101	–72	29	–129	–120	9
	B	–109	–102	7	–123	–103	20
	C	–119	–102	17	--	--	--
	D	–94	–104	10	–110	–100	10
225	A	–102	–80	22	--	–126	--
	B	–114	–91	23	–127	–100	27
	C	–122	–106	26	--	--	--
	D	–102	–88	14	–108	–81	27
450	A	–85	–55	30	–122	–108	14
	B	--	--	--	--	--	--
	C	–114	–93	21	--	--	--
	D	–112	–96	16	-113	–99	14

8. Recovery of Transmitters

After the implosion, the demolition contractor of the building recovered the transmitters so that we could examine them to determine whether the implosion destroyed them. This was needed to ensure that in the case that a signal for one particular transmitter was not detected after the implosion, non-detection of signals was a result of the signal attenuation through the rubble, not a result of the transmitter being destroyed. All the transmitters that were recovered from the stadium were in operational condition.

9. Summary of Results and Conclusion

This report summarized radio propagation measurements performed before, during, and after the implosion of the Veterans' Stadium in Philadelphia, PA. Three different types of experiments were performed during this effort. The first set of data, radio mapping, was collected a few days before the stadium was imploded. This involved carrying transmitters tuned to various frequencies through the stadium while recording the received signal at a site located outside the stadium as mentioned above. The purpose of these measurements was to investigate how the signals at the different frequencies couple into the stadium and to determine the field strength variability throughout the building. The results in this report indicate that the stadium caused about 50 to 60 dB of attenuation of the signals. These attenuation numbers were obtained by normalizing the signal to outside LOS values. Measurements around the outside perimeter of the stadium were also performed, and the results indicate that a walk around the exterior of the stadium would result in 70 to 75 dB of attenuation of the signals. Therefore, this 50 to 75 dB indicates the additional design margins that may be required in a link budget analysis of a communication system in order to achieve communication into a large structure of this type.

The results in Section 7.1 illustrated that the field strengths varied significantly throughout the stadium. In designing communication systems, the variability of the field strength is as important as the field strength itself. Some statistics of the field strength variability in the stadium were also investigated. The results in Section 7.2 show how the mean and standard deviation of the signals varied with both frequency and location in the building. These results show that the mean attenuation due to the building ranged from 25 to 50 dB and the standard deviation ranged from 7 to 16 dB, depending on frequency. These results indicate the variability in signal level that a communication system might experience throughout a building of this type.

These numbers can be compared to the implosion experiment performed in a 13-floor apartment building near New Orleans [5]. The results in the stadium are similar to those obtained in the apartment building. However, the stadium offers about 20 dB more shielding (or large attenuation) of the radio signals than that of the apartment biulding.

There are a number of other interesting studies and measurements published in the literature related to the attenuation of radio-frequency signals into buildings and through building materials [5, 8-17]. Many, if not most, of these studies concentrated on frequencies allocated to cellular and personal communications systems near 850 and 1900 MHz and the higher gigahertz bands using measurement scenarios that model some part of the commercial cellular network including

building interiors. While direct comparison of these results to our measurements is not possible, since each building and experimental setup is different, we can comment generally on how our data compare with the results in the literature.

A comprehensive review of earlier (pre-1991) building attenuation studies is given by Molkdar [10]. The author notes that the statistics of the received signal strengths depend strongly on the structural design, building materials, and contents of the building. The surrounding environment (i.e., adjacent structures) also had an effect. Results for building attenuation or penetration loss were tabulated for several distinct categories, including residential (–2 to 24 dB), office building in suburban areas (1.5 to 36 dB), and office building in urban areas (2 to 38 dB). Again, these results were for the higher cellular frequencies. Devasirvatham et al. [9] claimed that the statistics of signal attenuation within the interior of a large commercial stone and masonry building for four different frequencies (850 MHz, 1.9 GHz, 4.9 GHz, and 5.8 GHz) were nearly the same. They reported path losses ranging from 20 dB to near 70 dB and standard deviations from 3 to 9 dB. In more recent experiments, Ju et al. [11] show attenuation (path loss) between locations within an office building ranging from 20 to 80 dB at 1800 MHz with 15 to 35 dB from floor to floor. Tarng et al. [12] measured attenuation between floors in another office structure ranging from 20 to 47 dB at 900 MHz. The attenuation values of Ju et al. and Tarng et al. are similar to our measurements, but again, the measurement setups are quite different.

Walker [13] measured attenuation into several different buildings at 850 MHz and showed average attenuation that ranged from 15 to 20 dB with standard deviations ranging from 5 to 11 dB. These buildings were illuminated by multiple cellular transmitters at distant locations, and the exterior and interior signal strength measurements were extensively averaged. Davidson et al. [15] also measured building penetration loss using cellular base transmitters some distance from the buildings (similar to Walker [13]). These measurements favored the side of the building facing the transmitter. The mean attenuation of all the buildings measured was 10.8 dB at 900 MHz and 10.2 dB at 1500 MHz, while standard deviations of 5.8 dB and 5.6 dB, respectively. In similar measurements, Tanis et al. [15] reported attenuation ranging from 16 to 19 dB for 880 MHz and 1922 MHz. The measurements of Loew et al. [16] are more similar to our configuration. They measured the path loss from a street level transmitter near the building (both line-of-sight and shadowed by another structure) to various points within multistory commercial structures. These measurements showed mean attenuation of as much as 22 dB to 33 dB for 912 MHz and 1920 MHz for specific buildings. Standard deviations varied from 8.8 to 14.5 dB. In one of the few studies at the lower VHF frequencies, Rice [17] measured several structures and reported a mean penetration loss of 24.8 dB at 35 MHz with a standard deviation of 14 dB and 23 dB loss at 150 MHz with a standard deviation of 12 dB.

We see there is huge variability in the experimental setup and objectives, the definition of the reference measurement, the building properties, and the surrounding environment in the various studies of building penetration loss. However, there is a consistent message in the data, namely that there is always some attenuating effect on the radio-frequency energy caused by the building. This attenuation is usually on the order of 10 to 30 dB but in certain situations it can climb as high as 80 dB or more.

In the second type of data collection, radio transmitters were placed in four fixed sites throughout the stadium interior. Signals received at listening stations exterior to the stadium were collected before, during, and after the implosion. Our receiving sites in this case were both fixed and mobile. A receiving system mounted on a modified garden cart was pulled around the perimeter of the stadium both before and after the implosion, enabling direct comparison of signal strength as a function of azimuth angle through the standing stadium and the resulting pile of rubble. The implosion is indicated in the results by the dramatic change in the signal levels. In fact, the results show that some signals experienced large amounts of attenuation, while other signals increased during the implosion but then decreased to a final level. This is explained by the fact that the stadium collapsed around the perimeter in a 60 second sequence. Hence, portions of the structure had fallen out of the signal path for some period of time before the section directly above the transmitter cache came down and effectively blocked the signals. Measurements for the transmitters in the different sites were made before the implosion such that a pre- and post-signal strength comparison could be made. These results show that large amounts of stadium rubble caused at least 30 to 50 dB of attenuation of the signal. Thus, if someone is trapped under such a rubble pile and is trying to communicate with an emergency responder with a two-way radio or cell phone, their communication link would have to overcome 30 to 50 dB of attenuation.

It is interesting to note that the increases in signal attenuation after the collapse of the stadium were not as large as observed during the apartment building implosion (60 to 70 dB, see [5]). This can be explained by the fact the stadium had such massive amounts of concrete and steel throughout the stadium that the signal propagating through the interior of the stadium behaved similarly to the signal propagating through collapsed rubble piles.

The third set of data, referred to as "debris radiators," was collected by connecting instruments to the stadium rubble and by using a directional antenna connected to our instruments placed in proximity of metallic debris. The purpose of this experiment was to investigate the probability of detecting radio signals from transmitter(s) under the rubble that might couple onto these metal objects and radiate signals to the edges of the rubble pile. Use of debris radiators may improve reception of signals emitted from deep within a stadium in collapsed building or other weak-signal scenarios. The results show that use of the directional receive antenna in close proximity to the debris radiator generally resulted in a higher received signal level than did use of direct connection. However, at some frequencies and at some locations, direct connection to the metallic debris yielded results comparable to that of the antenna. Through experiments such as these, we are beginning to gain an understanding of what conditions make debris radiators more effective. Further tests in the field and in the laboratory have been carried out and will be discussed in subsequent publications.

The results in this report are the second in a series of reports detailing implosion experiments performed by NIST in order to better understand the first responder's radio propagation environment and to investigate new methods for weak-signal detection. The first set of implosion experiments was performed in an apartment building in New Orleans. The results of similar implosion experiments performed at the Washington D.C. Convention Center are the subject of a separate report. Besides implosion experiments, NIST has also performed radio-mapping experiments in various other large structures, including apartment and office buildings, sports

stadiums, stores, malls, hotels, a convention center, and warehouses. The results of the signal-strength measurements and statistical distribution for these radio-mapping experiments will also be published separately.

This work was sponsored by the U.S. Department of Justice and the U.S. Department of Homeland Security through the Office of Law Enforcement Standards of NIST. We thank William Moore, Mike Casbon, Jim Santora, and Jim Morgan of Brandenburg and Steven R. Pettigrew and Jeffrey S. Sizemore of Demolition Dynamics for their assistance during this experiment. Without their help, this experiment would not have been possible. We also thank members of the technical staff of the Electromagnetics Division 818, who pulled together the equipment in a short time, including Dennis Friday, Perry Wilson, and Robert Judish for managerial support.

10. References

[1] Statement of Requirements: Background on Public Safety Wireless Communications, *The SAFECOM Program,* Department of Homeland Security, Vol.1.0, March 10, 2004.

[2] M. Worrell and A. MacFarlane, Phoenix Fire Department Radio System Safety Project, Phoenix Fire Dept. Final Report, Oct. 8, 2004, http://www.ci.phoenix.az.us/FIRE/radioreport.pdf.

[3] 9/11 Commission Report, *National Commission on Terrorist Attacks Upon the United States*, 2004.

[4] Final Report for September 11, 2001 New York World Trade Center terrorist attack, *Wireless Emergency Response Team (WERT),* Oct. 2001.

[5] C.L. Holloway, G. Koepke, D. Camell, K.A. Remley, D.F. Williams, S. Schima, S. Canales, and D.T. Tamura, "Propagation and Detection of Radio Signals Before, During and After the Implosion of a Thirteen Story Apartment Building," *NIST Technical Note 1540*, Boulder, CO, May 2005.

[6] C.L. Holloway, G. Koepke, D. Camell, K.A. Remley, and D.F. Williams, "Radio Propagation Measurements During a Building Collapse: Applications for First Responders," *Proc. Intl. Symp. Advanced Radio Tech.*, Boulder, CO, March 2005, pp. 61-63.

[7] APCO International, APCO Project 25 Standards for Public Safety Digital Radio, Aug. 1995, http://www.apcointl.org/frequency/project25/information.html#documents.

[8] Rubinstein, T.N., "Clutter losses and environmental noise characteristics associated with various LULC categories," *IEEE Trans. Broadcasting*, 44(3): 286-293; Sept. 1998.

[9] D.M.J. Devasirvatham, C. Banerjee, R.R. Murray, and D.A. Rappaport, "Four-frequency radiowave propagation measurements of the indoor environment in a large metropolitan commercial building," *Proc. GLOBECOM 1991*, Phoenix, AZ, 2-5 Dec. 1991, pp. 1282-1286.

[10] D. Molkdar, "Review on radio propagation into and within building," *IEE Proceeding-H,* 38(1): 61-73; Feb. 1991.

[11] K.M. Ju, C.C. Chiang, H.S. Liaw, S.L. Her, "Radio propagation in office building at 1.8 GHz," *Proc. 7th IEEE Intl. Symp. on Personal, Indoor and Mobile Radio Communications*, Taipei, 15-18 Oct., 1996, pp. 766-770.

[12] J.H. Tarng and D.W. Perng, "Modeling and measurement of UHF radio propagating through floors in a multifloored building," *Proc. IEE, Microwave Antennas Propagat.*, 144(5): 359-363; Oct. 1997.

[13] E. Walker, "Penetration of radio signals into building in the cellular radio environment," *Bell Syst. Tech. J.,* 62(9), Nov. 1983.

[14] A. Davidson and C. Hill, "Measurement of building penetration into medium buildings at 900 and 1500 MHz," *IEEE Trans. Veh. Technol.*, 46(1): 161-168; Feb. 1997.

[15] W.J. Tanis and G.J. Pilato, "Building penetration characteristics of 880 MHz and 1922 MHz radio waves," *Proc. 43th IEEE Veh. Technol. Conf.,* Secaucus, NJ, 18-20 May 1993, pp. 206-209.

[16] L.H. Loew, Y. Lo, M.G. Lafin, and E.E. Pol, "Building penetration measurements from low-height base stations at 912, 1920, and 5990 MHz," *NTIA Report 95-325,* National Telecommunications and Information Administration, Sept. 1995.

[17] L.P. Rice, "Radio transmission into buildings at 35 and 150 mc," Bell Syst. Tech. J., pp. 197-210, Jan. 1959.

Figure 1. Veterans' Stadium.

Figure 2. Pre-implosion deconstruction of the stadium.

Figure 3. Pre-implosion preparation inside the stadium.

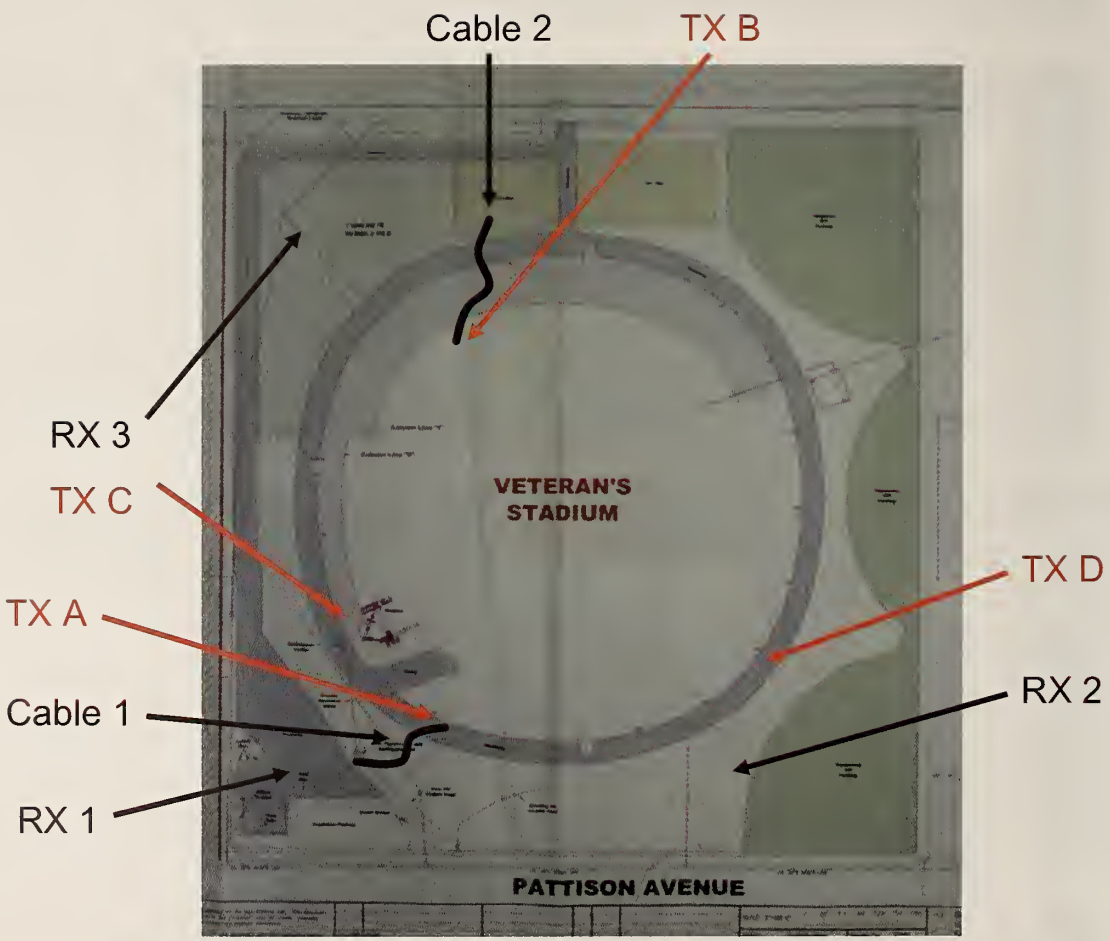

Figure 4. Stadium overview. TX refers to the transmitter locations and RX refers to the receiver locations during the implosion. The cable locations for the debris radiator tests are also noted on the drawing.

Figure 5. Typical transmitters used for the lower four frequency bands.

Figure 6. Transmitters used for the two higher frequency bands.

Figure 7. Transmitter in the NIST Boulder anechoic chamber.

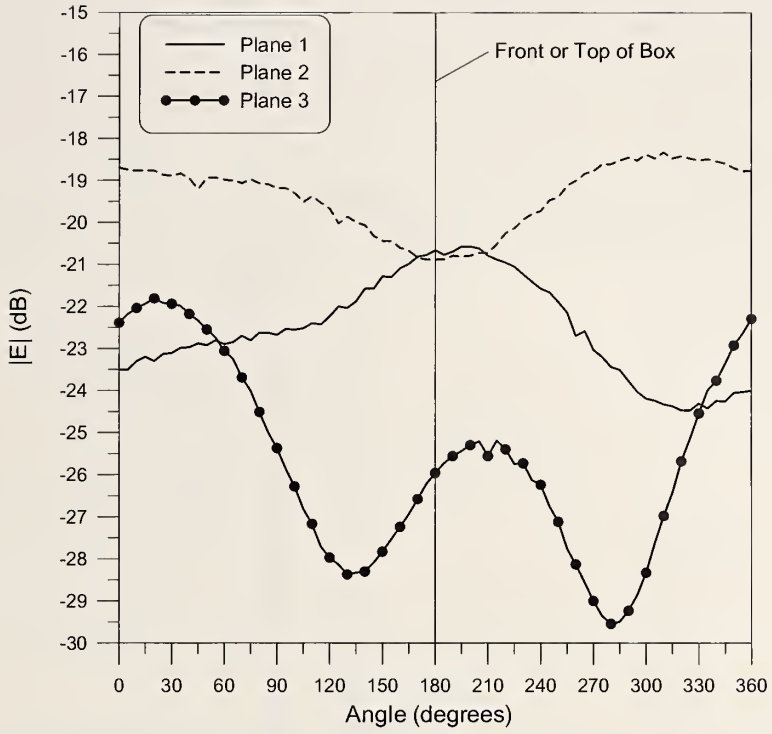

Figure 8. Radiation pattern of a 164 MHz transmitter in a protective case.

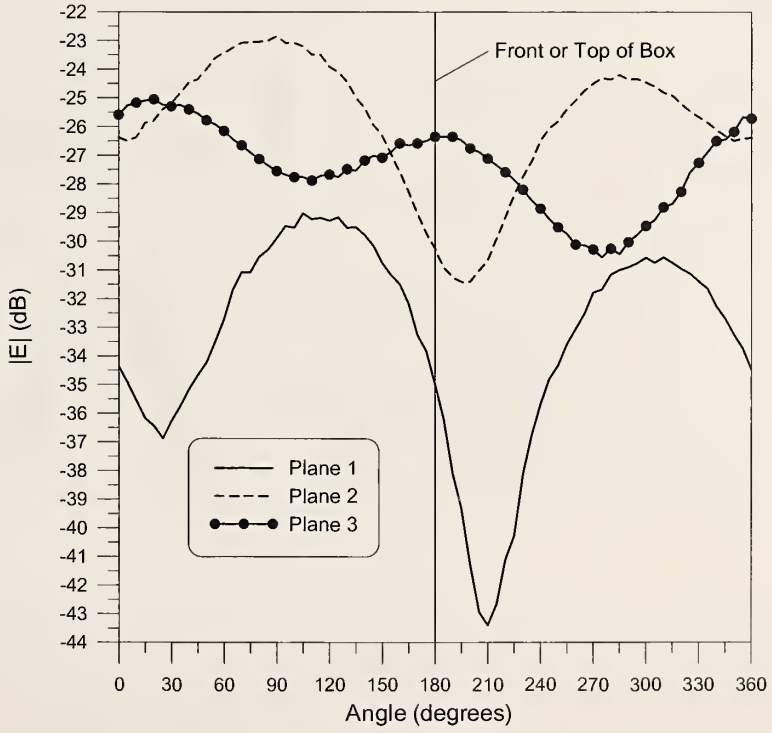

Figure 9. Radiation pattern of a 225 MHz transmitter in a protective case.

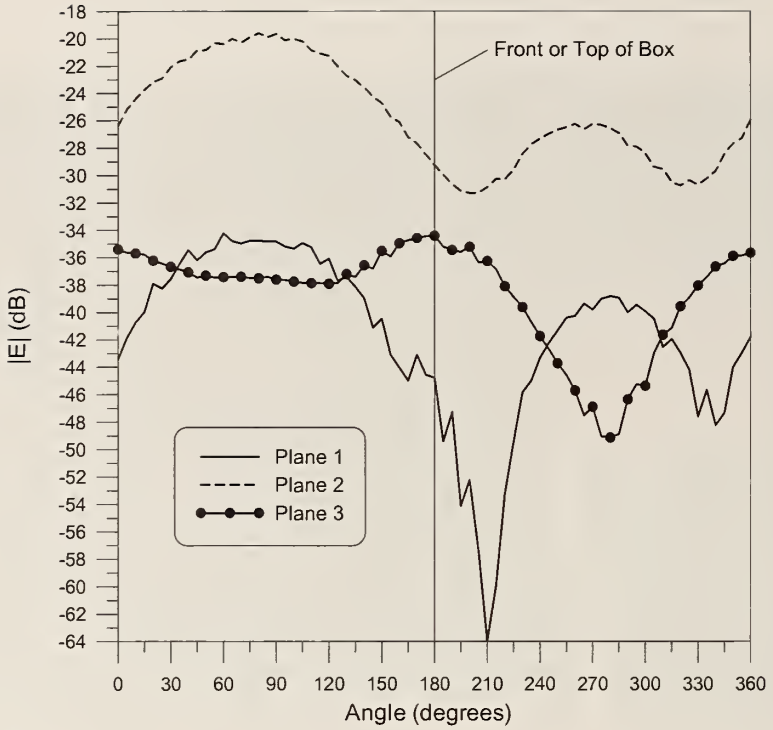

Figure 10. Radiation pattern of a 448 MHz transmitter in a protective case.

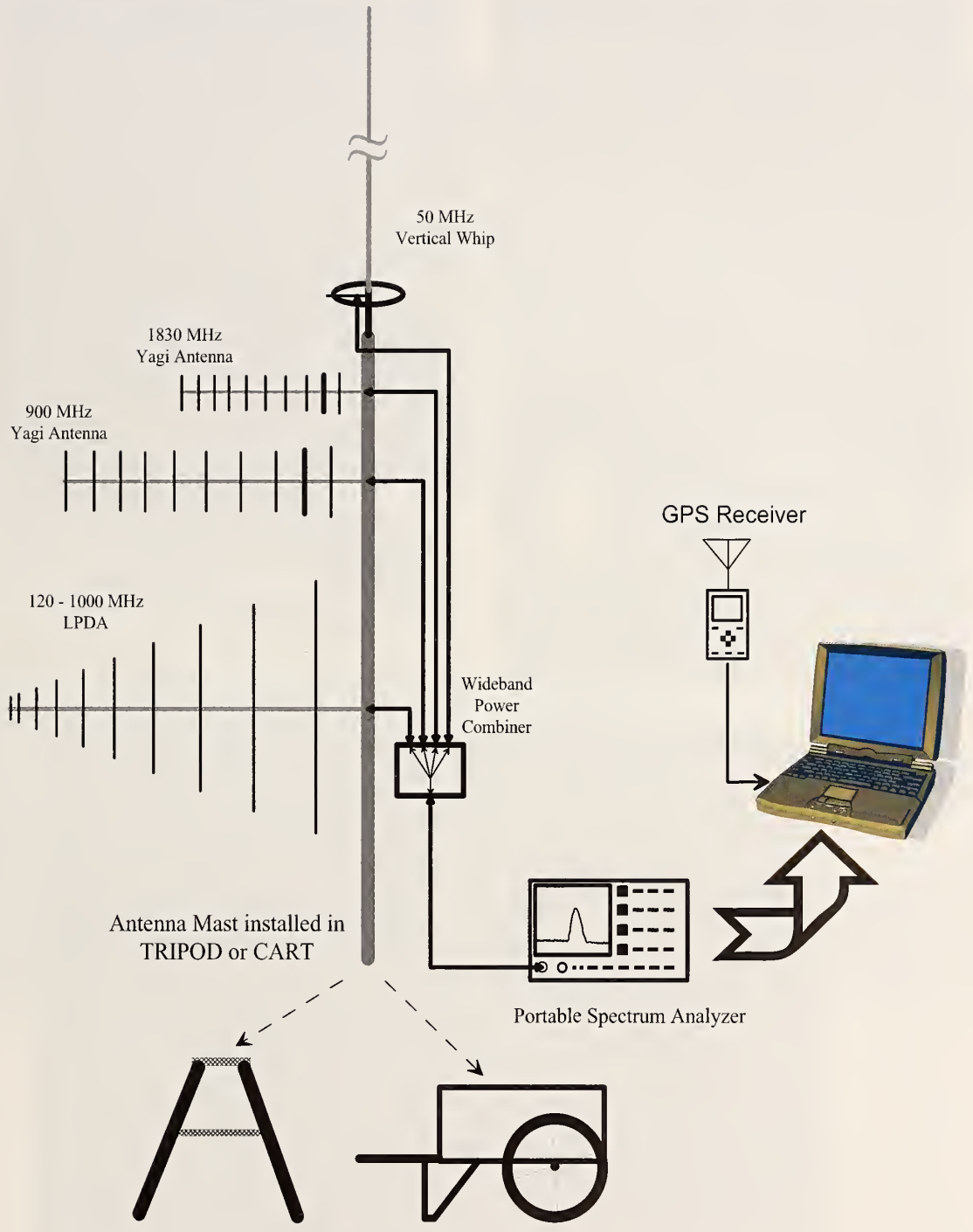

Figure 11. Schematic of the receiving system for the building penetration and field-mapping experiments.

Figure 12. Photos of the weather-resistant antenna system mounted on a tripod and mounted to the mobile cart. The receiving instruments are protected inside the container in the tripod system and under the plastic in the cart system.

Figure 13. Receiving site on the south perimeter of the stadium.

Figure 14. Carrying and driving transmitters through the stadium.

Figure 15. Fixed transmitter location TX A on south-side of sub-level.

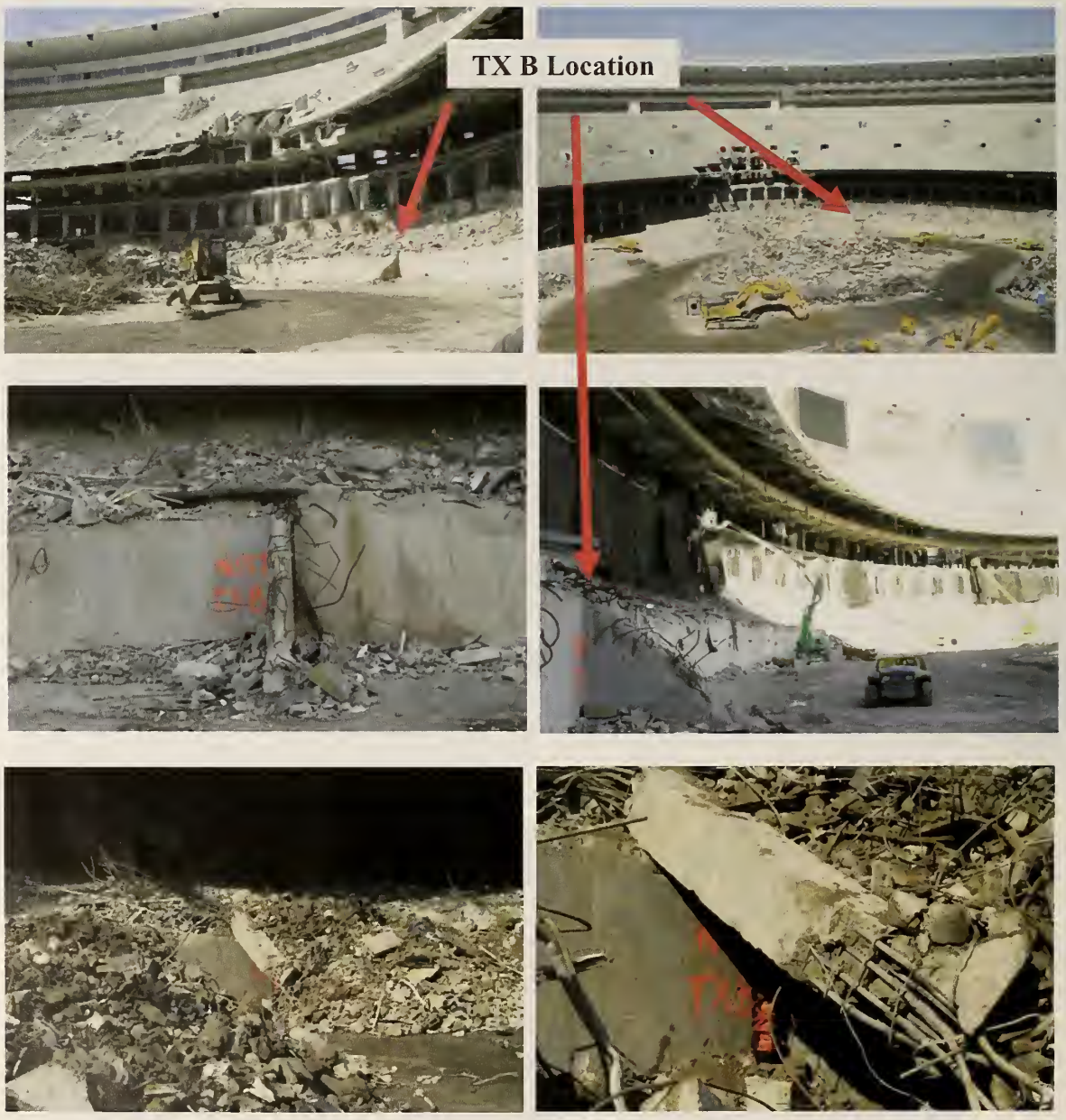

Figure 16. Fixed transmitter location TX B on the playing field.

.

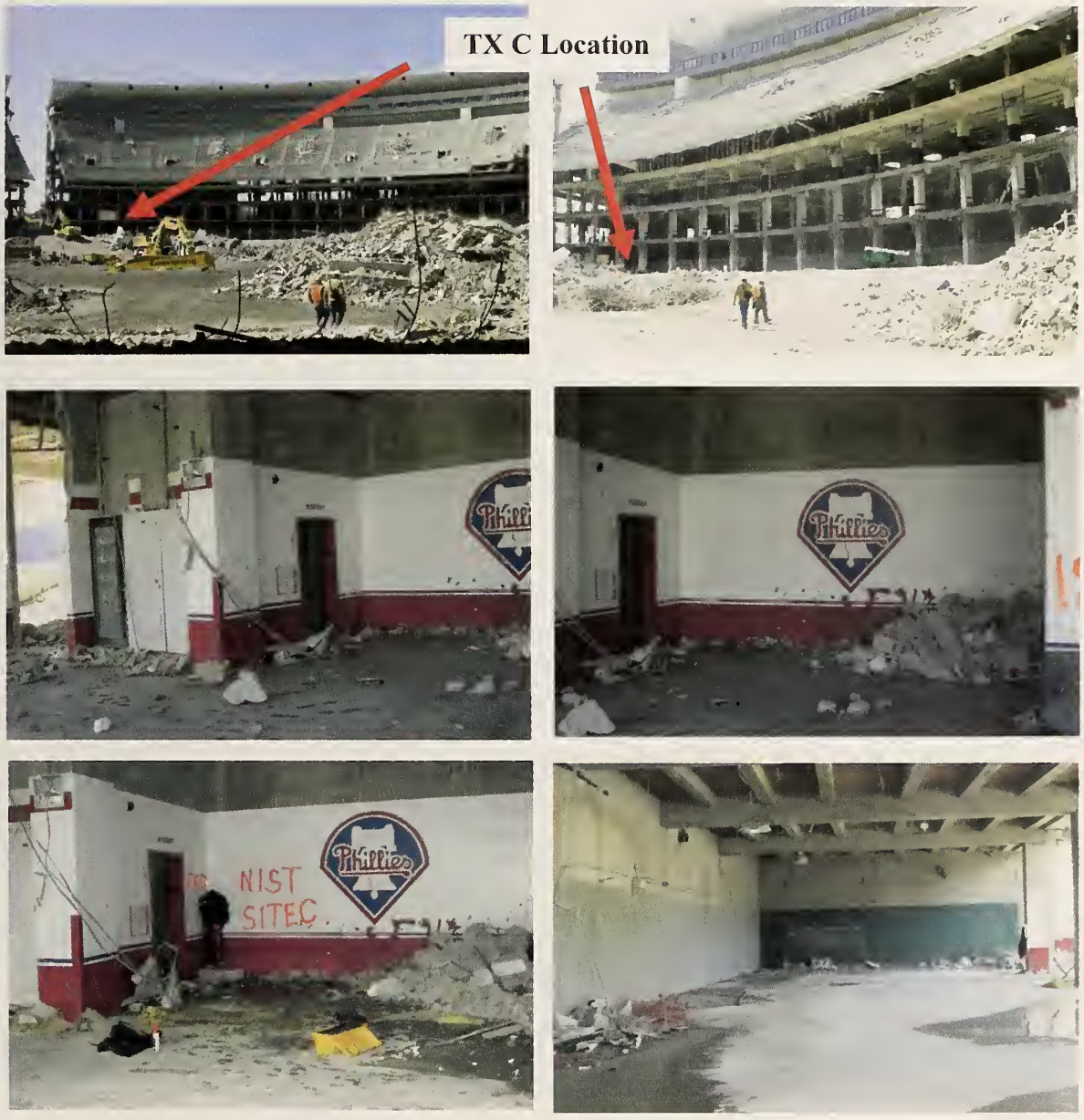

Figure 17. Fixed transmitter location TX C on west side of sub-level.

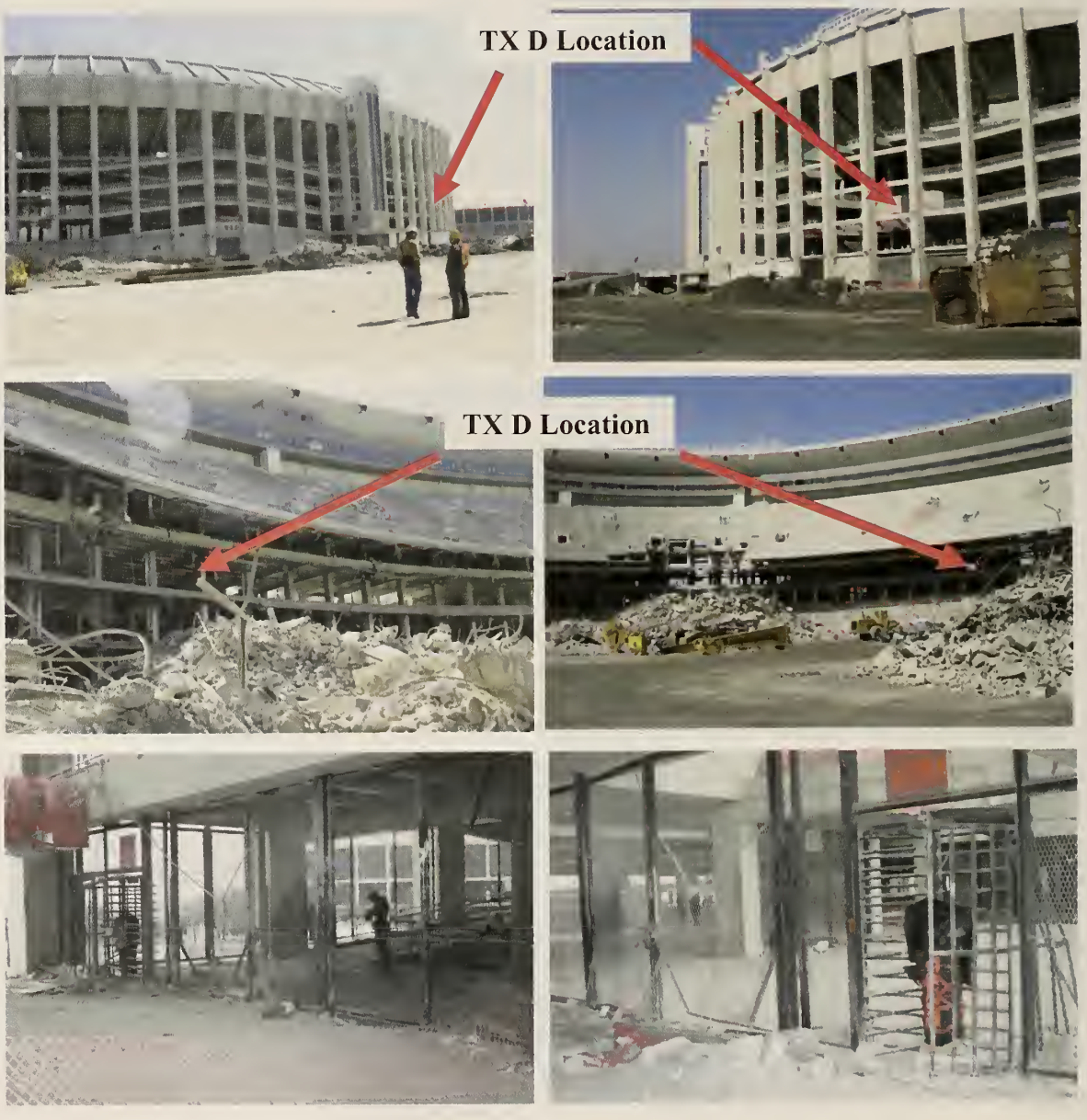

Figure 18. Fixed transmitter location TX D on the third level.

(a) (b)

(c) (d)

Figure 19. Final installation of transmitters with protective blast cloth; (a) south wall: TX A location, (b) playing field: TX B location, (c) west wall: TX C location, and (d) third level in turnstyle: TX D location.

(a)

Figure 20(a). Fixed receiving site RX 1: south-west site (unstaffed site, 53 m away).

(b)

Figure 20(b). Fixed receiving site RX 2: south-east site (unstaffed, 37 m away).

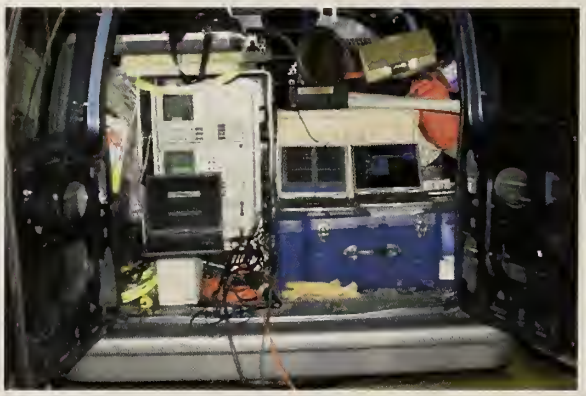

(c)

Figure 20(c). Fixed receiving site RX 3: north-west site (unstaffed, 53 m away).

Figure 21. Mobile measurement cart.

Figure 22. Cable on north side of stadium. This cable was run from the transmitter site on the playing field (TX B).

Figure 23. Cable on south side of stadium. This cable was run from the transmitter site at the south wall (TX A).

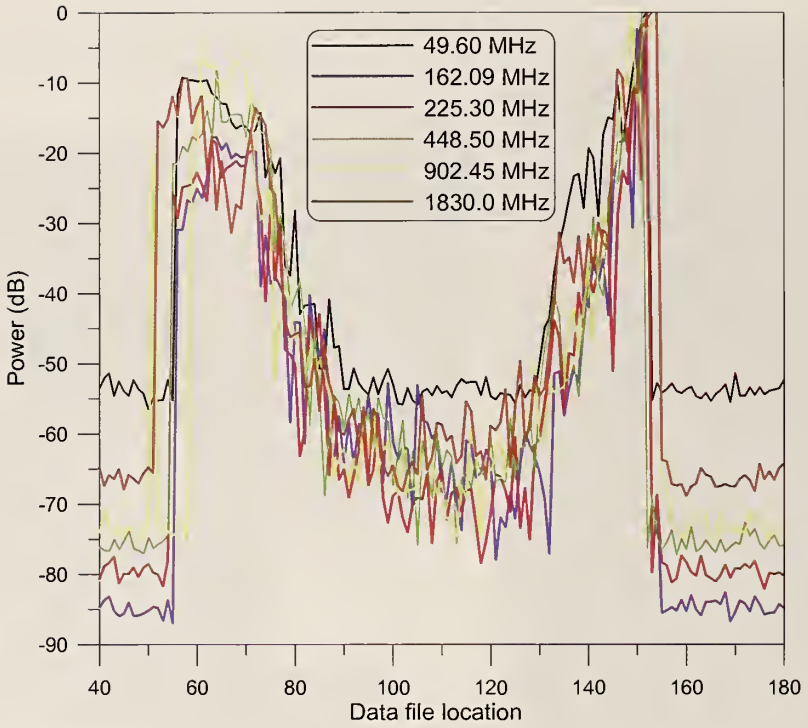

Figure 24. Stadium perimeter walk around for vertically polarized receiving antennas.

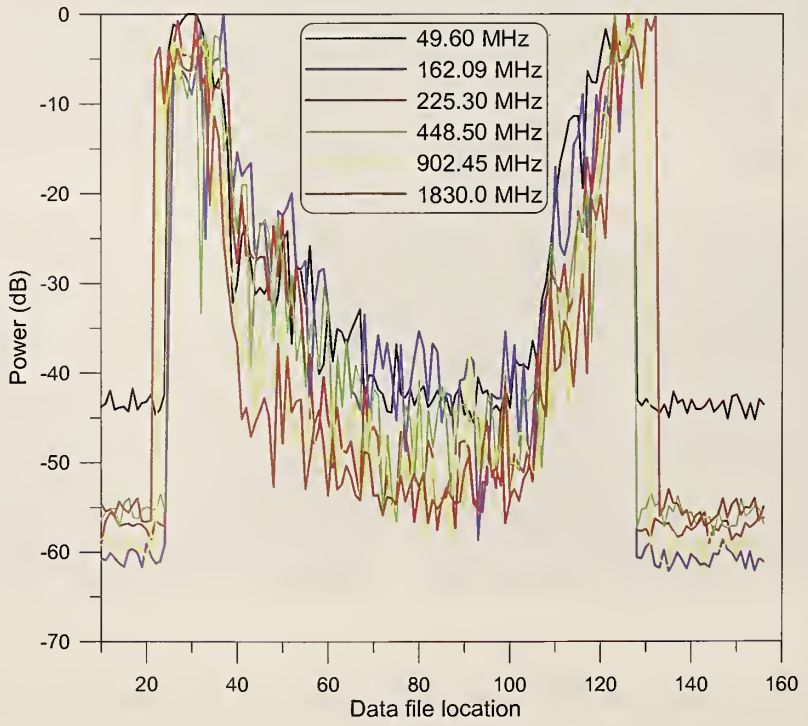

Figure 25. Stadium perimeter walk around for horizontally polarized receiving antennas.

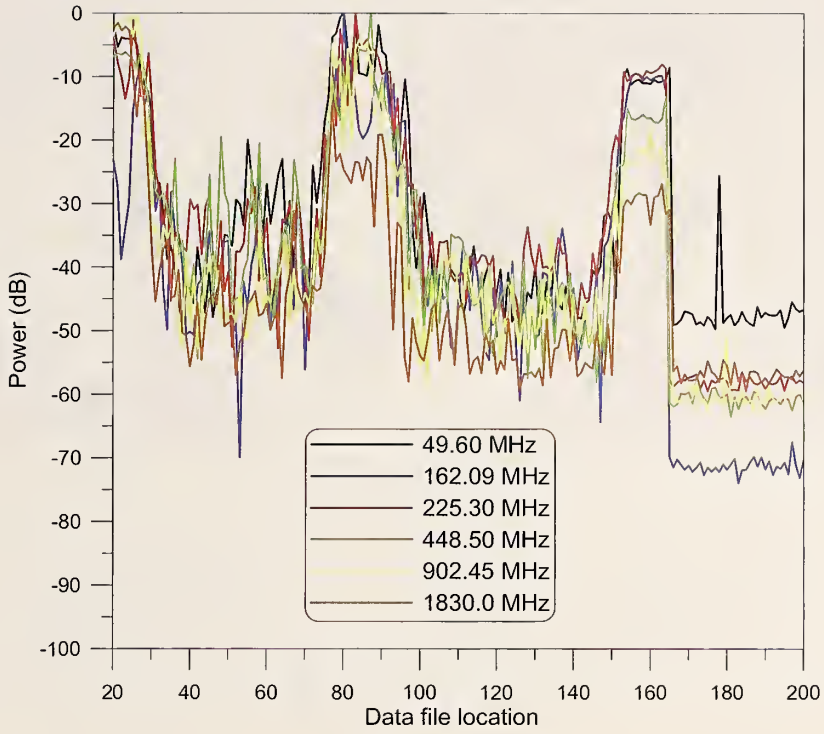

Figure 26. Stadium walk-through for horizontally polarized receiving antennas.

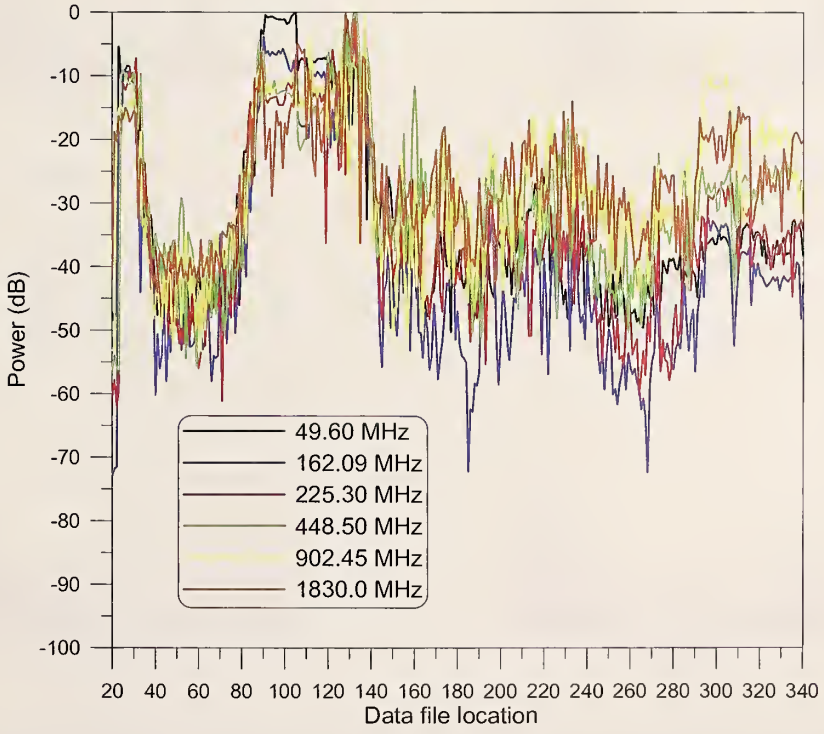

Figure 27. Stadium walk-through for vertically polarized receiving antennas.

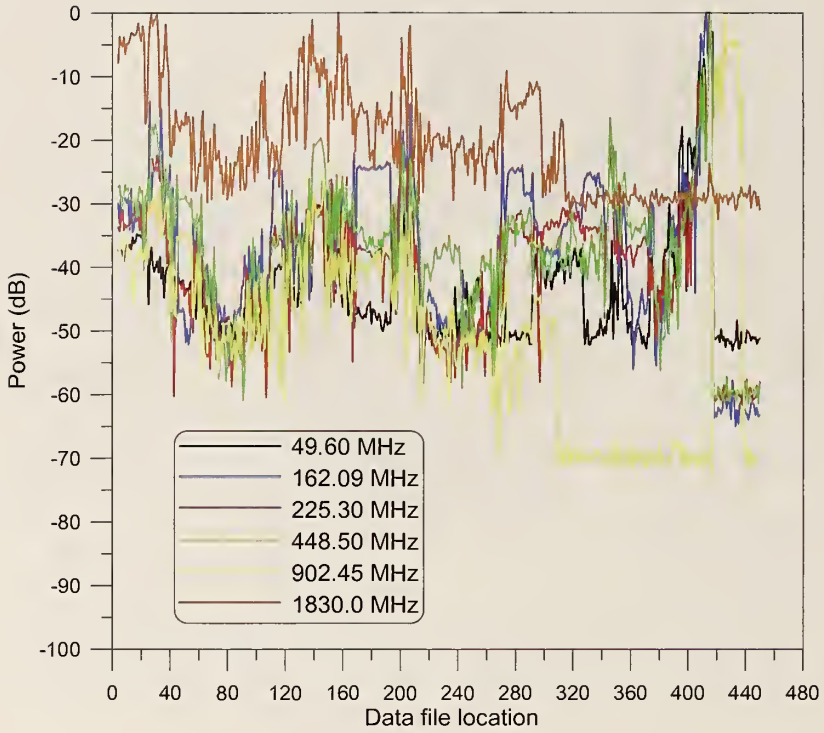

Figure 28. Stadium walk-through for horizontally polarized receiving antennas (playing field).

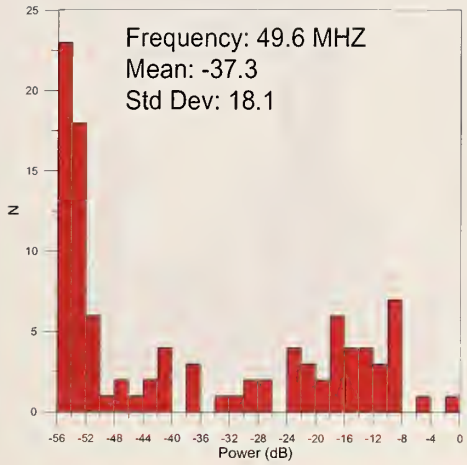

(a)

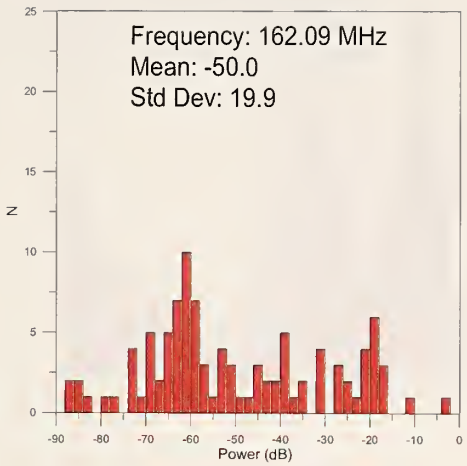

(b)

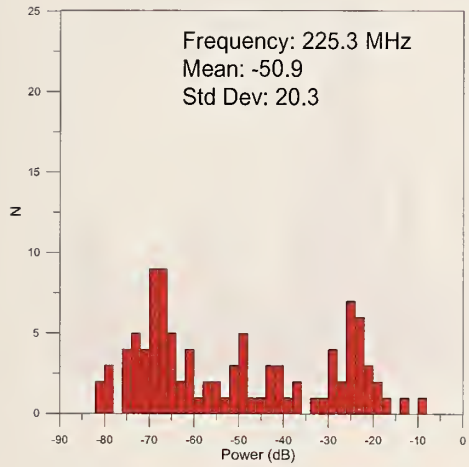

(c)

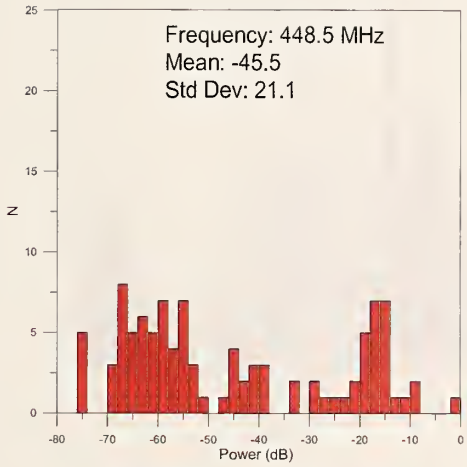

(d)

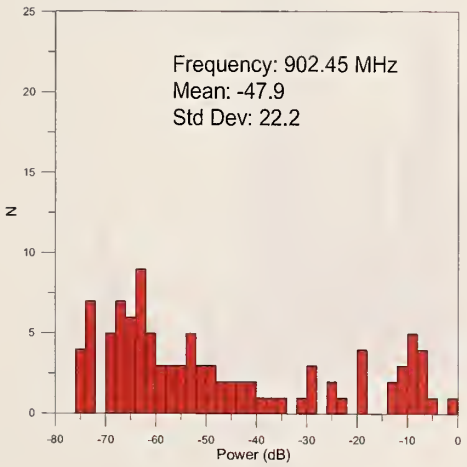

(e)

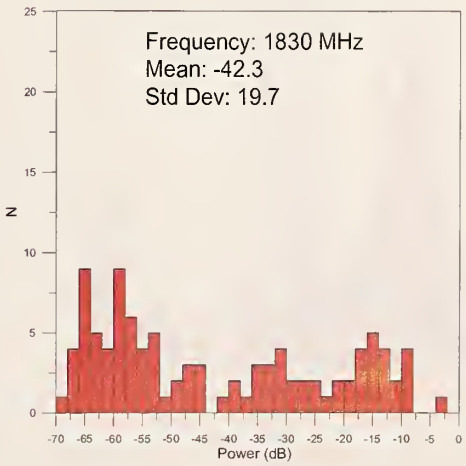

(f)

Figure 29. Histograms for the perimeter measurements for vertically polarized receiving antennas.

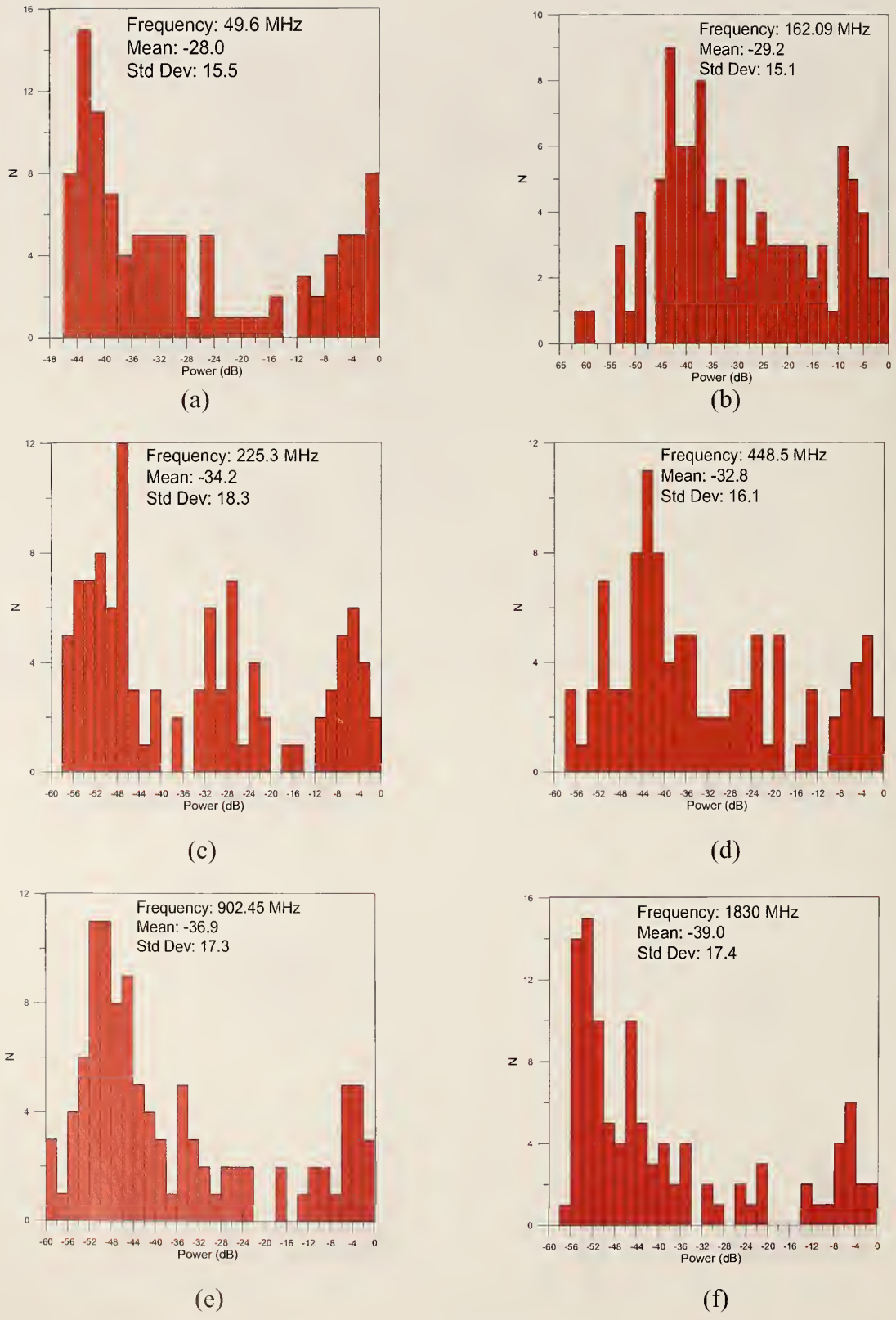

Figure 30. Histograms for the perimeter measurements for horizontally polarized receiving antennas.

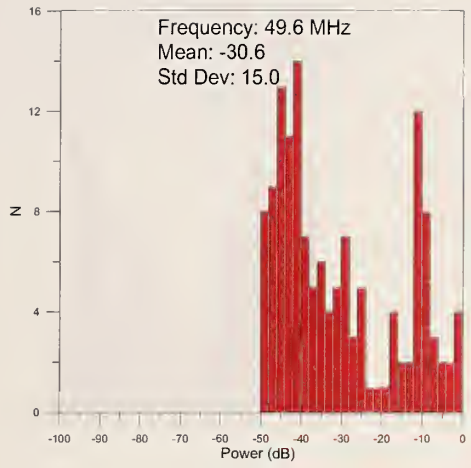

(a)

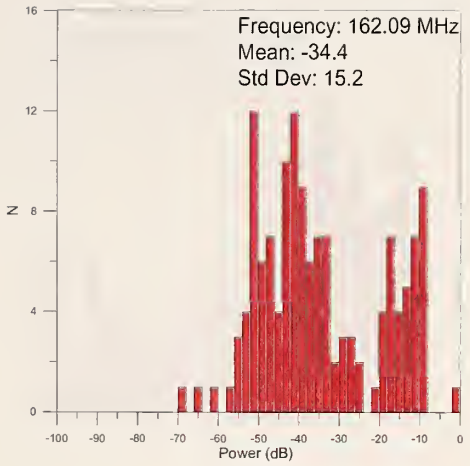

(b)

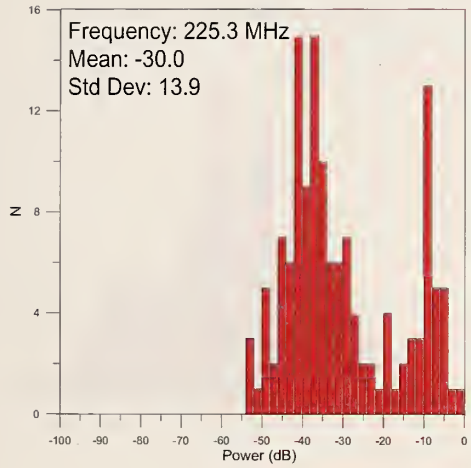

(c)

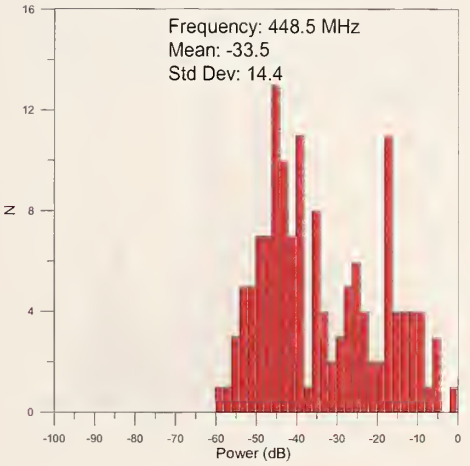

(d)

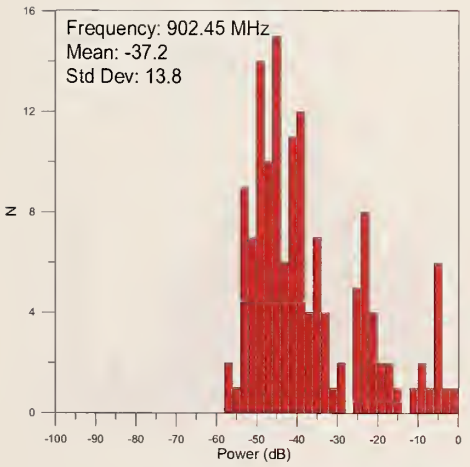

(e)

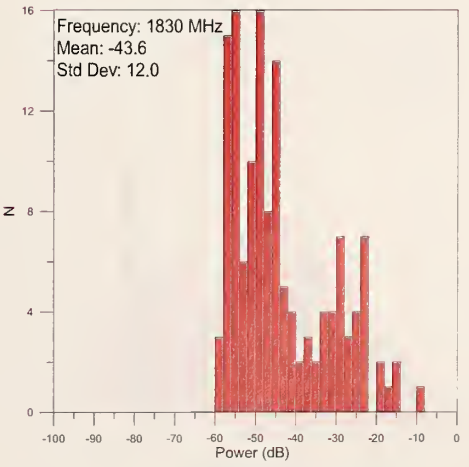

(f)

Figure 31. Histograms for the upper level measurements for horizontally polarized receiving antennas.

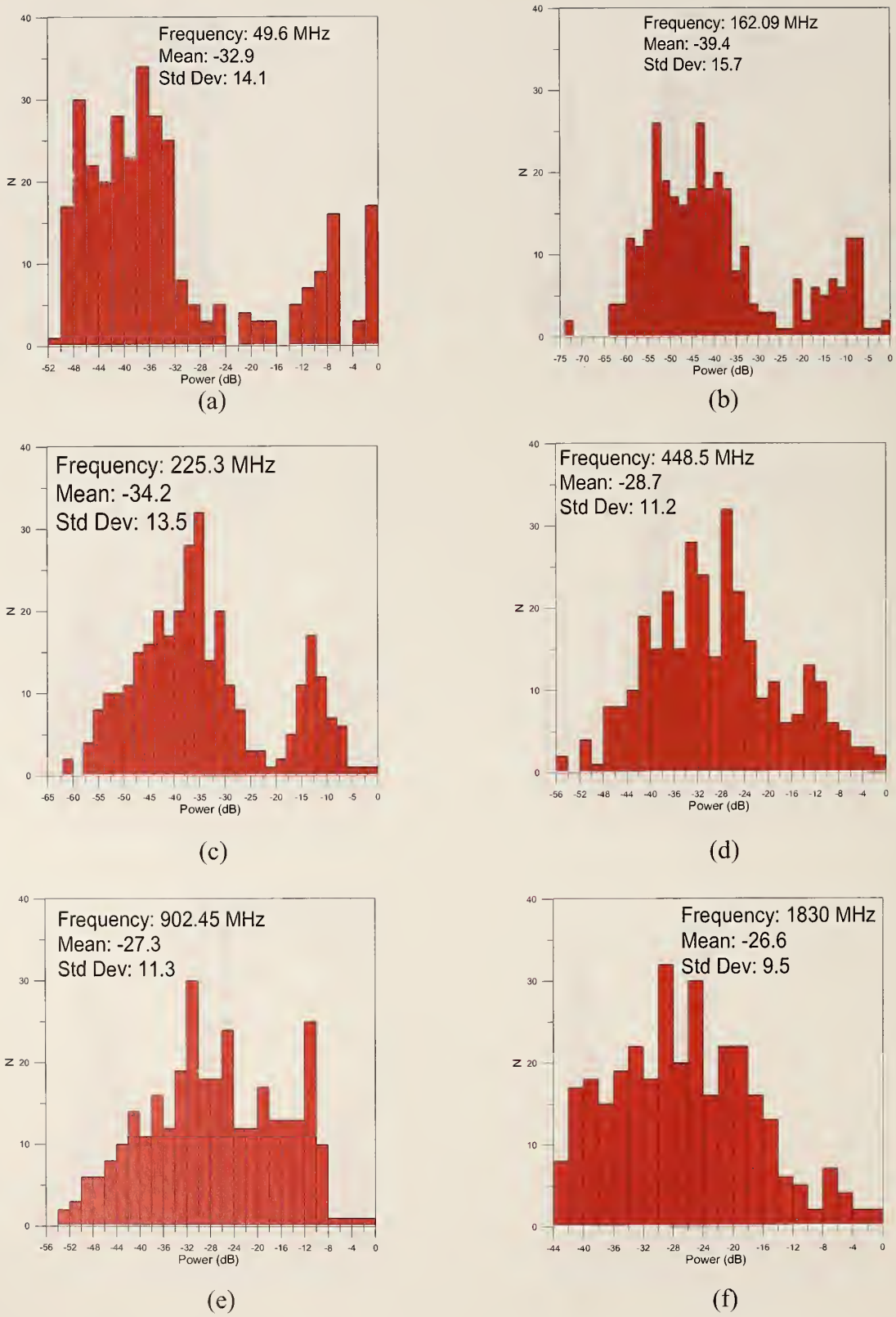

Figure 32. Histograms for data collected throughout the upper levels of the stadium to the play field for vertically polarized receiving antennas.

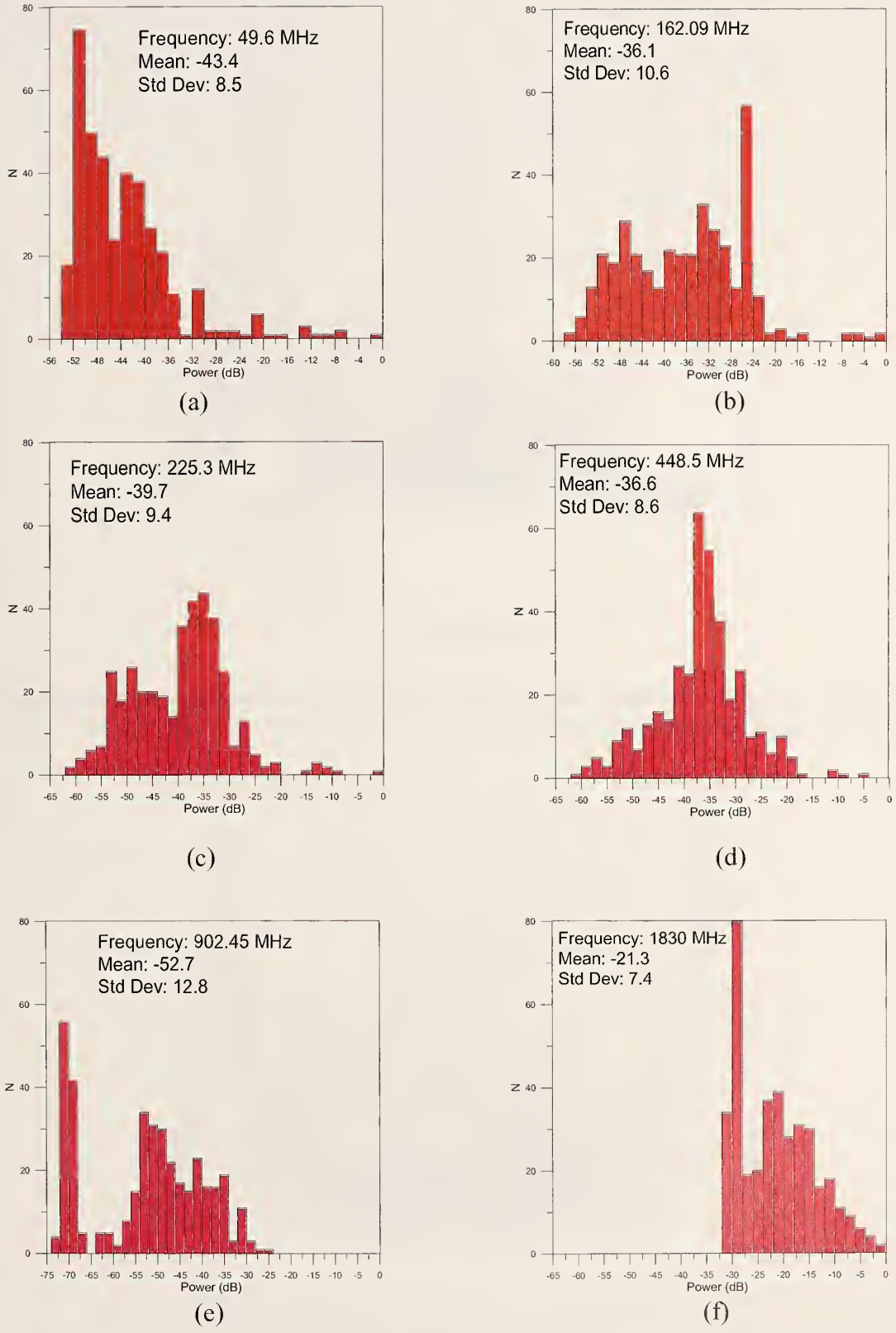

Figure 33. Histograms for data collected for the lower levels and the play field for horizontally polarized receiving antennas.

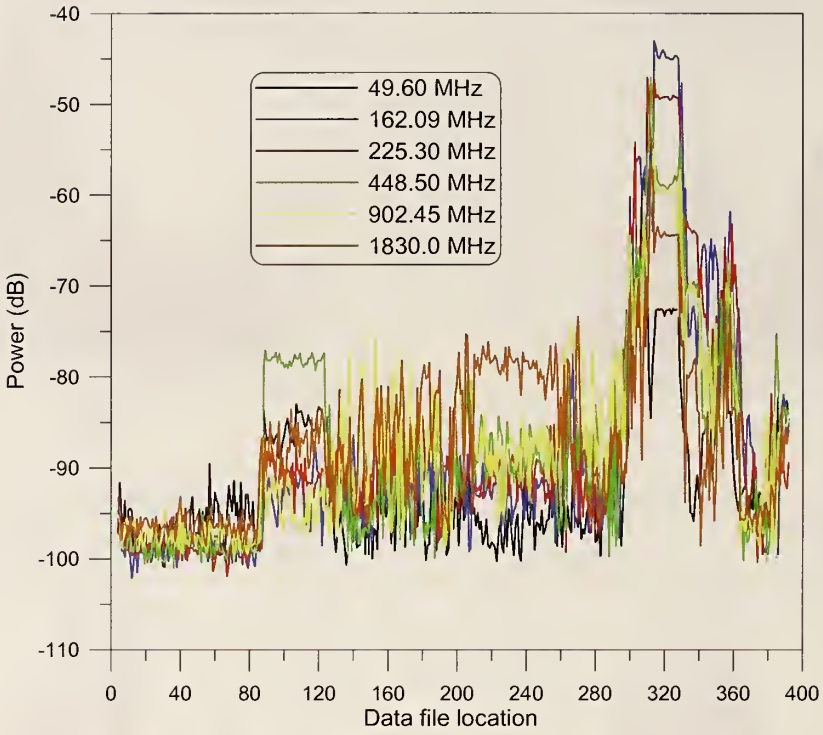

Figure 34. Signal strength measurements around the perimeter of the stadium for the transmitters located at fixed Site A and vertically polarized receiving antennas.

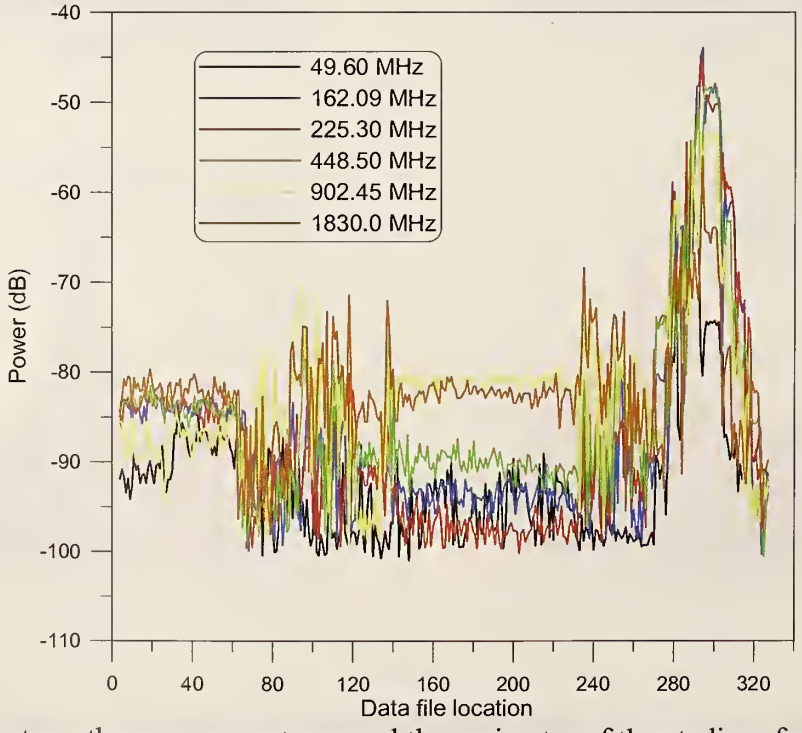

Figure 35. Signal strength measurements around the perimeter of the stadium for the transmitters located at fixed Site A and horizontally polarized receiving antennas.

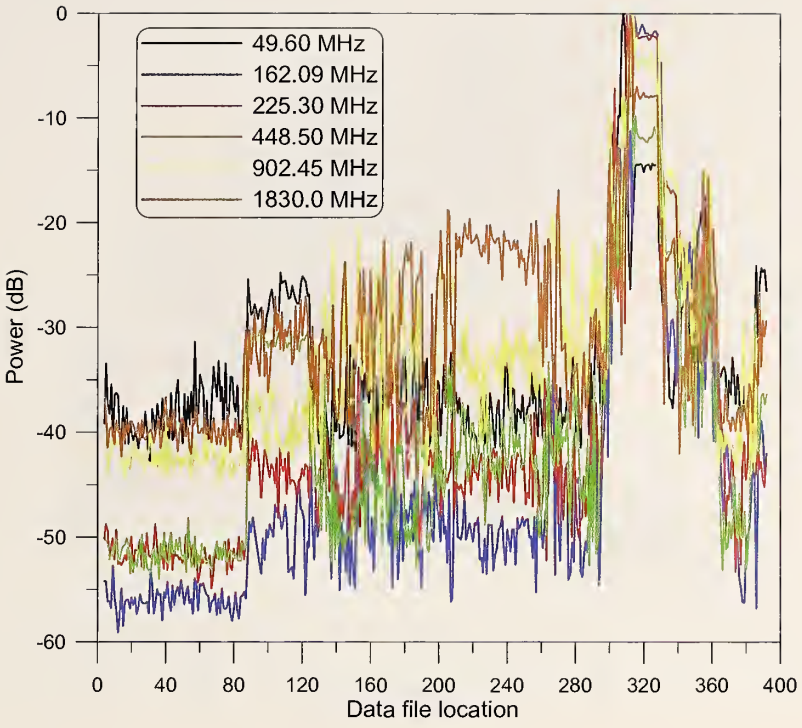

Figure 36. Normalized signal strength for the perimeter measurements of the stadium for the transmitters located at fixed Site A and vertically polarized receiving antennas.

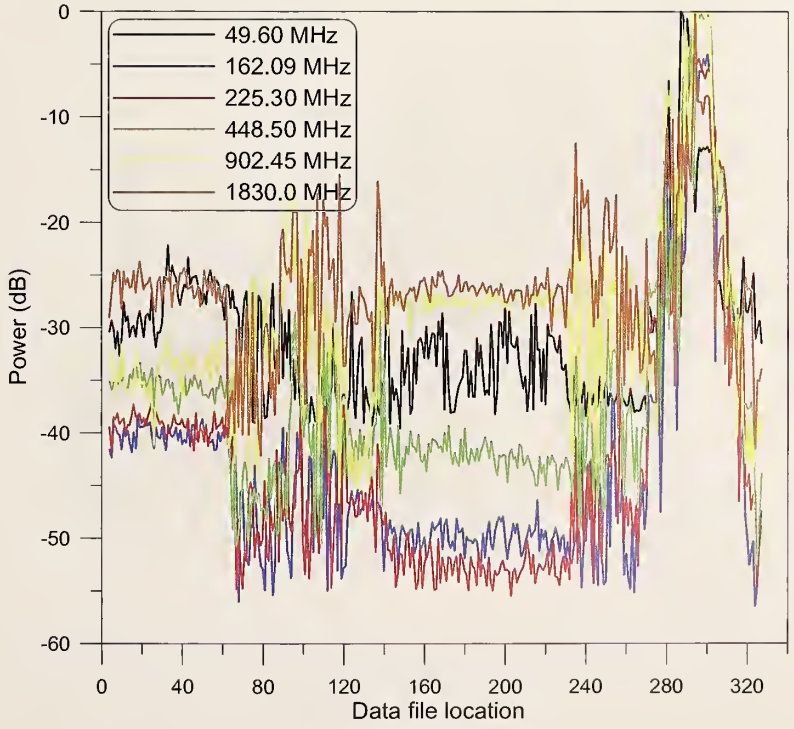

Figure 37. Normalized signal strength for the perimeter measurements of the stadium for the transmitters located at fixed Site A and horizontally polarized receiving antennas.

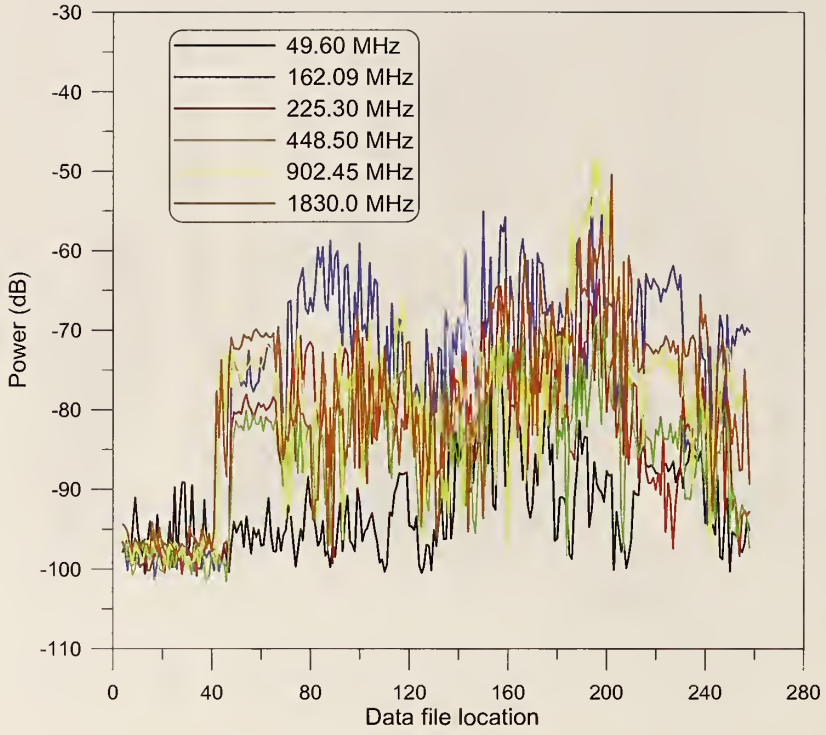

Figure 38. Signal strength measurements around the perimeter of the stadium for the transmitters located at fixed Site B and vertically polarized receiving antennas.

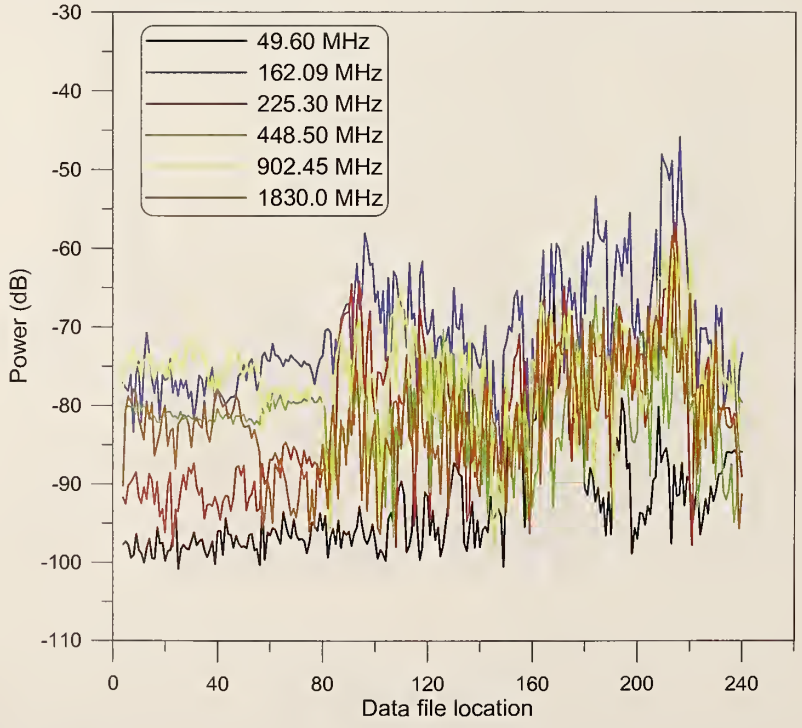

Figure 39. Signal strength measurements around the perimeter of the stadium for the transmitters located at fixed Site B and horizontally polarized receiving antennas.

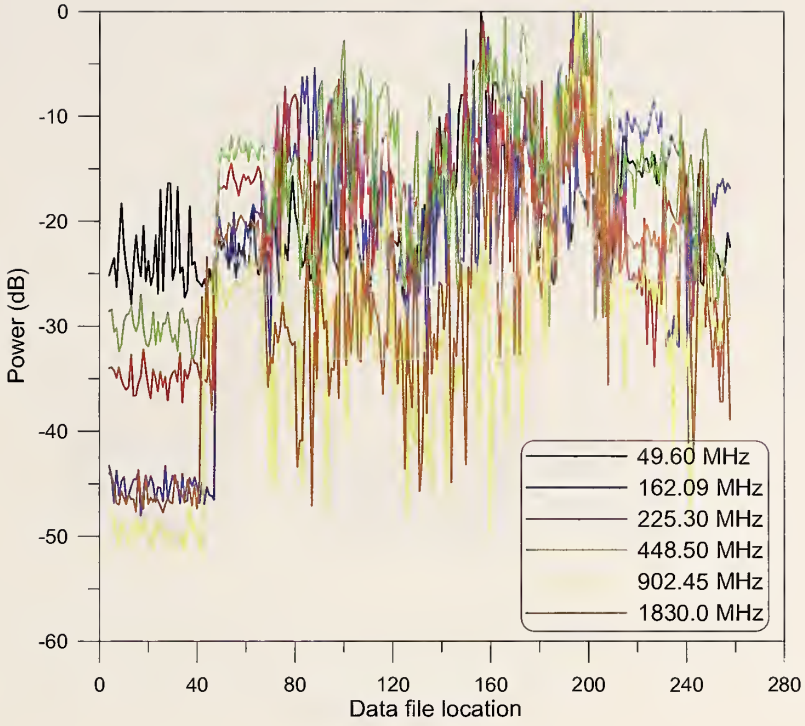

Figure 40. Normalized signal strength for the perimeter measurements of the stadium for the transmitters located at fixed Site B and vertically polarized receiving antennas.

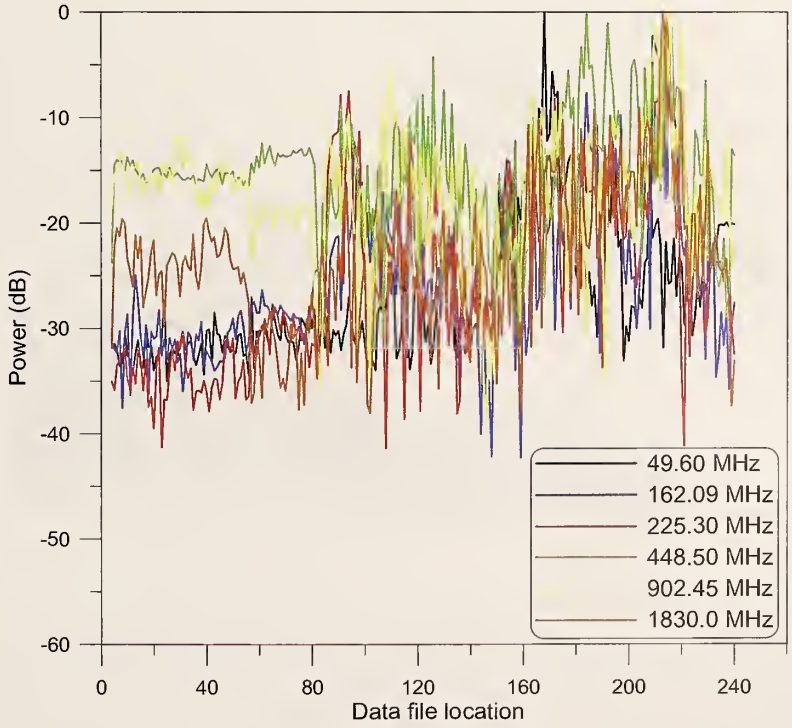

Figure 41. Normalized signal strength for the perimeter measurements of the stadium for the transmitters located at fixed Site B and horizontally polarized receiving antennas.

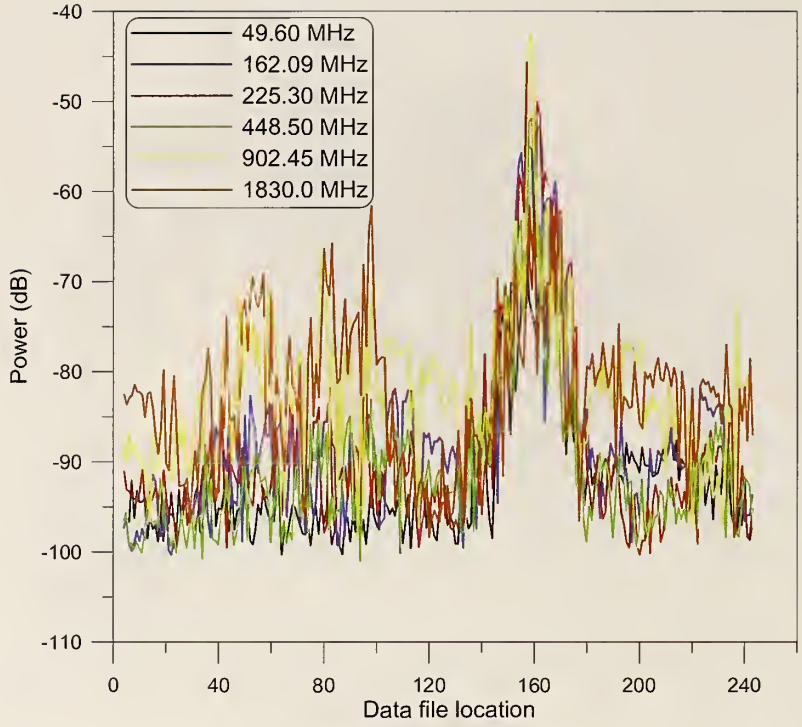

Figure 42. Signal strength measurements around the perimeter of the stadium for the transmitters located at fixed Site C and vertically polarized receiving antennas.

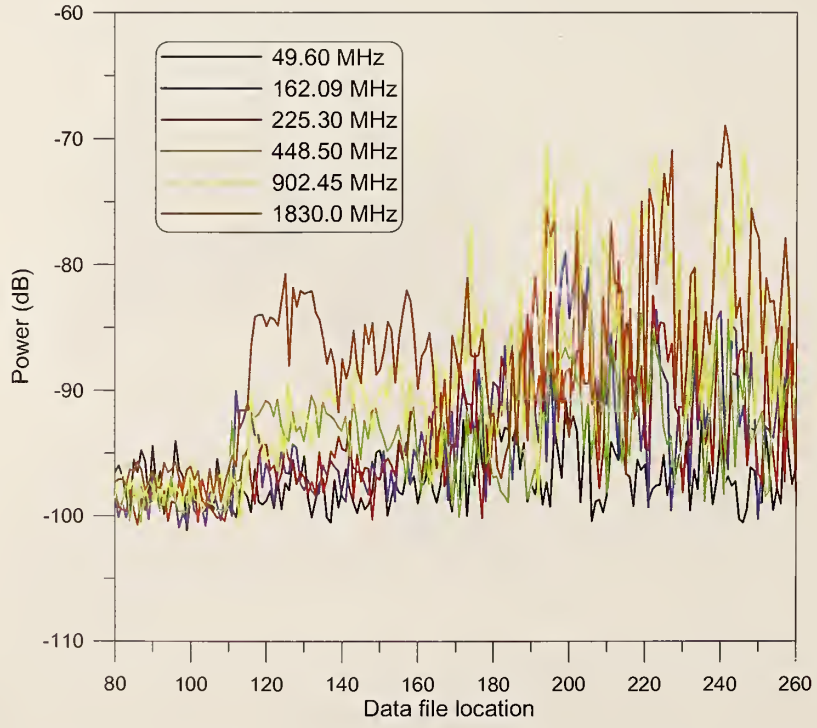

Figure 43. Signal strength measurements around the perimeter of the stadium for the transmitters located at fixed Site C and horizontally polarized receiving antennas.

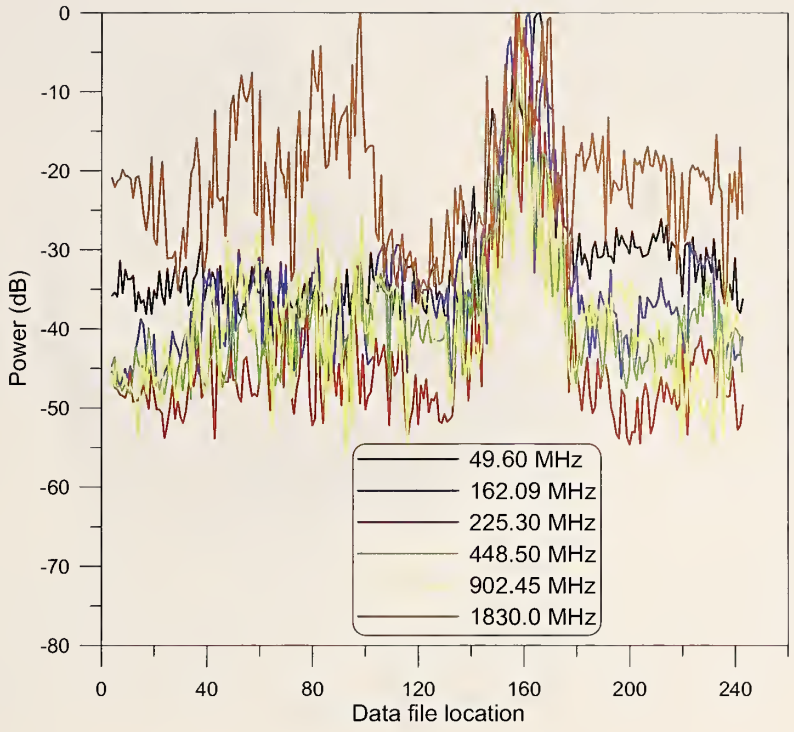

Figure 44. Normalized signal strength for the perimeter measurements of the stadium for the transmitters located at fixed Site C and vertically polarized receiving antennas.

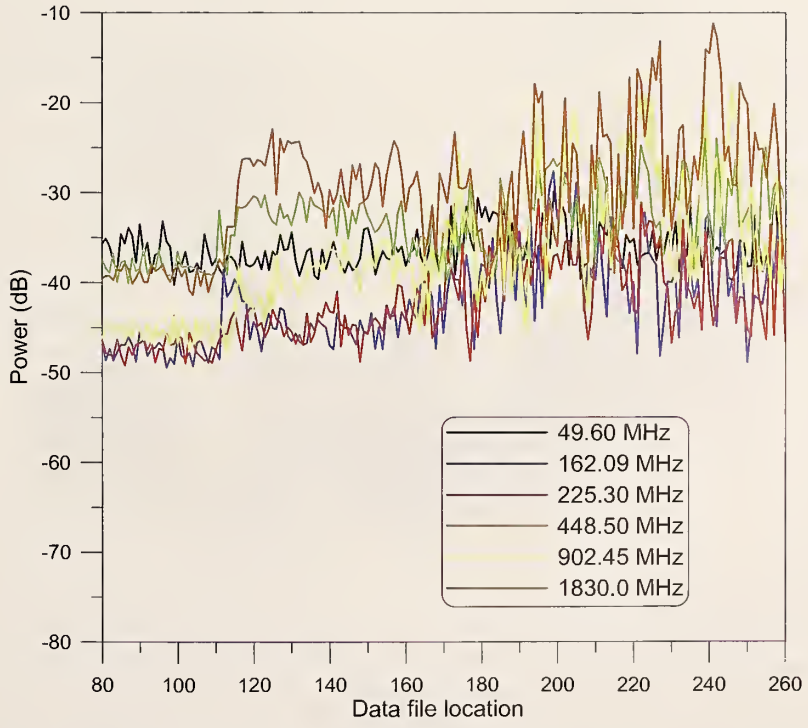

Figure 45. Normalized signal strength for the perimeter measurements of the stadium for the transmitters located at fixed Site C and horizontally polarized receiving antennas.

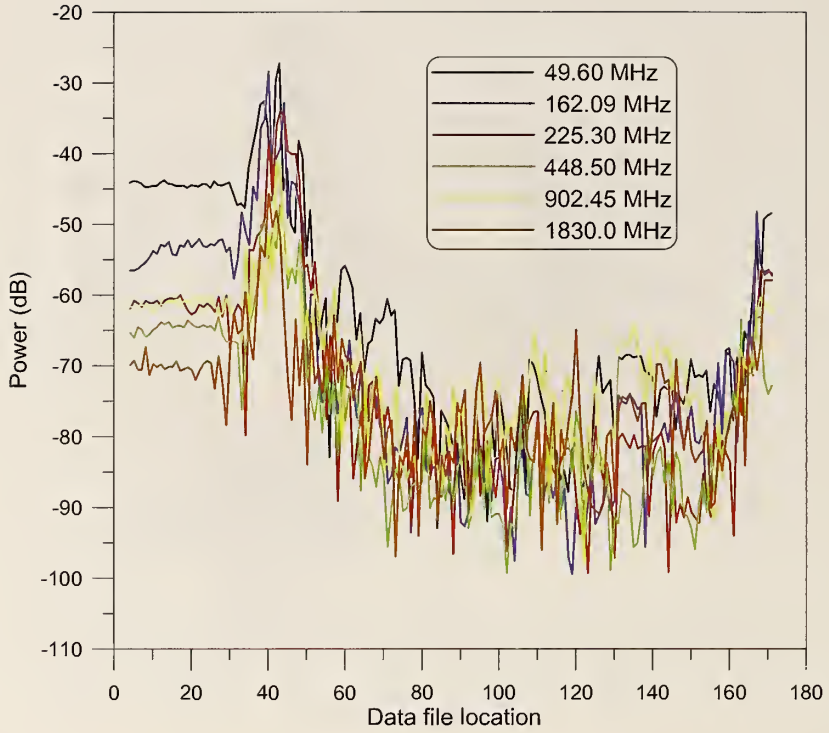

Figure 46. Signal strength measurements around the perimeter of the stadium for the transmitters located at fixed Site D and vertically polarized receiving antennas.

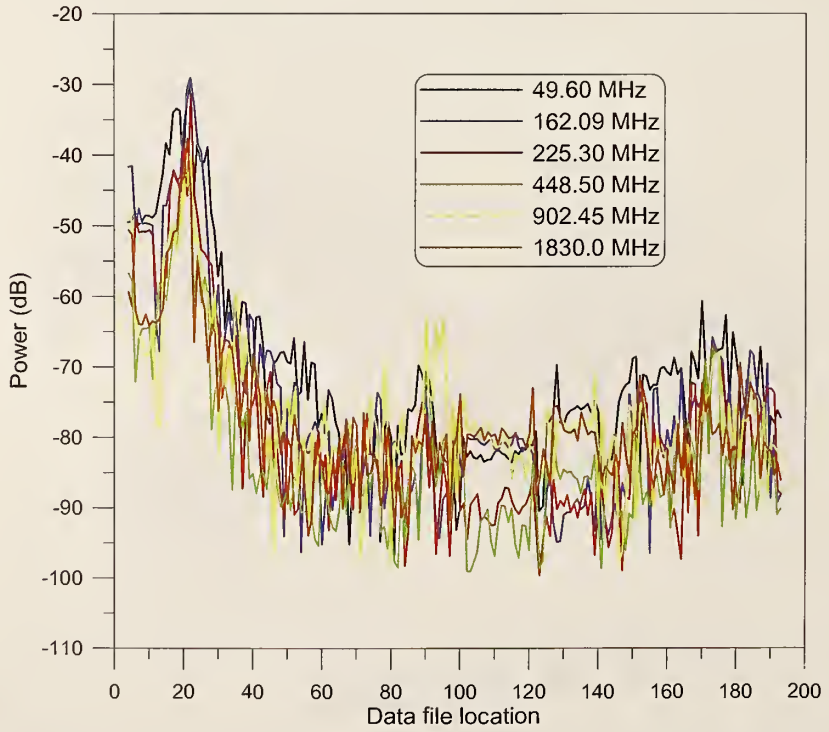

Figure 47. Signal strength measurements around the perimeter of the stadium for the transmitters located at fixed Site D and horizontally polarized receiving antennas.

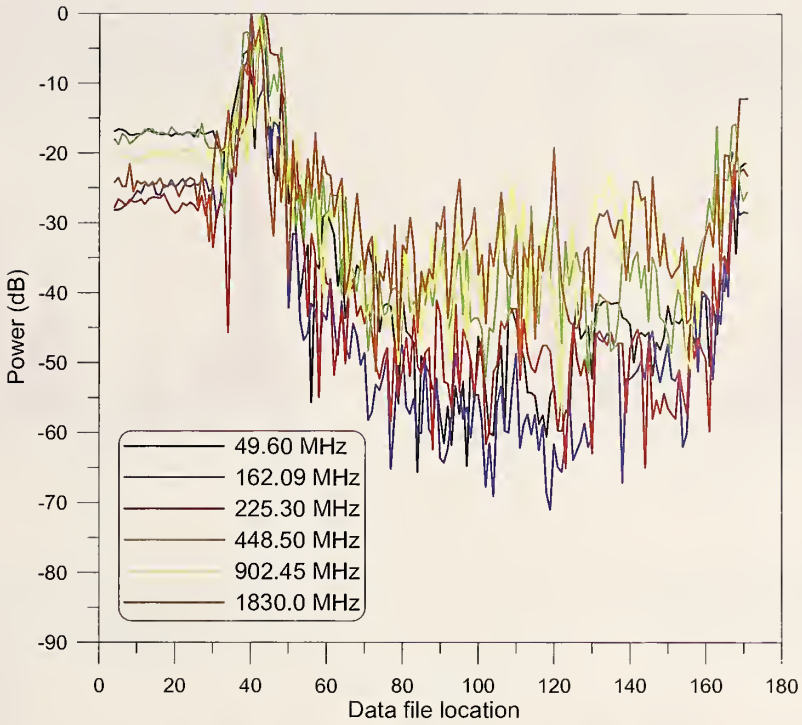

Figure 48. Normalized signal strength for the perimeter measurements of the stadium for the transmitters located at fixed Site D and vertically polarized receiving antennas.

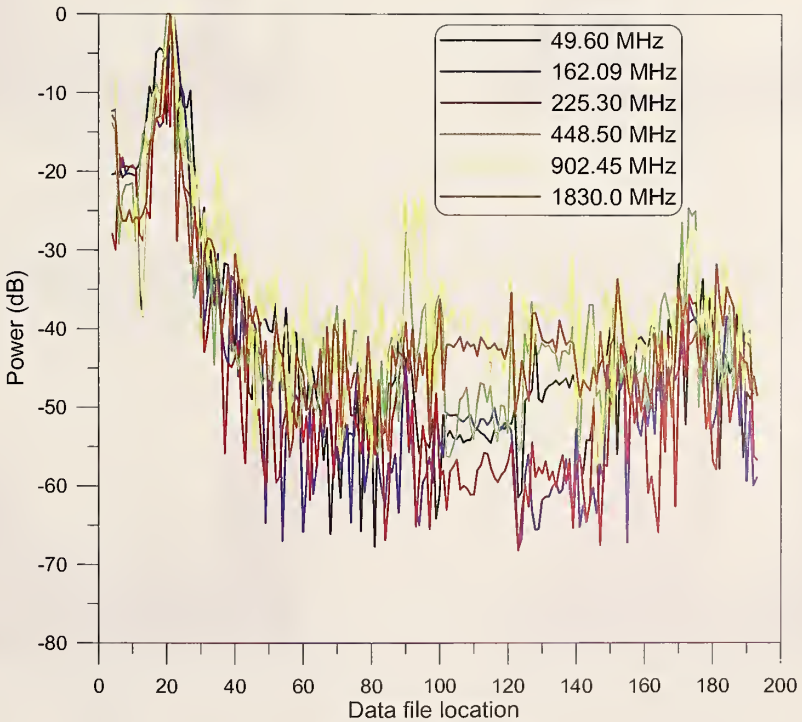

Figure 49. Normalized signal strength for the perimeter measurements of the stadium for the transmitters located at fixed Site D and horizontally polarized receiving antennas.

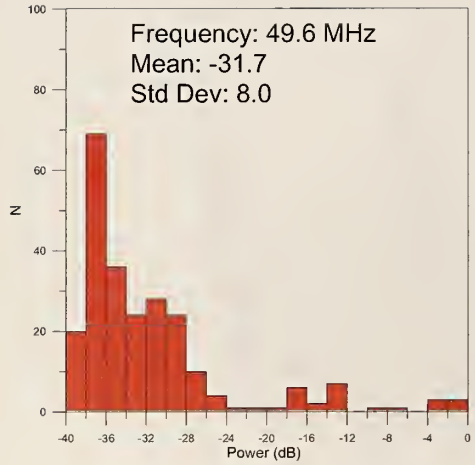

(a)

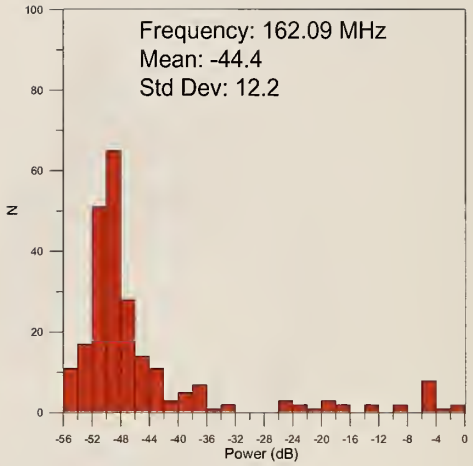

(b)

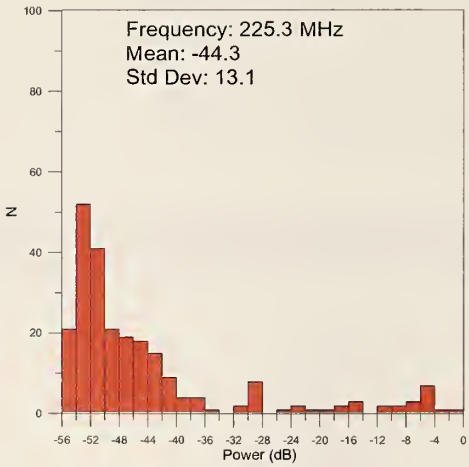

(c)

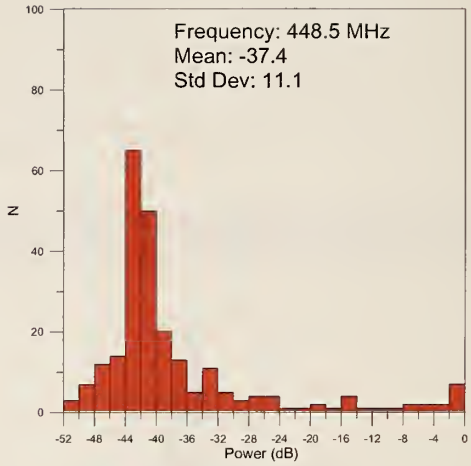

(d)

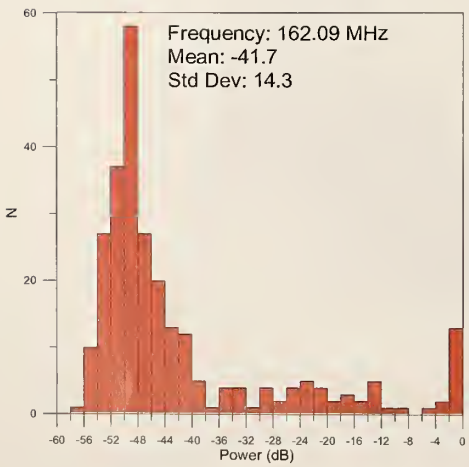

(e)

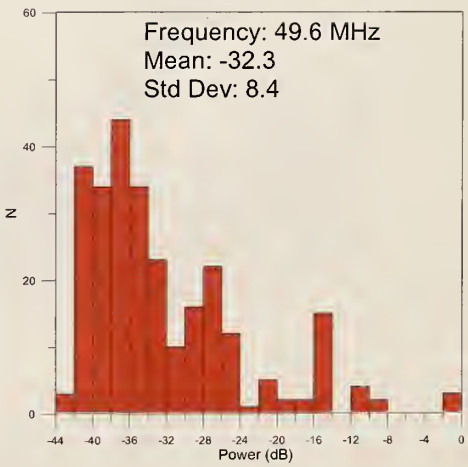

(f)

Figure 50. Histograms for the perimeter measurements for Site A fixed transmitters and vertically polarized receiving antennas.

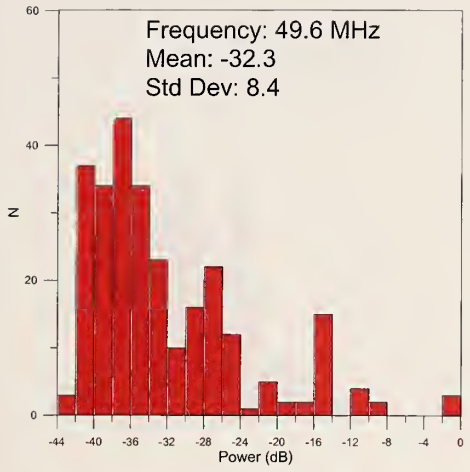

(a)

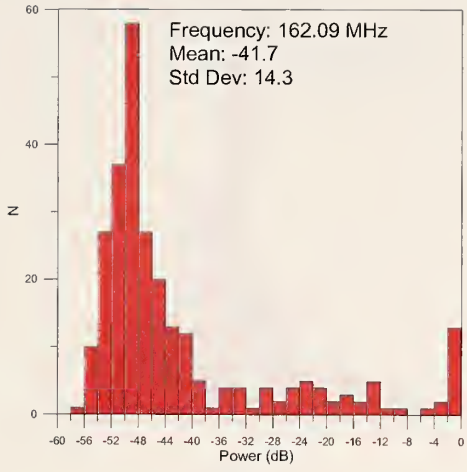

(b)

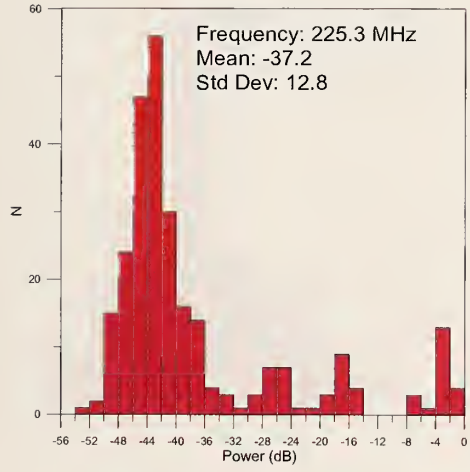

(c)

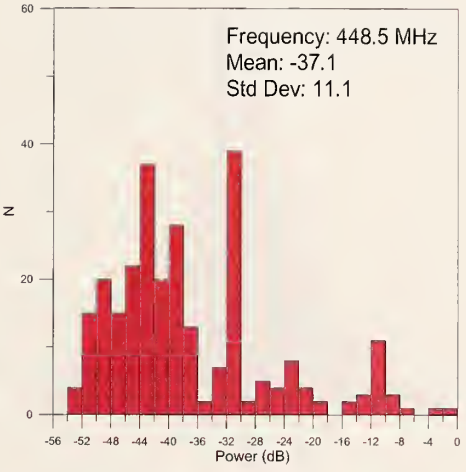

(d)

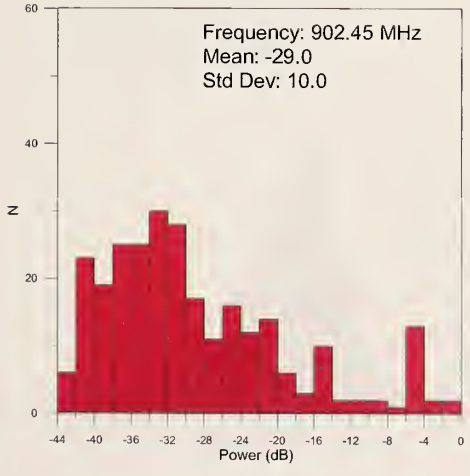

(e)

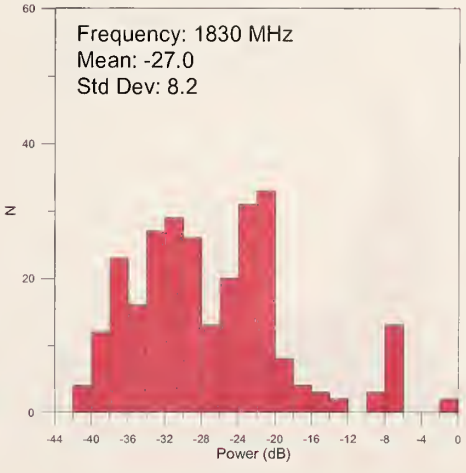

(f)

Figure 51. Histograms for the perimeter measurements for Site A fixed transmitters and horizontally polarized receiving antennas.

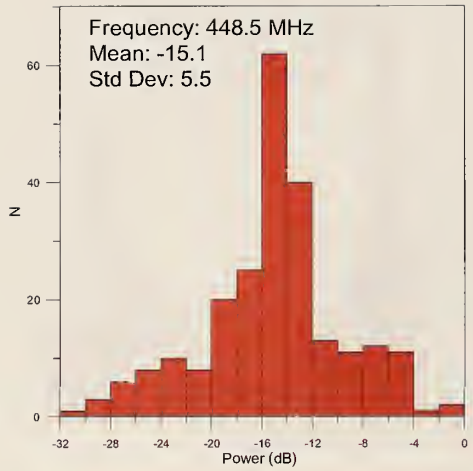

(a)

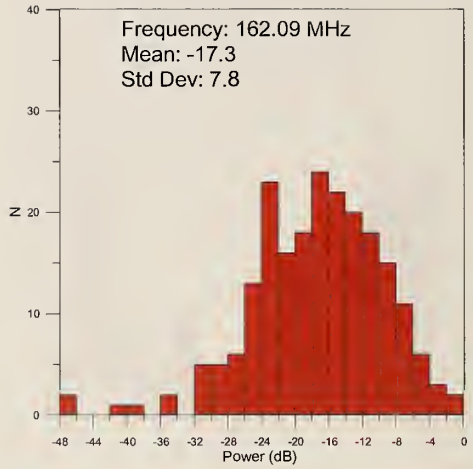

(b)

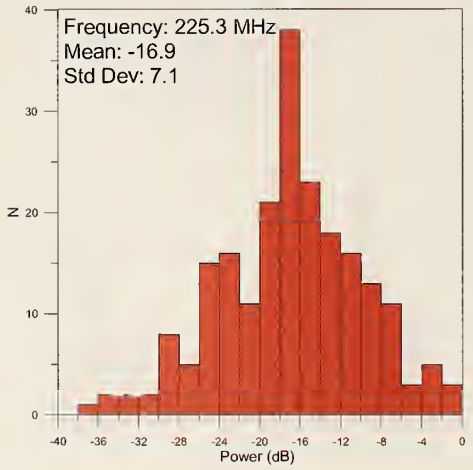

(c)

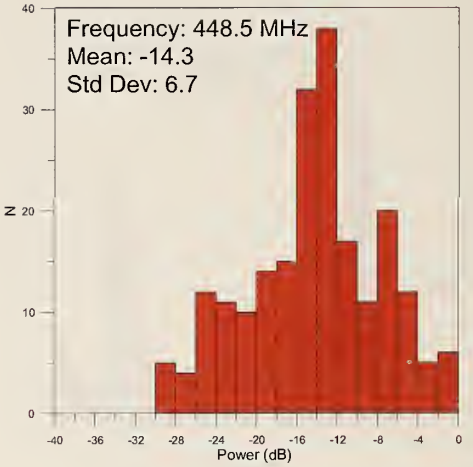

(d)

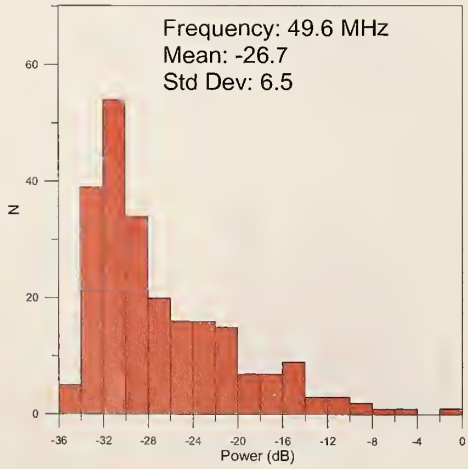

(e)

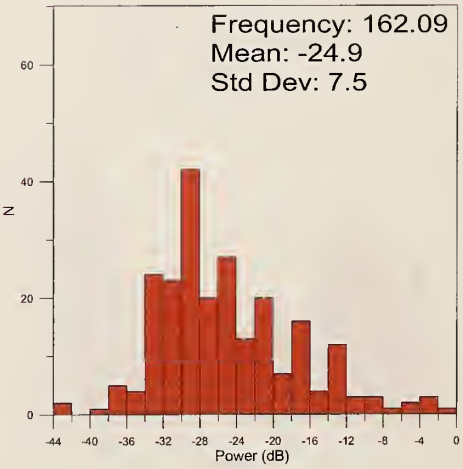

(f)

Figure 52. Histograms for the perimeter measurements for Site B fixed transmitters and vertically polarized receiving antennas.

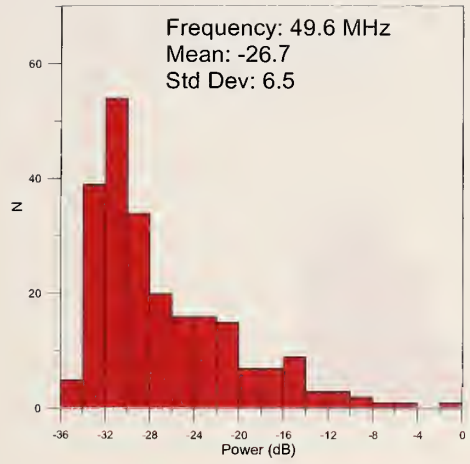

(a)

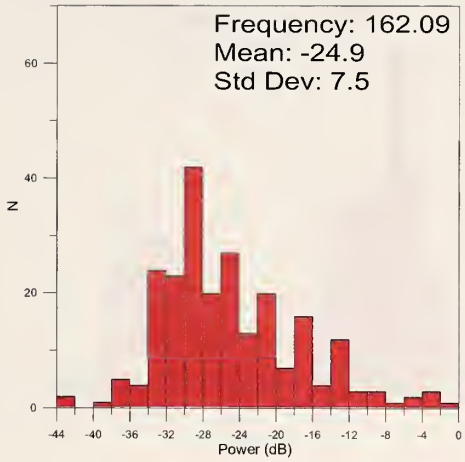

(b)

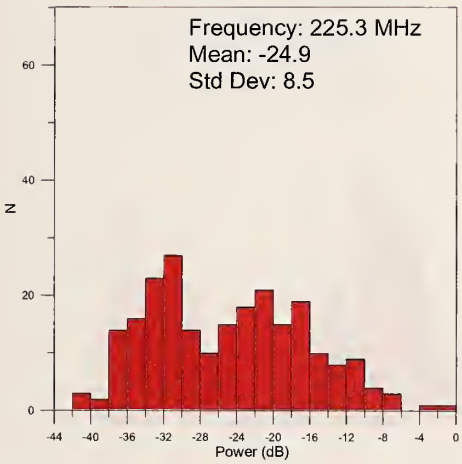

(c)

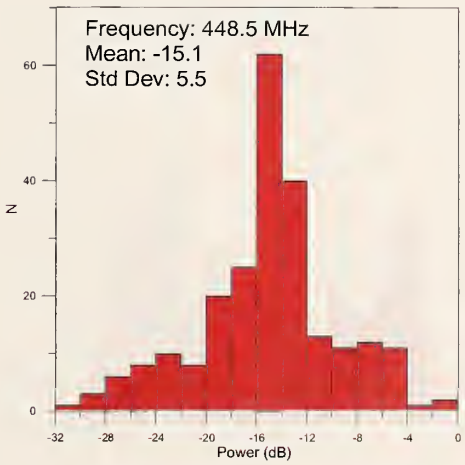

(d)

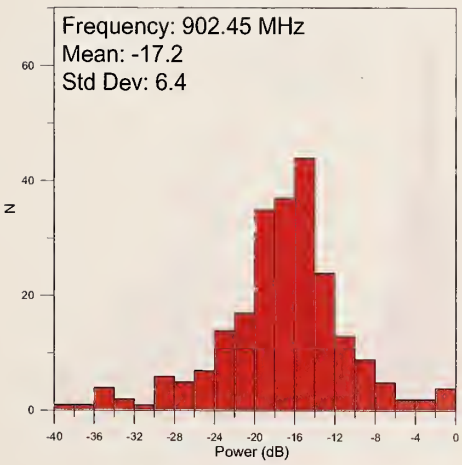

(e)

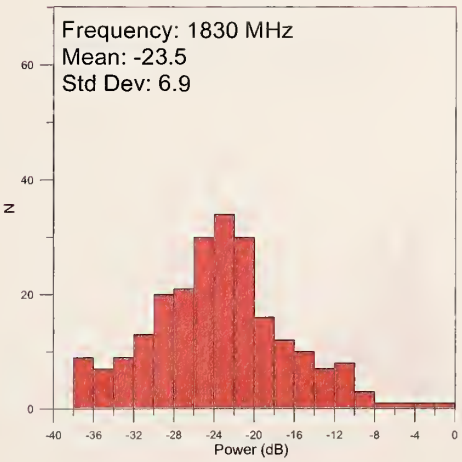

(f)

Figure 53. Histograms for the perimeter measurements for Site B fixed transmitters and horizontally polarized receiving antennas.

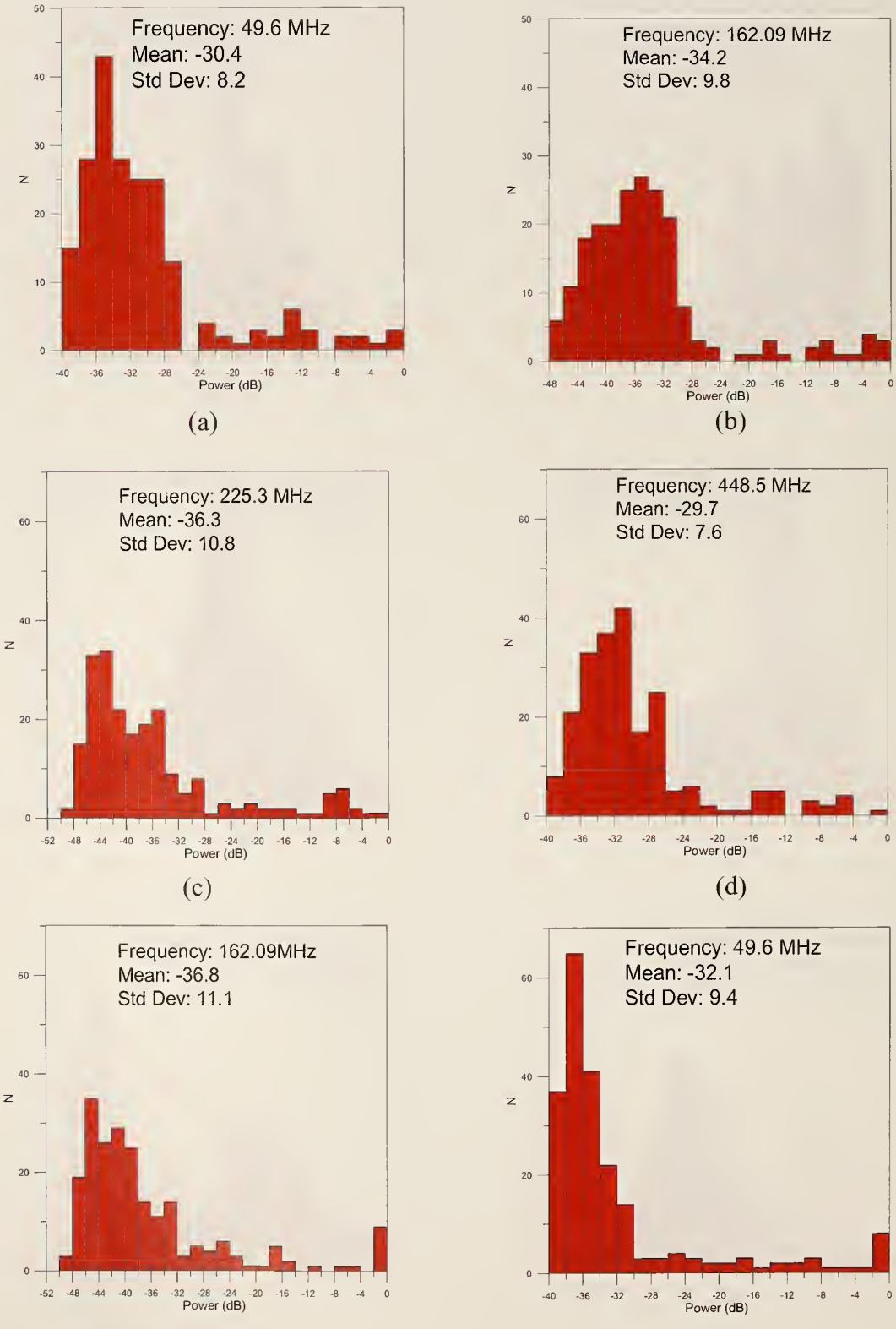

Figure 54. Histograms for the perimeter measurements for Site C fixed transmitters and vertically polarized receiving antennas.

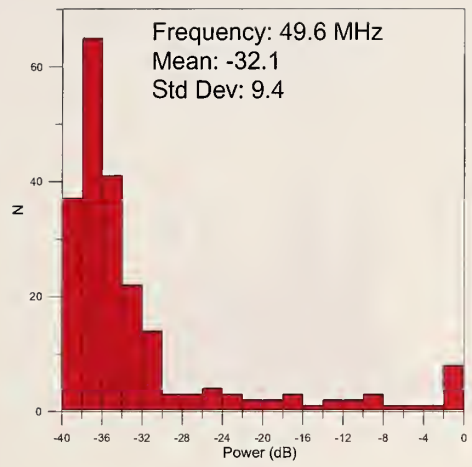

(a)

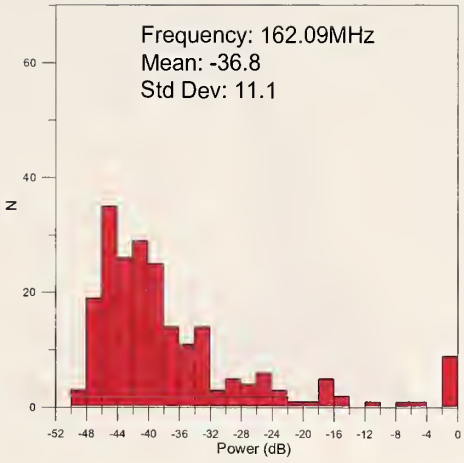

(b)

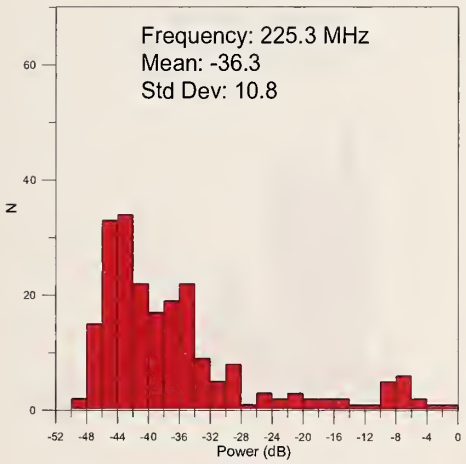

(c)

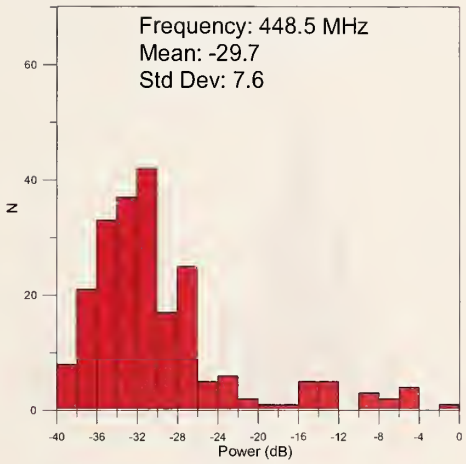

(d)

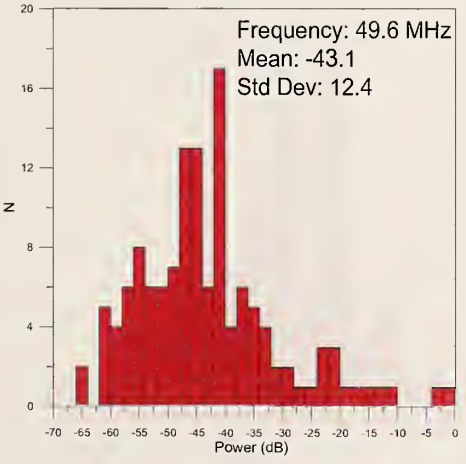

(e)

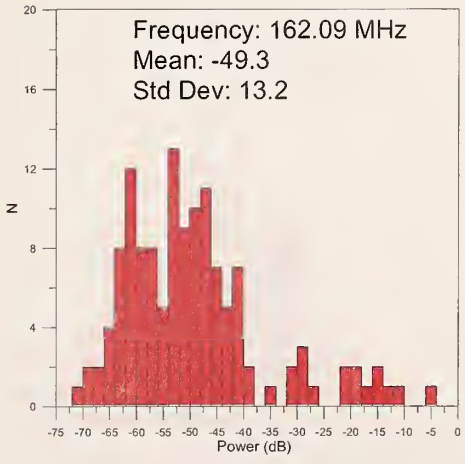

(f)

Figure 55. Histograms for the perimeter measurements for Site C fixed transmitters and horizontally polarized receiving antennas.

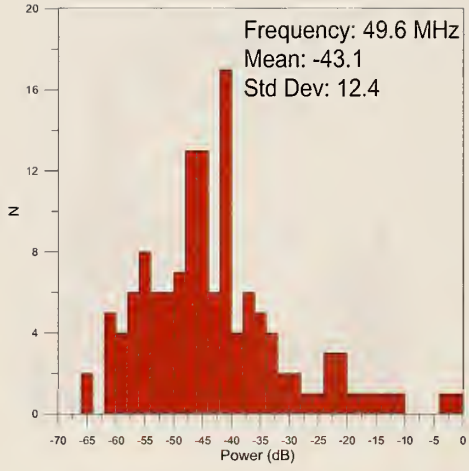

(a)

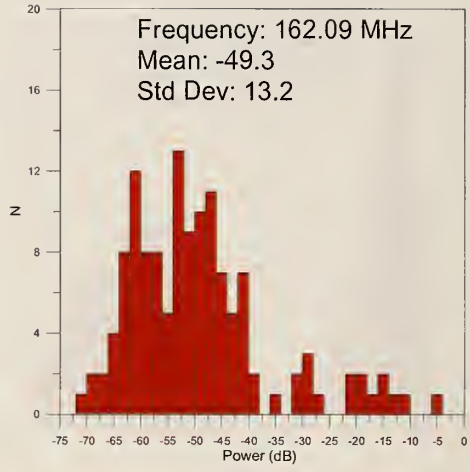

(b)

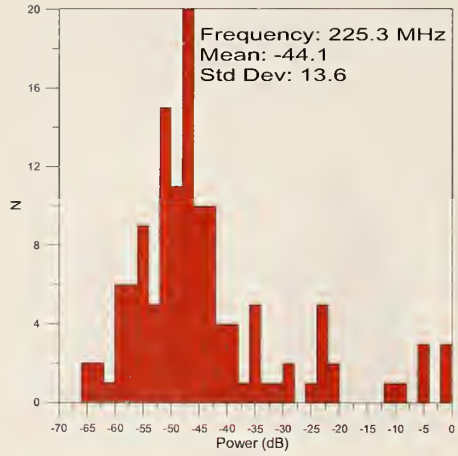

(c)

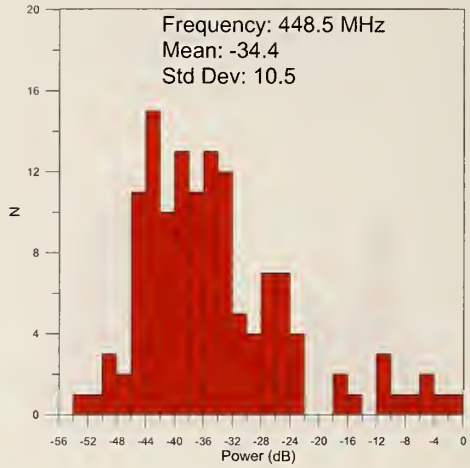

(d)

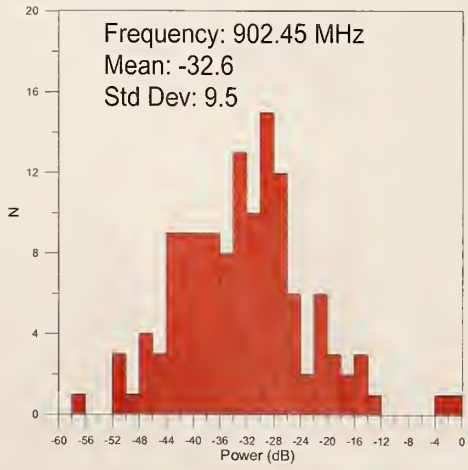

(e)

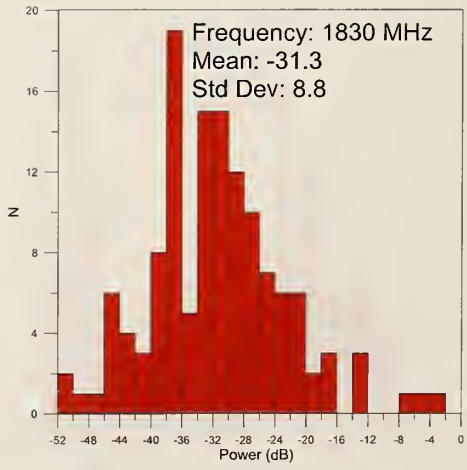

(f)

Figure 56. Histograms for the perimeter measurements for Site D fixed transmitters and vertically polarized receiving antennas.

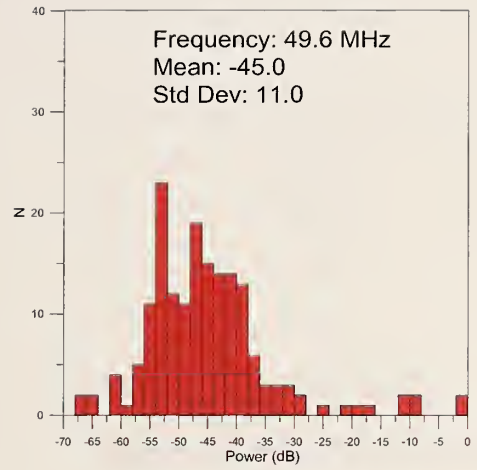

(a)

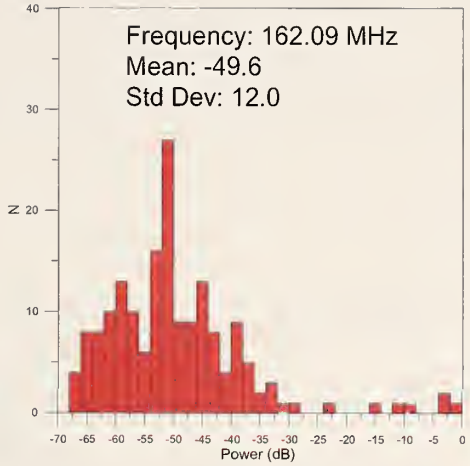

(b)

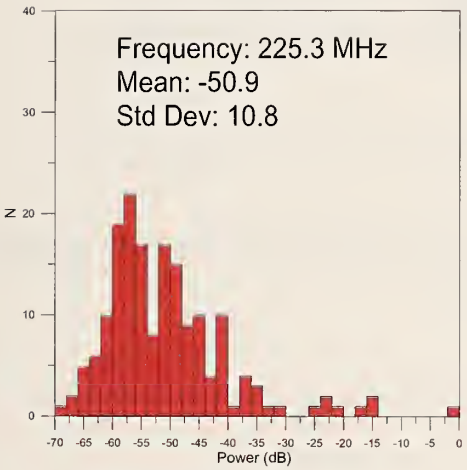

(c)

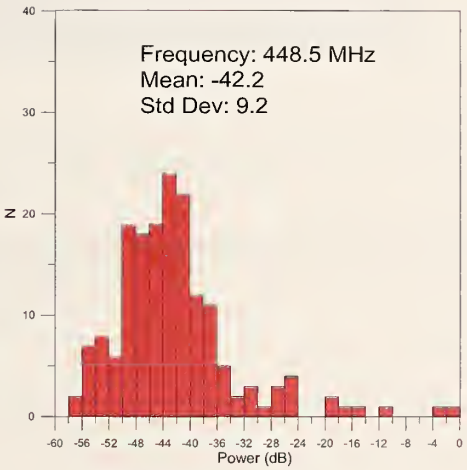

(d)

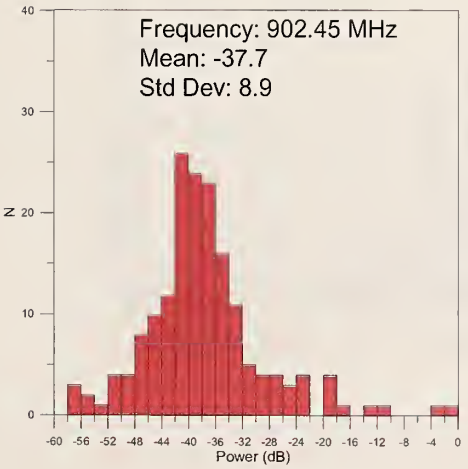

(e)

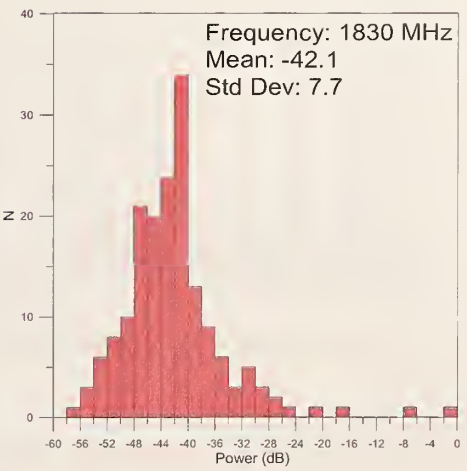

(f)

Figure 57. Histograms for the perimeter measurements for Site D fixed transmitters and horizontally polarized receiving antennas.

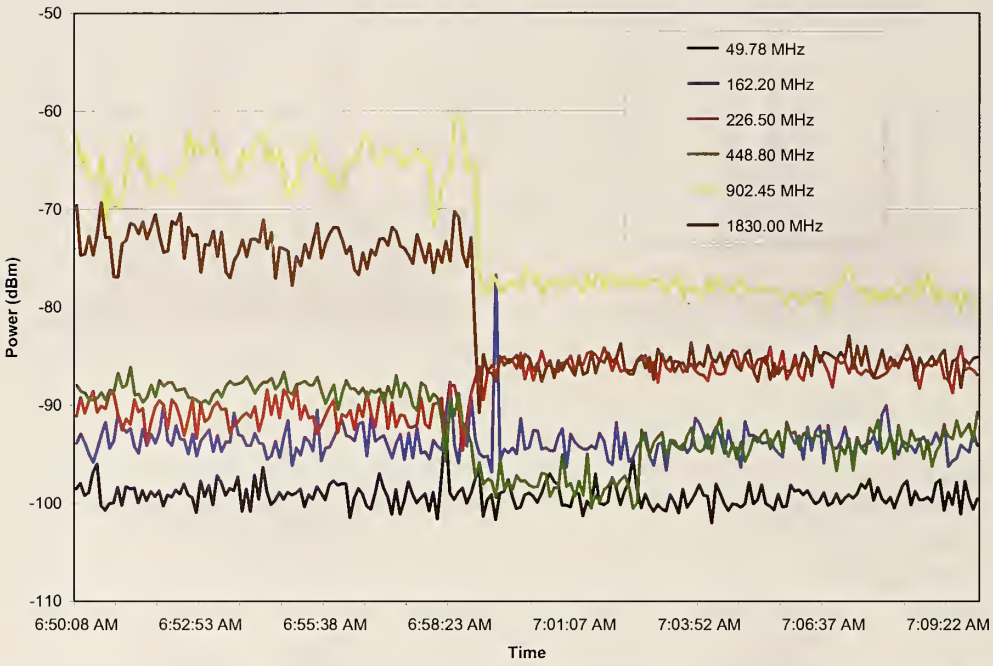

Figure 58. Pre- and post-implosion data collected from Receiver Site 1 for the transmitters located at Site A.

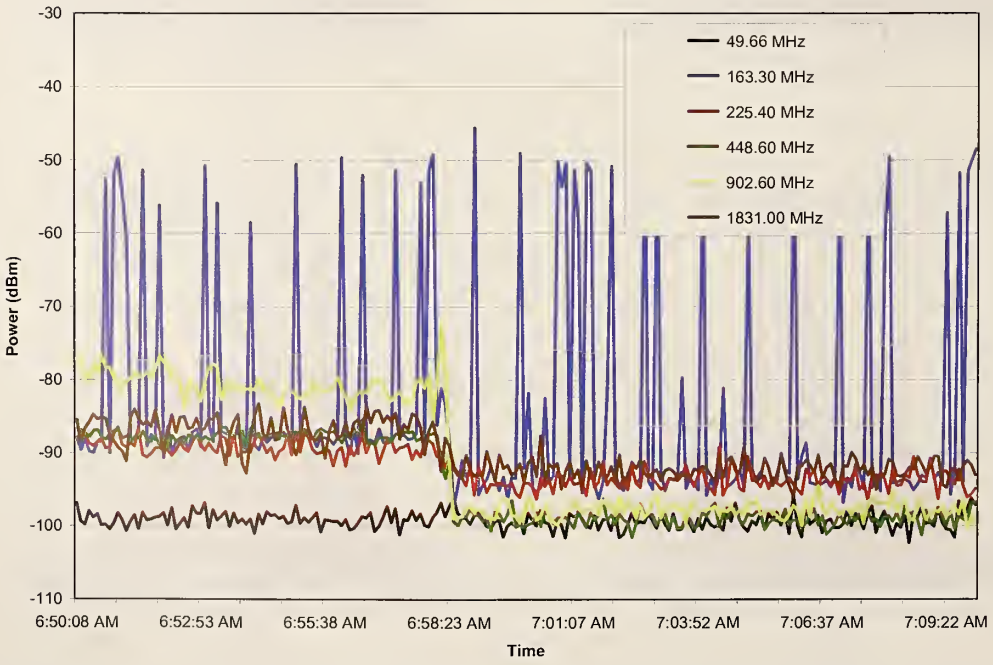

Figure 59. Pre- and post-implosion data collected from Receiver Site 1 for the transmitters located at Site B.

Figure 60. Pre- and post-implosion data collected from Receiver Site 1 for the transmitters located at Site C.

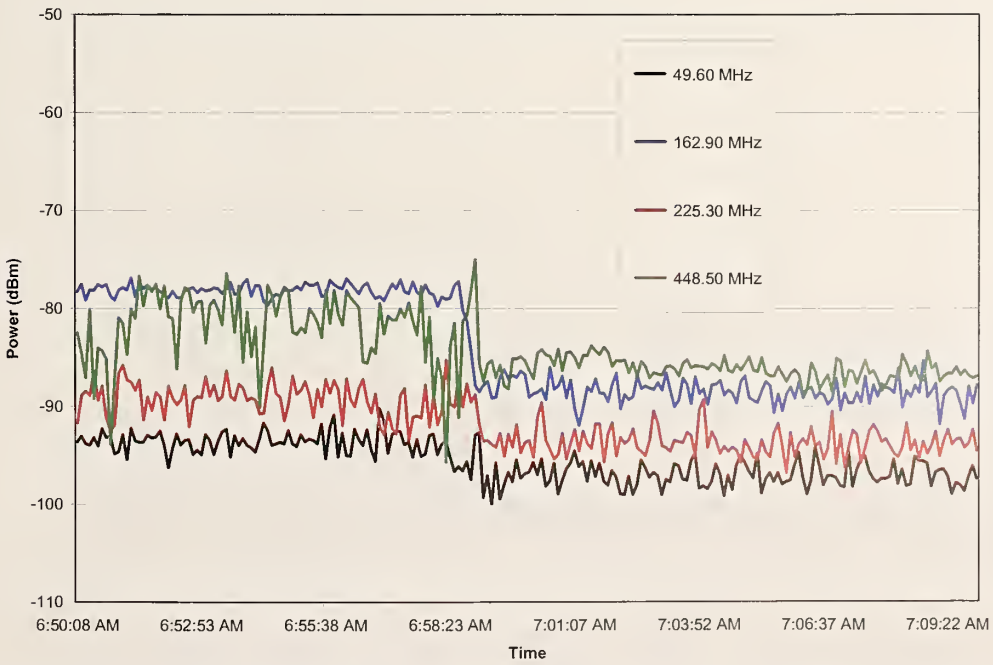

Figure 61. Pre- and post-implosion data collected from Receiver Site 1 for the transmitters located at Site D.

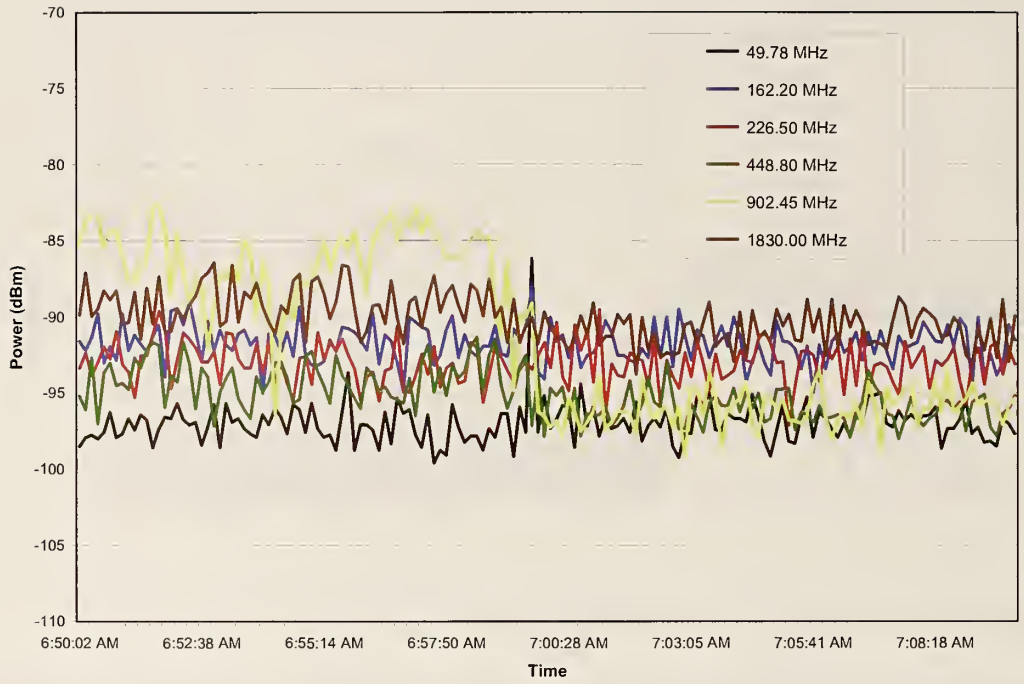

Figure 62. Pre- and post-implosion data collected from Receiver Site 2 for the transmitters located at Site A.

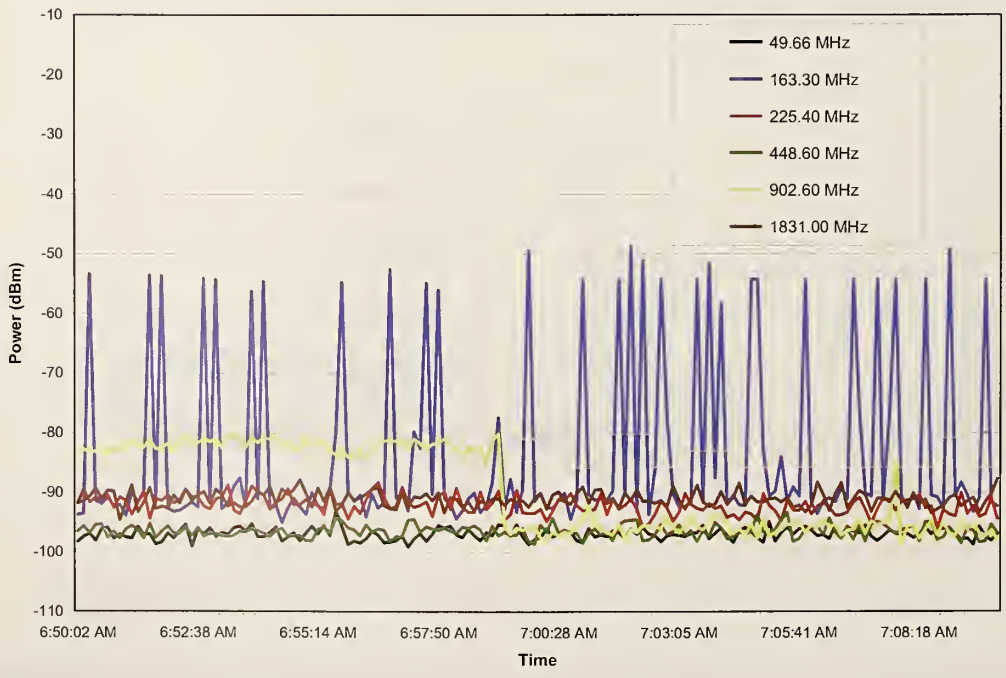

Figure 63. Pre- and post-implosion data collected from Receiver Site 2 for the transmitters located at Site B.

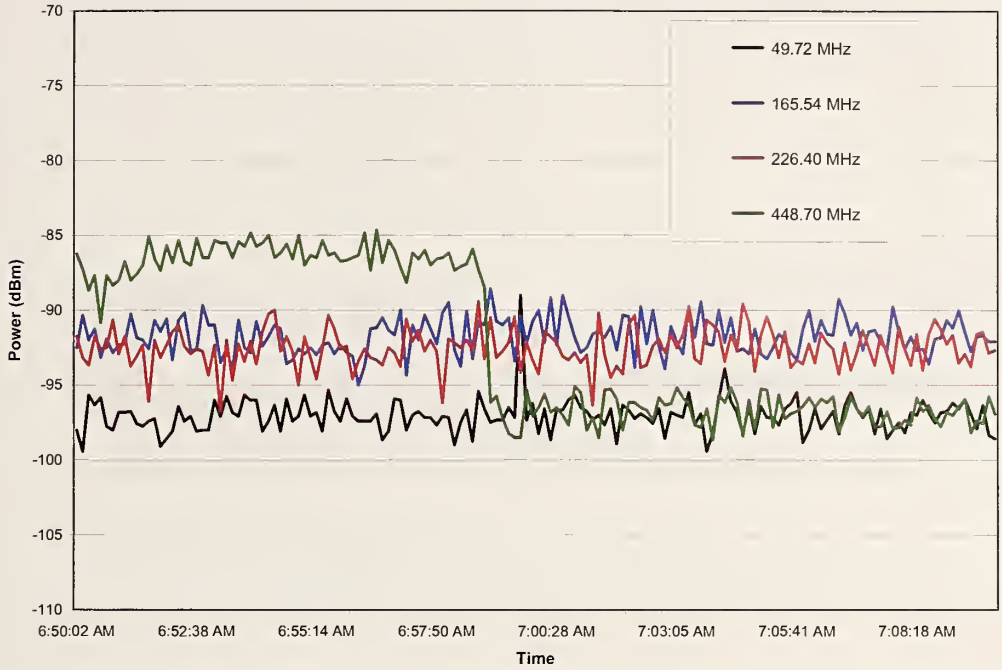

Figure 64. Pre- and post-implosion data collected from Receiver Site 2 for the transmitters located at Site C.

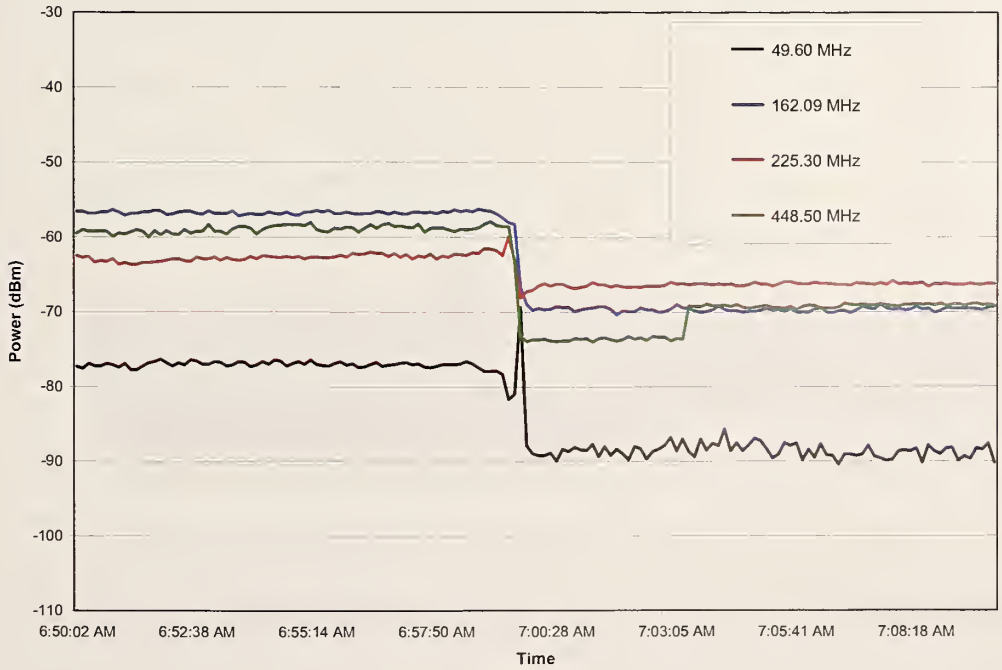

Figure 65. Pre- and post-implosion data collected from Receiver Site 2 for the transmitters located at Site D.

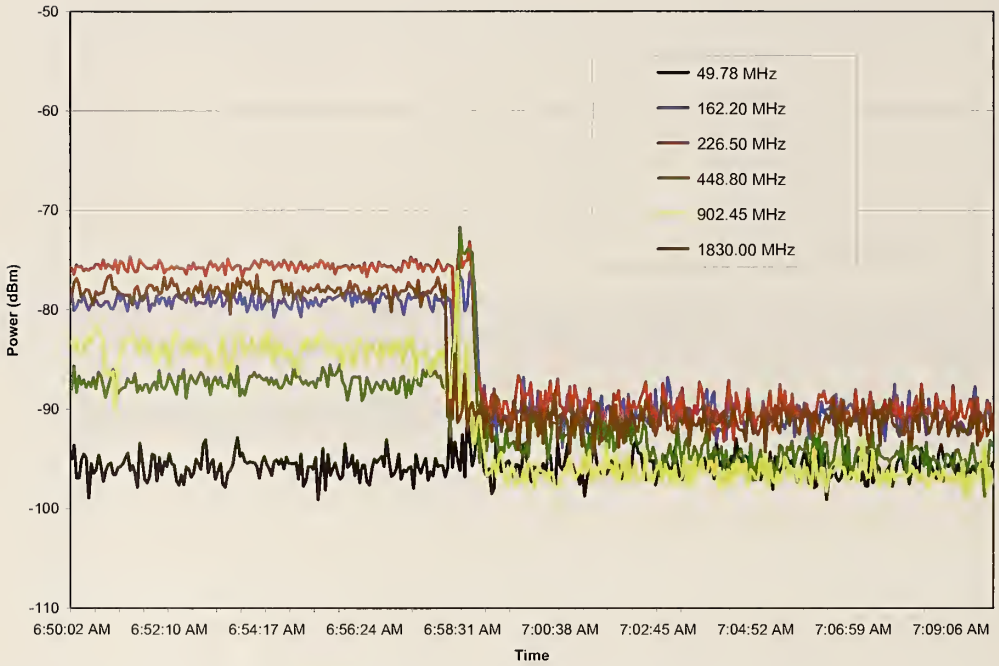

Figure 66. Pre- and post-implosion data collected from Receiver Site 3 for the transmitters located at Site A.

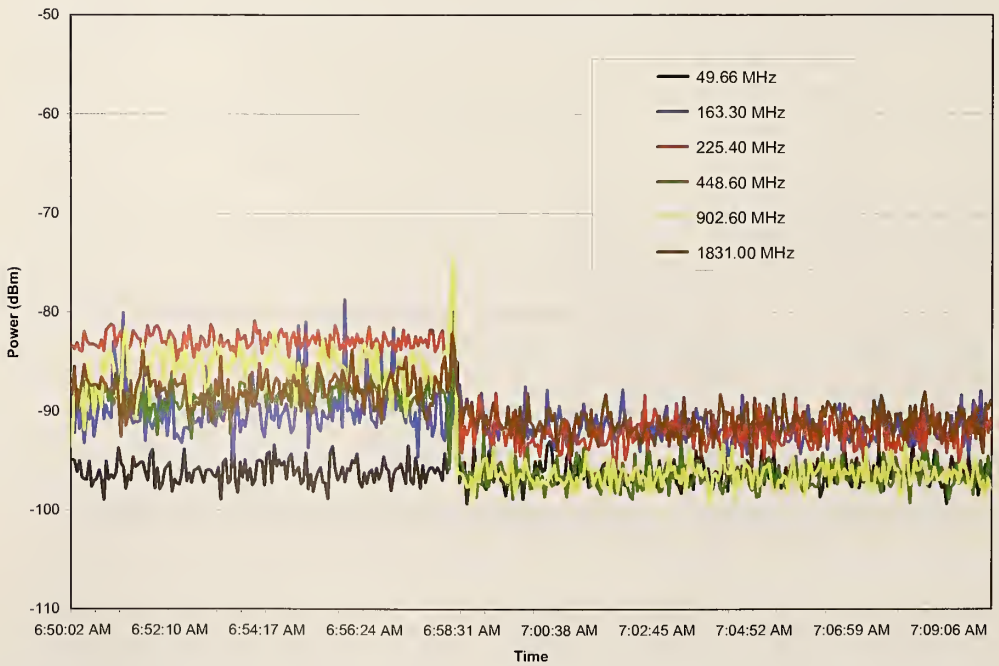

Figure 67. Pre- and post-implosion data collected from Receiver Site 3 for the transmitters located at Site B.

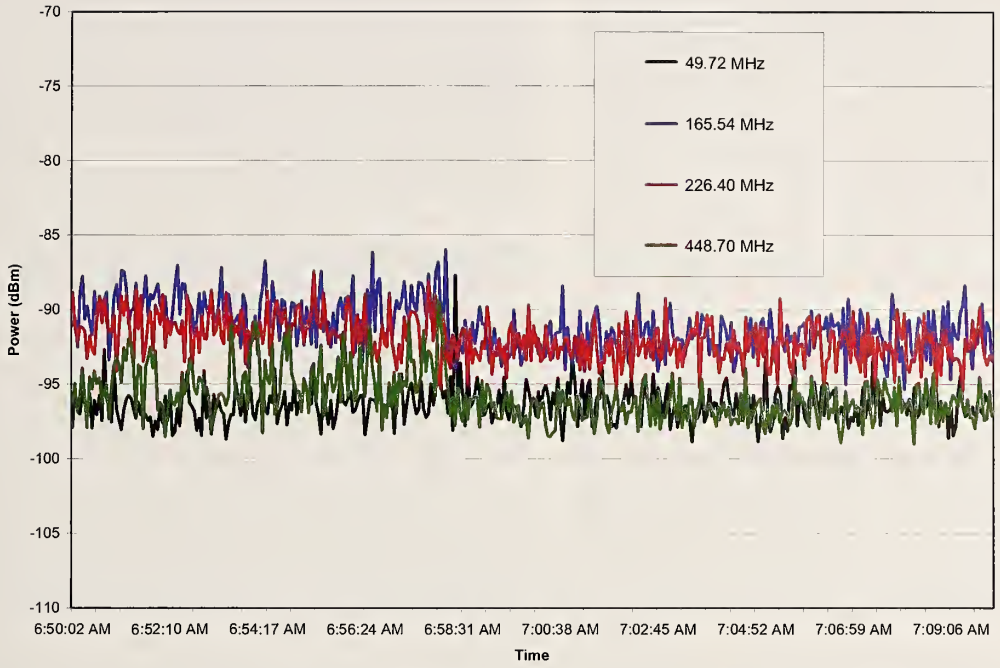

Figure 68. Pre- and post-implosion data collected from Receiver Site 3 for the transmitters located at Site C.

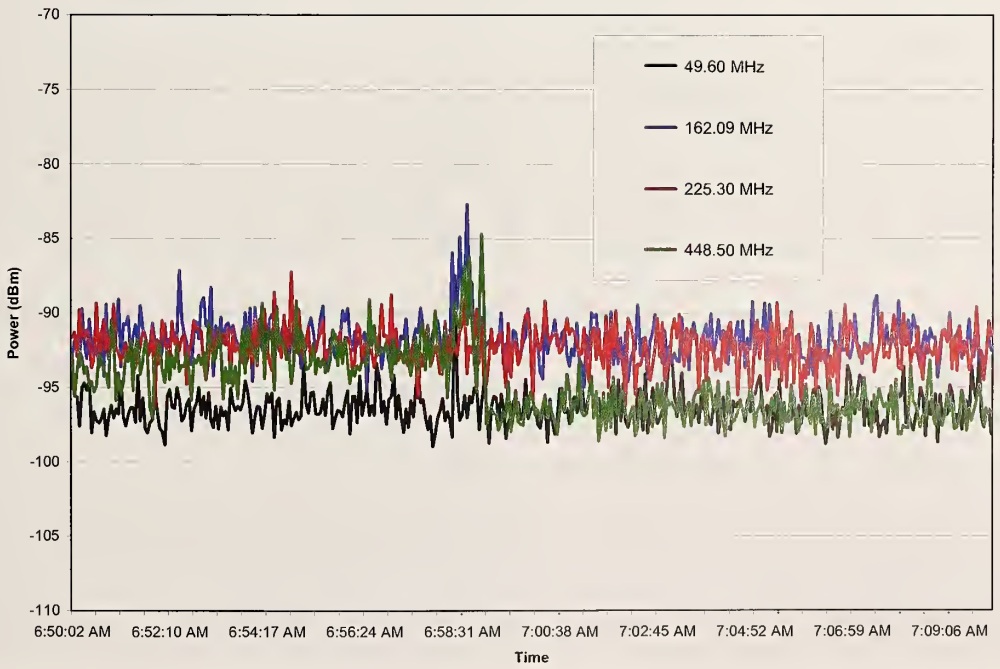

Figure 69. Pre- and post-implosion data collected from Receiver Site 3 for the transmitters located at Site D.

Figure 70. The stadium collapses during the implosion sequence.

Figure 71. Photos of stadium after the implosion.

Figure 72. Photos of stadium after the implosion.

(a)

(b)

(c)

Figure 73. Receiving sites before and after implosion (a) Site 1, (b) Site 2, and (c) Site 3.

Figure 74. Illustration of measurements with mobile cart.

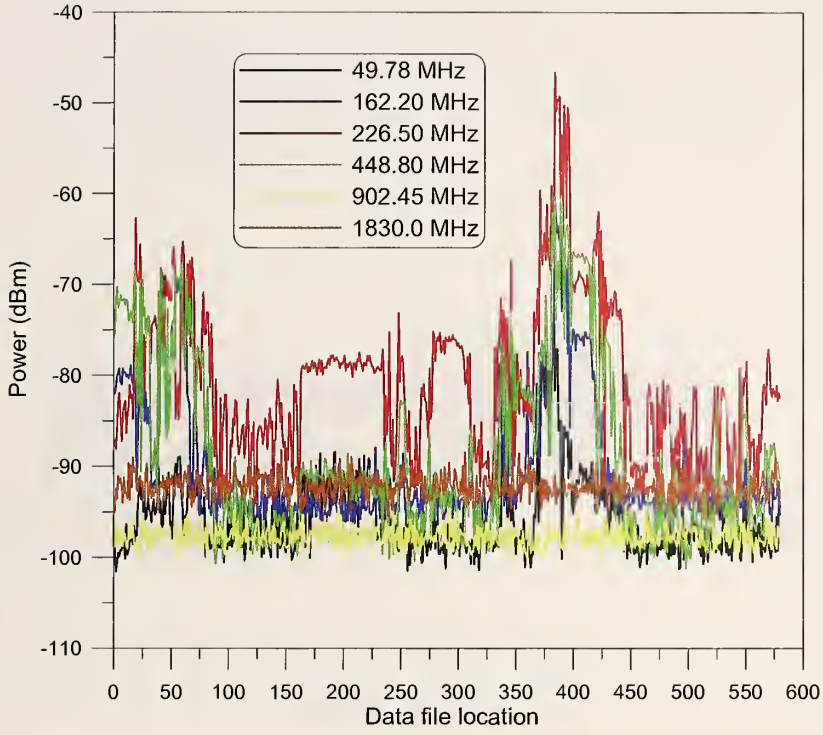

Figure 75. Post-implosion mobile cart perimeter measurements for the transmitters at transmitter Site A for horizontally polarized receiving antennas.

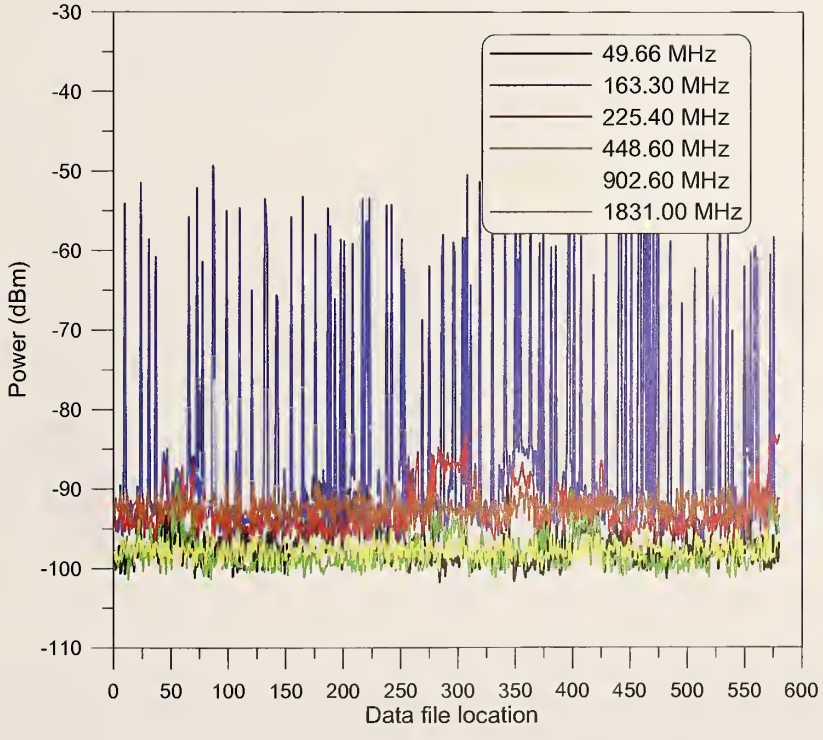

Figure 76. Post-implosion mobile cart perimeter measurements for the transmitters at transmitter Site B for horizontally polarized receiving antennas.

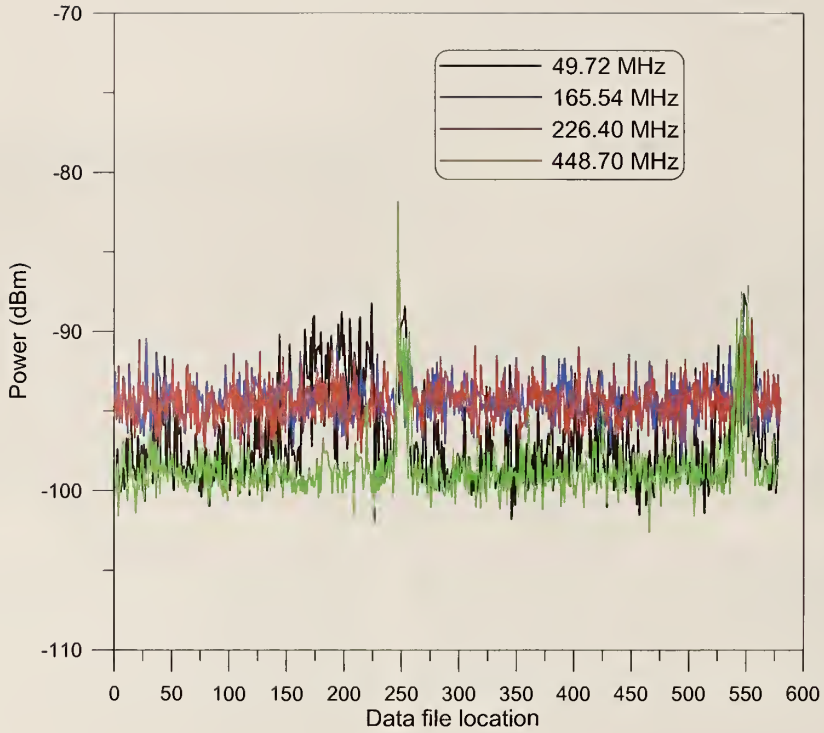

Figure 77. Post-implosion mobile cart perimeter measurements for the transmitters at transmitter Site C for horizontally polarized receiving antennas.

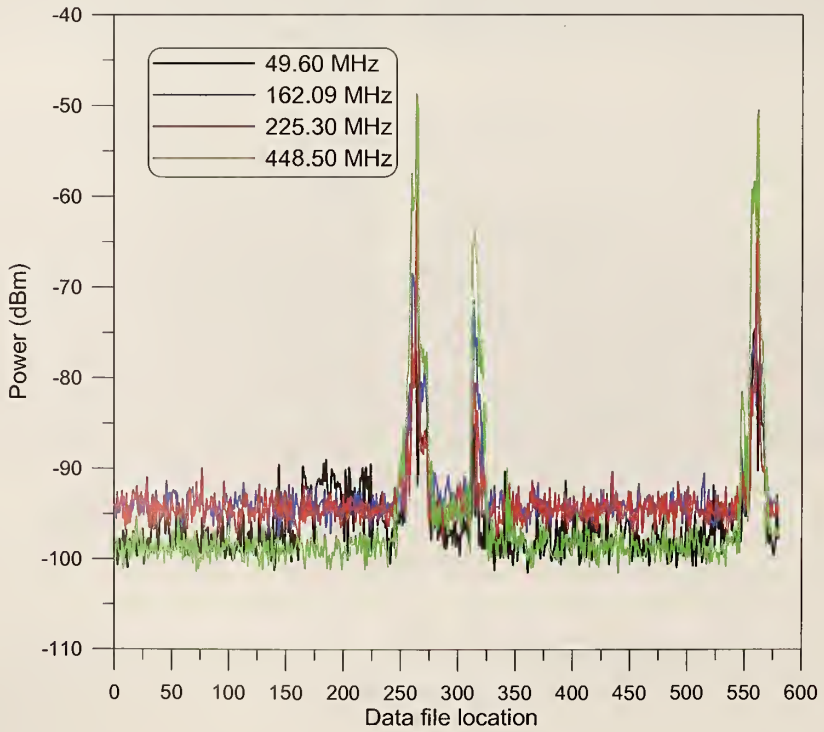

Figure 78. Post-implosion mobile cart perimeter measurements for the transmitters at transmitter Site D for horizontally polarized receiving antennas.

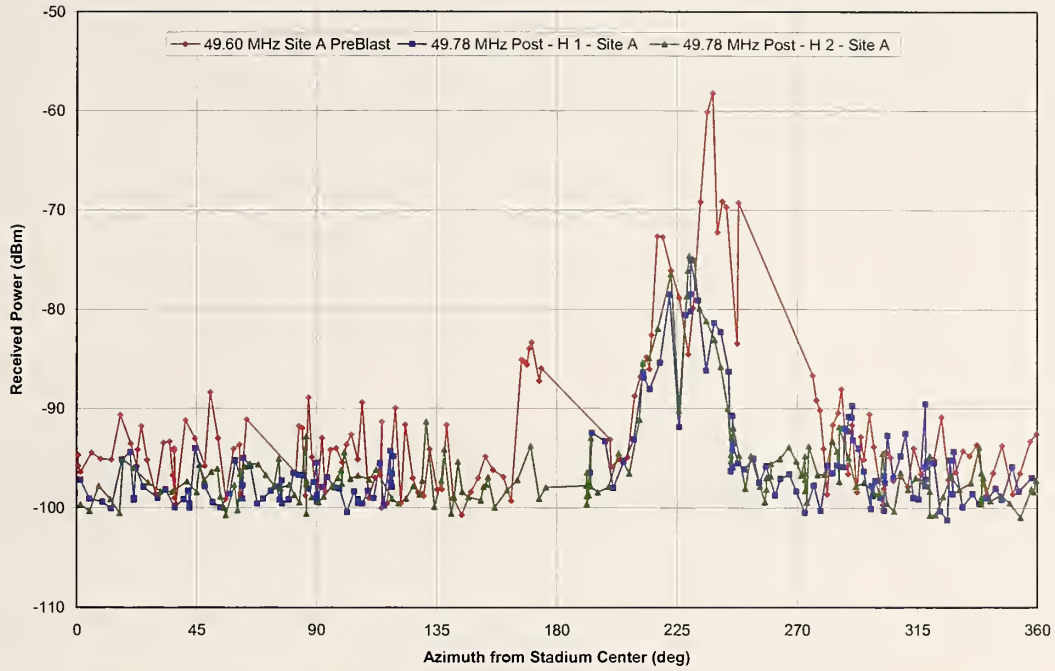

Figure 79. Comparison of pre- and post-implosion mobile cart perimeter measurements for the transmitters at transmitter Site A for horizontally polarized receiving antennas: 49 MHz band.

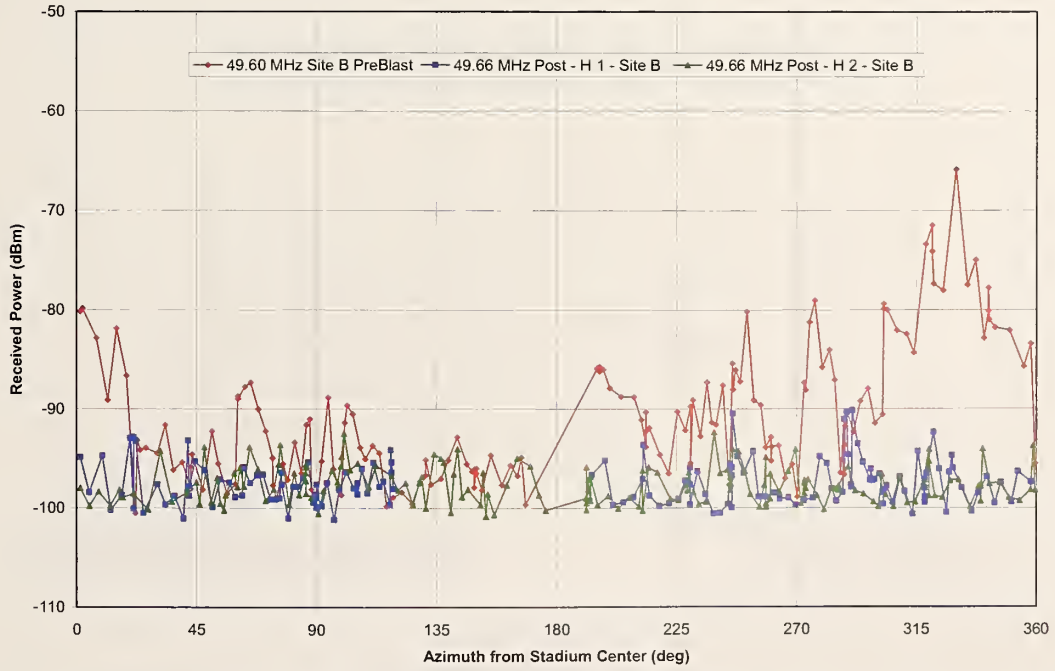

Figure 80. Comparison of pre- and post-implosion mobile cart perimeter measurements for the transmitters at transmitter Site B for horizontally polarized receiving antennas: 49 MHz band.

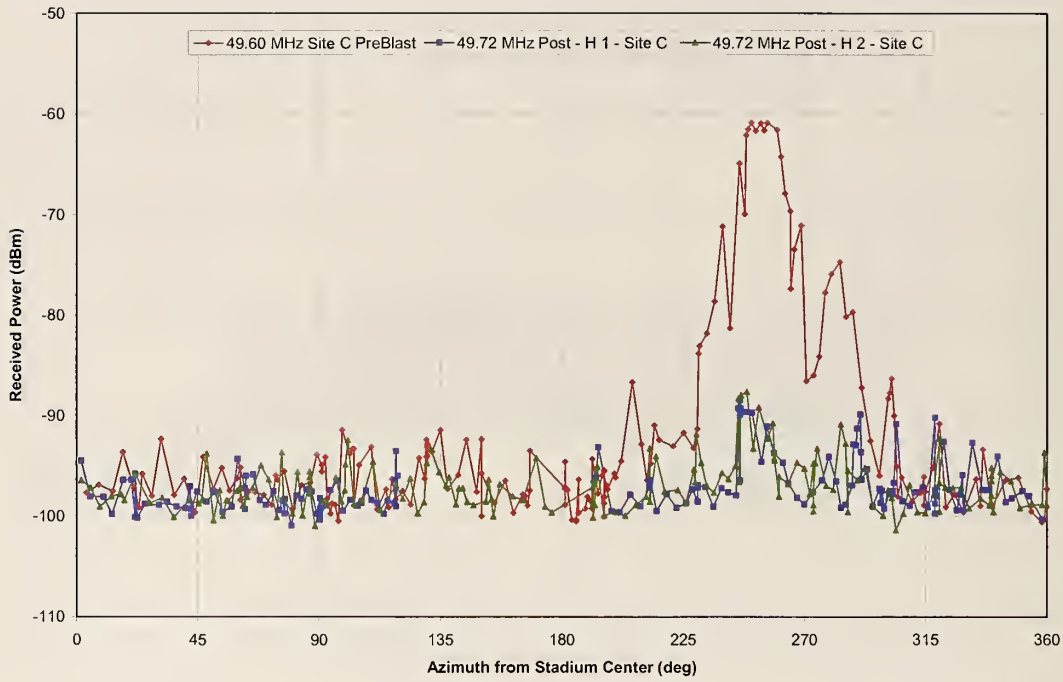

Figure 81. Comparison of pre- and post-implosion mobile cart perimeter measurements for the transmitters at transmitter Site C for horizontally polarized receiving antennas: 49 MHz band.

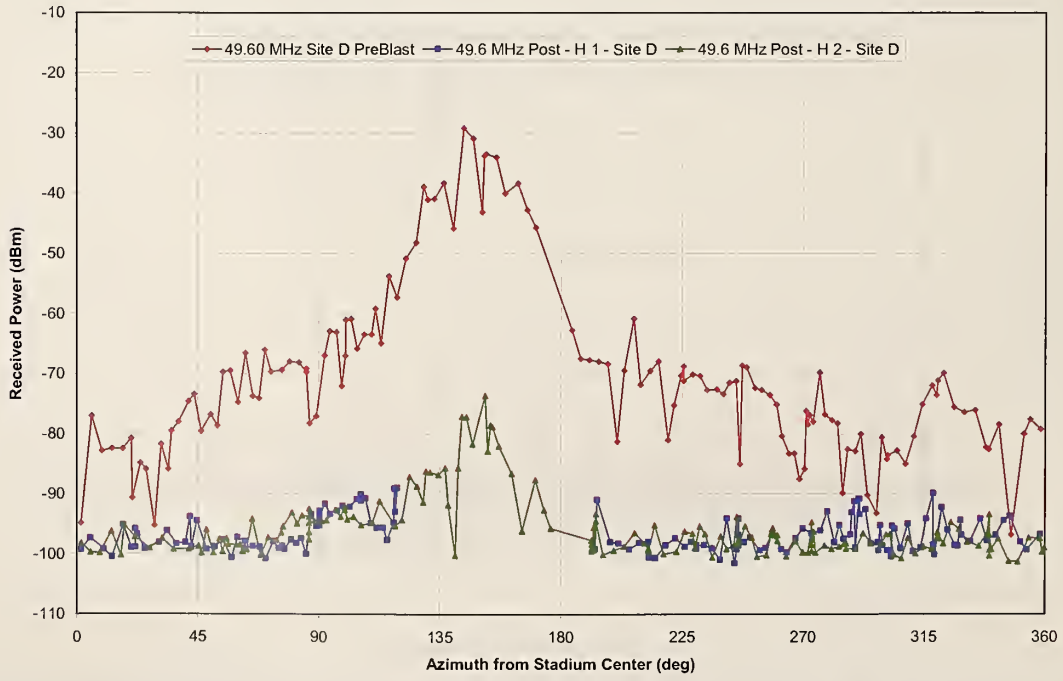

Figure 82. Comparison of pre- and post-implosion mobile cart perimeter measurements for the transmitters at transmitter Site D for horizontally polarized receiving antennas: 49 MHz band.

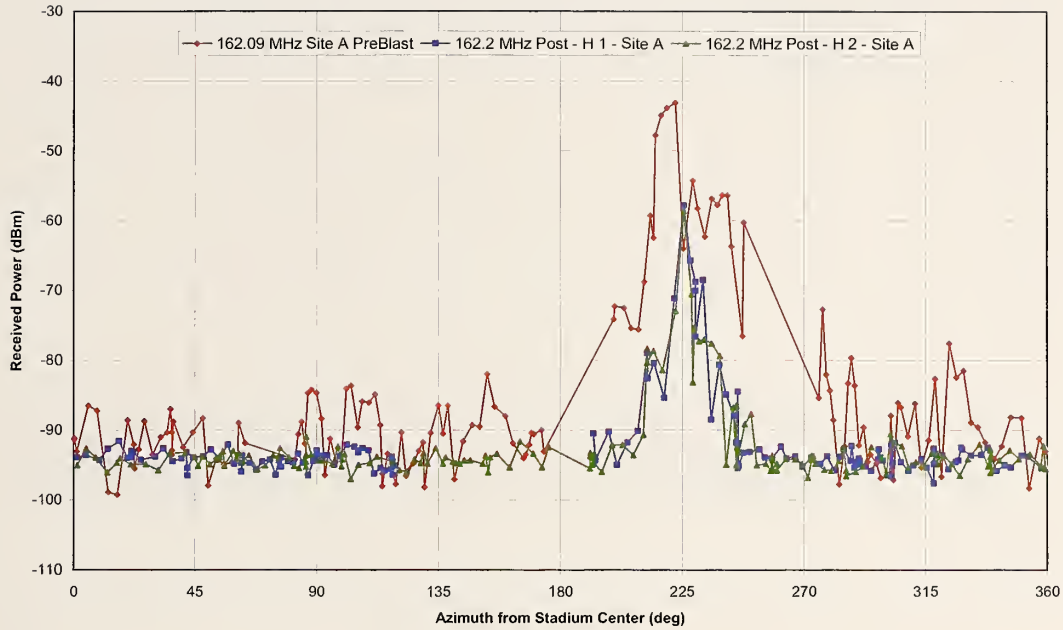

Figure 83. Comparison of pre- and post-implosion mobile cart perimeter measurements for the transmitters at transmitter Site A for horizontally polarized receiving antennas: 160 MHz band.

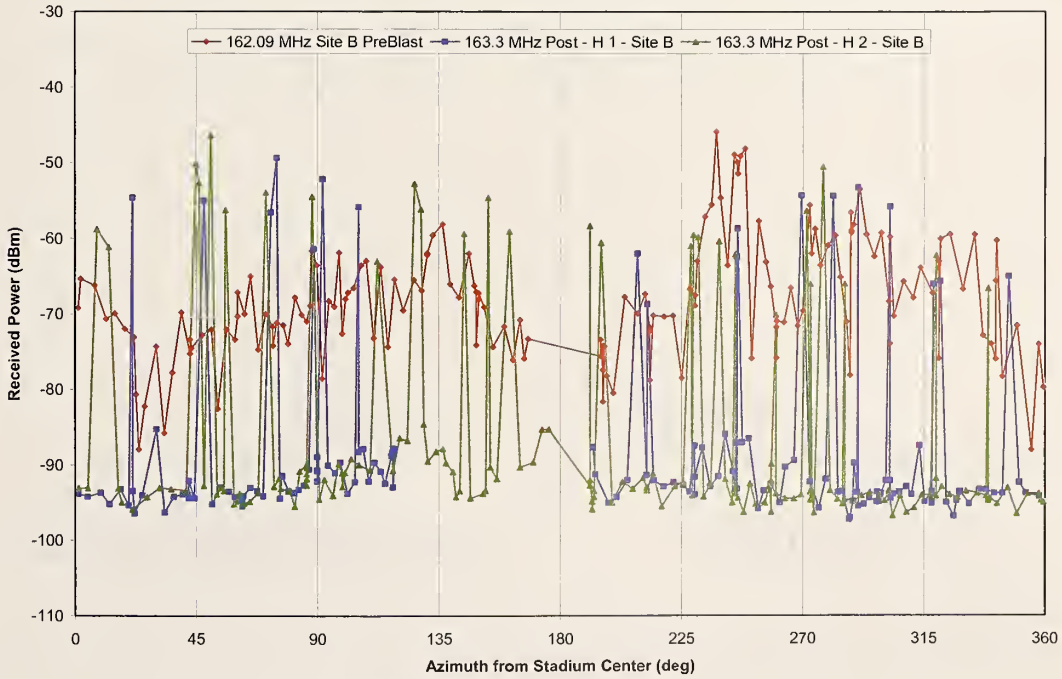

Figure 84. Comparison of pre- and post-implosion mobile cart perimeter measurements for the transmitters at transmitter Site B for horizontally polarized receiving antennas: 160 MHz band.

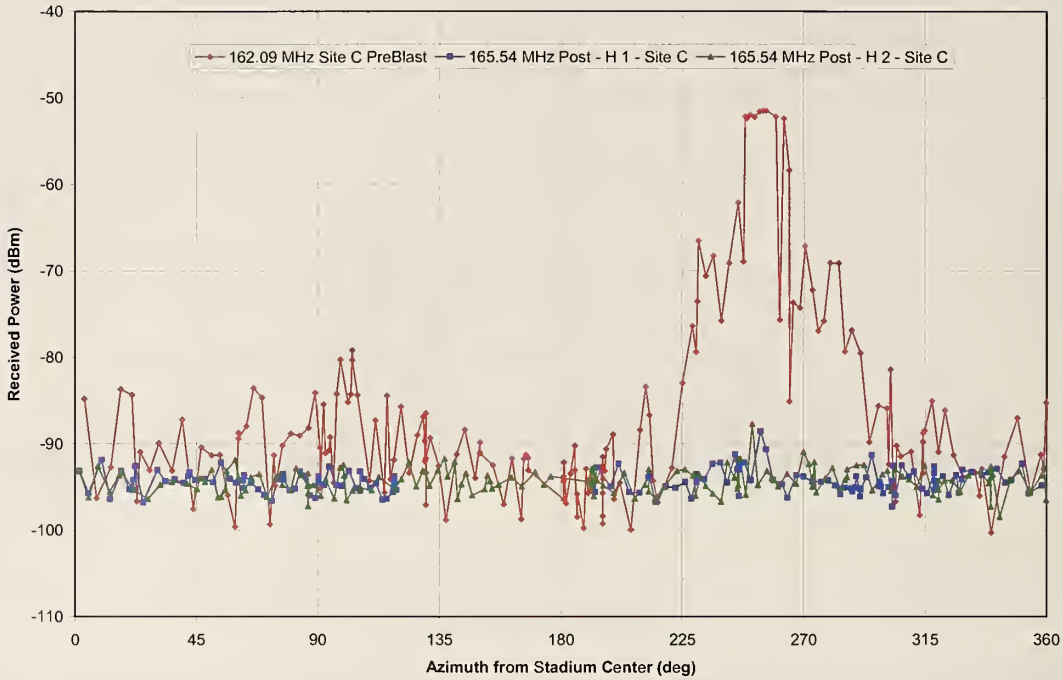

Figure 85. Comparison of pre- and post-implosion mobile cart perimeter measurements for the transmitters at transmitter Site C for horizontally polarized receiving antennas: 160 MHz band.

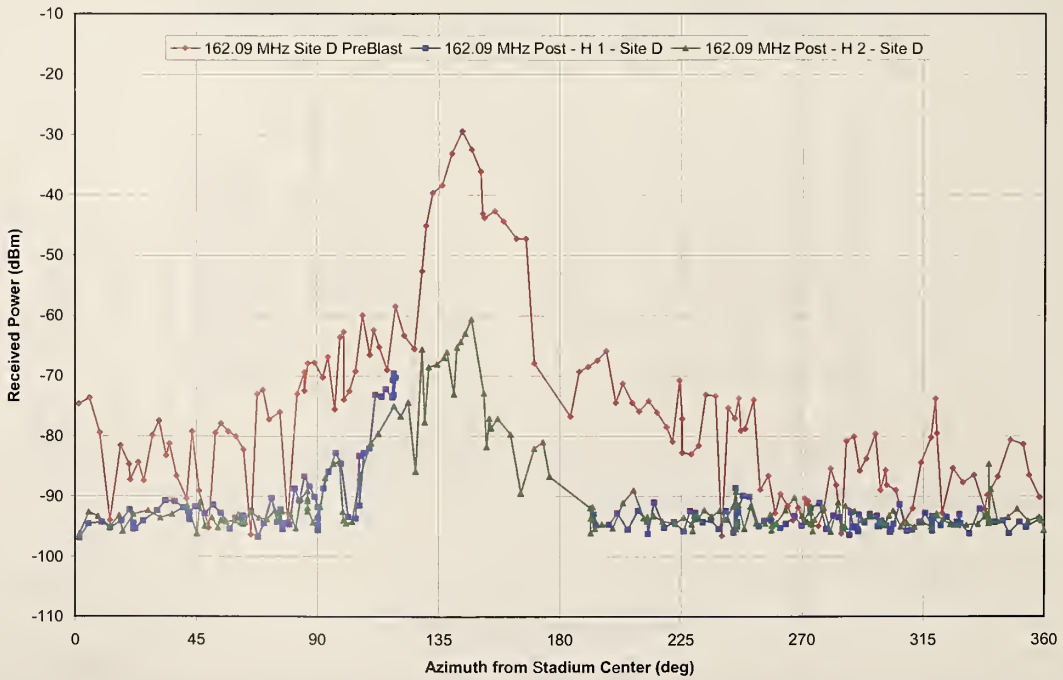

Figure 86. Comparison of pre- and post-implosion mobile cart perimeter measurements for the transmitters at transmitter Site D for horizontally polarized receiving antennas: 160 MHz band.

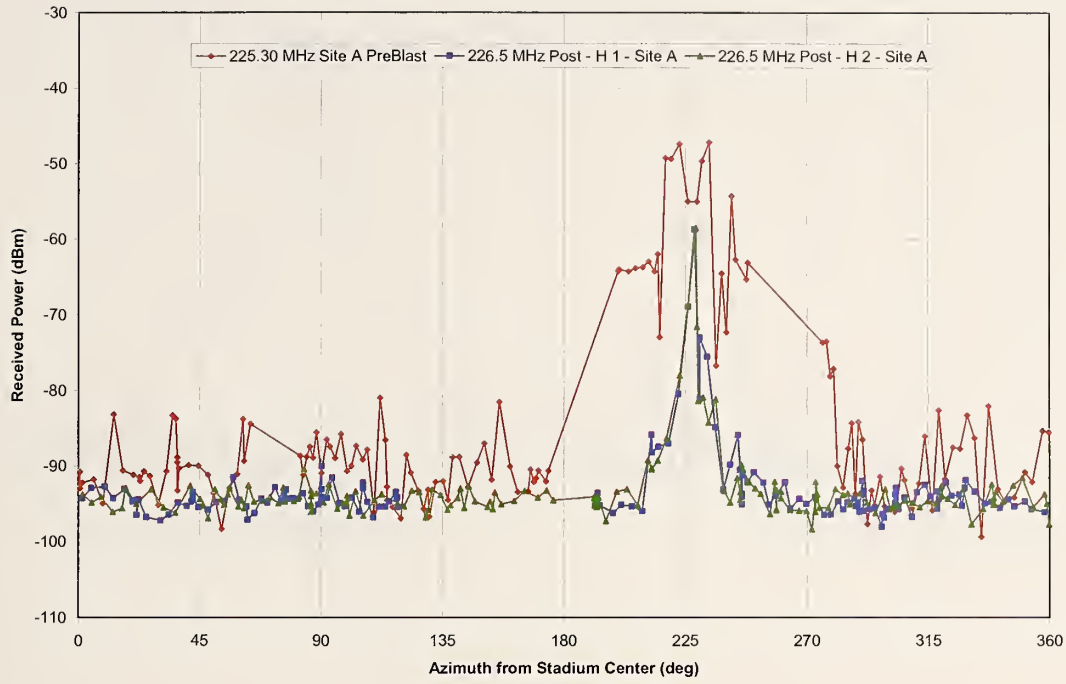

Figure 87. Comparison of pre- and post-implosion mobile cart perimeter measurements for the transmitters at transmitter Site A for horizontally polarized receiving antennas: 225 MHz band.

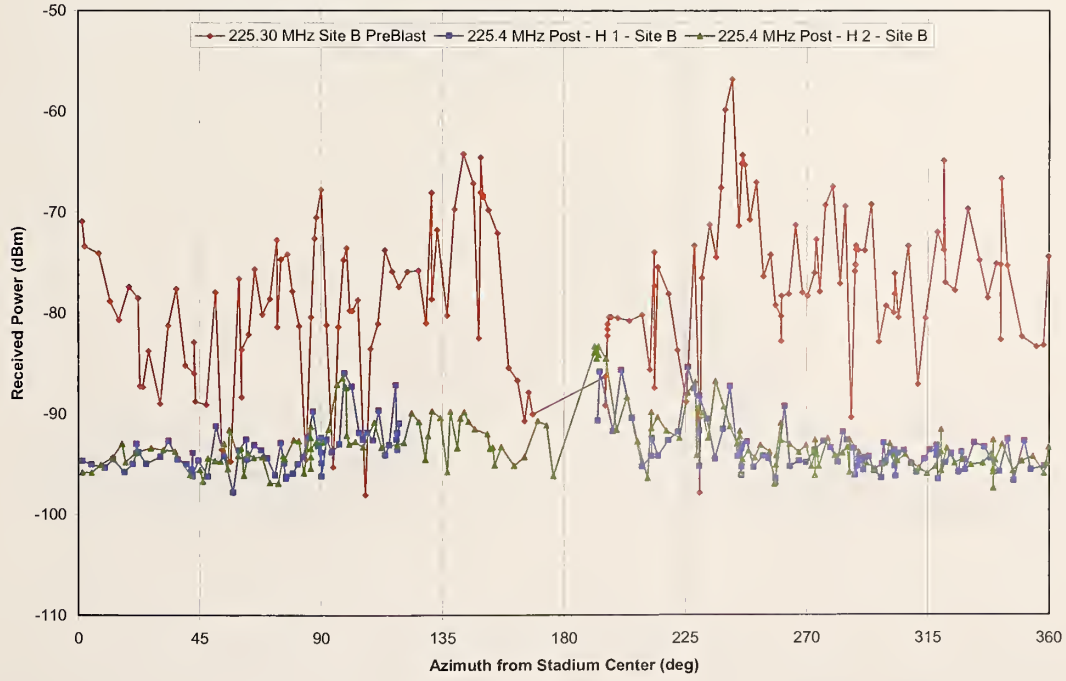

Figure 88. Comparison of pre- and post-implosion mobile cart perimeter measurements for the transmitters at transmitter Site B for horizontally polarized receiving antennas: 225 MHz band.

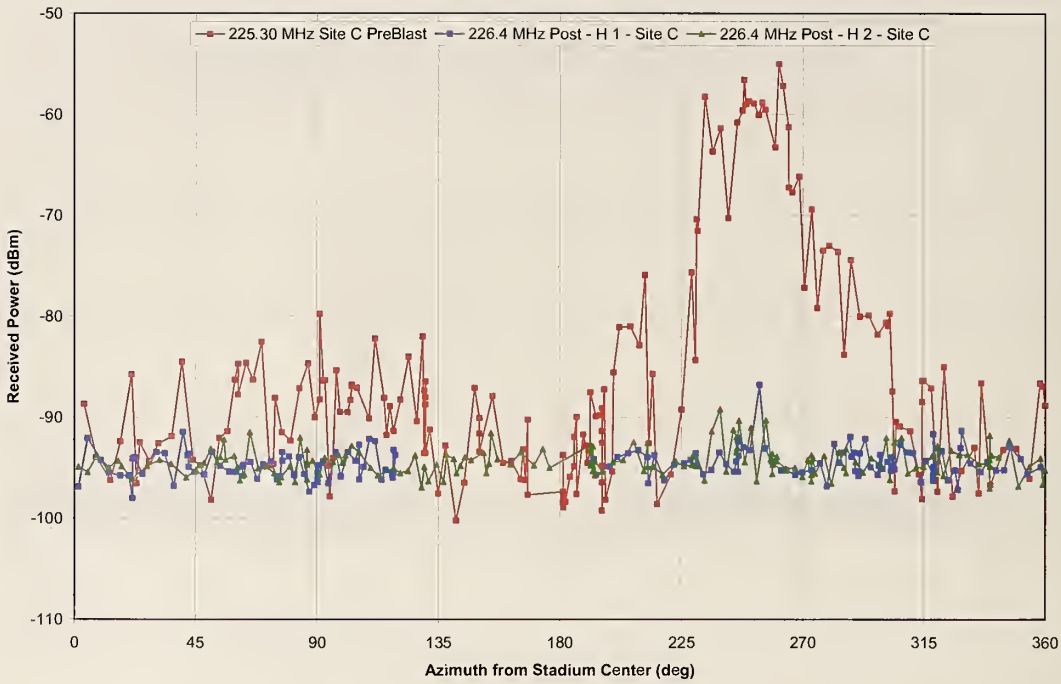

Figure 89. Comparison of pre- and post-implosion mobile cart perimeter measurements for the transmitters at transmitter Site C for horizontally polarized receiving antennas: 225 MHz band.

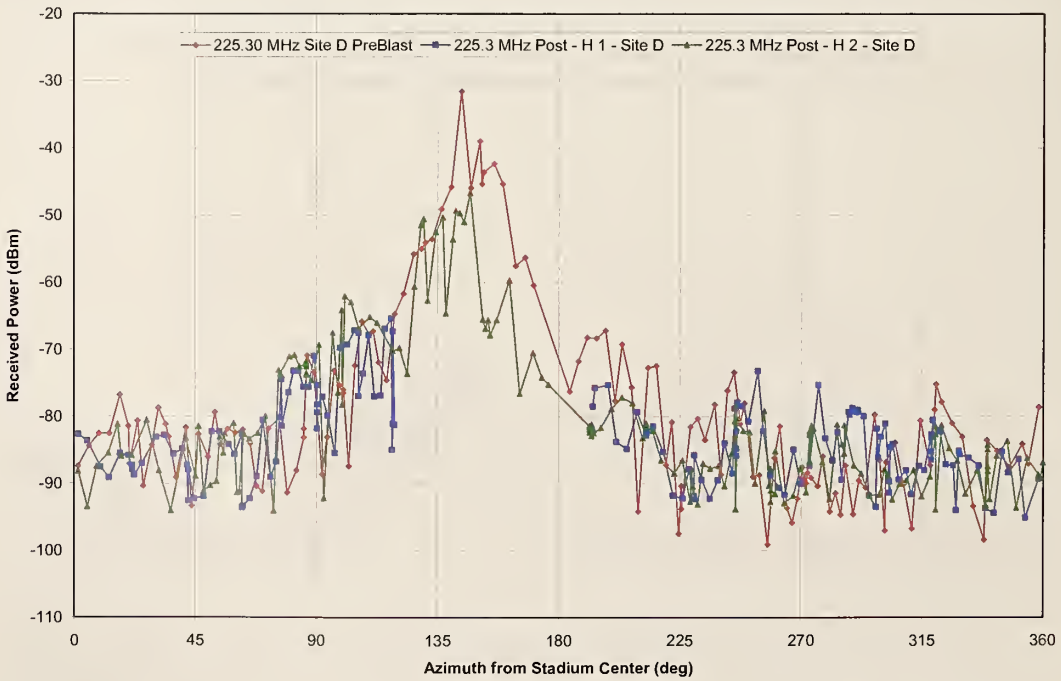

Figure 90. Comparison of pre- and post-implosion mobile cart perimeter measurements for the transmitters at transmitter Site D for horizontally polarized receiving antennas: 225 MHz band.

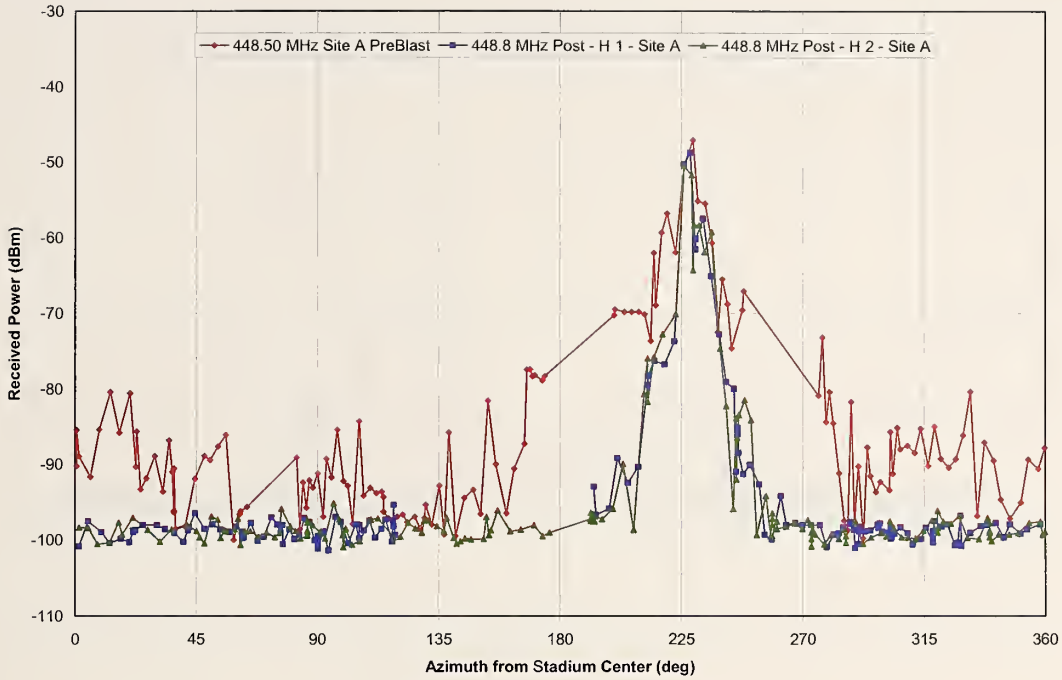

Figure 91. Comparison of pre- and post-implosion mobile cart perimeter measurements for the transmitters at transmitter Site A for horizontally polarized receiving antennas: 450 MHz band.

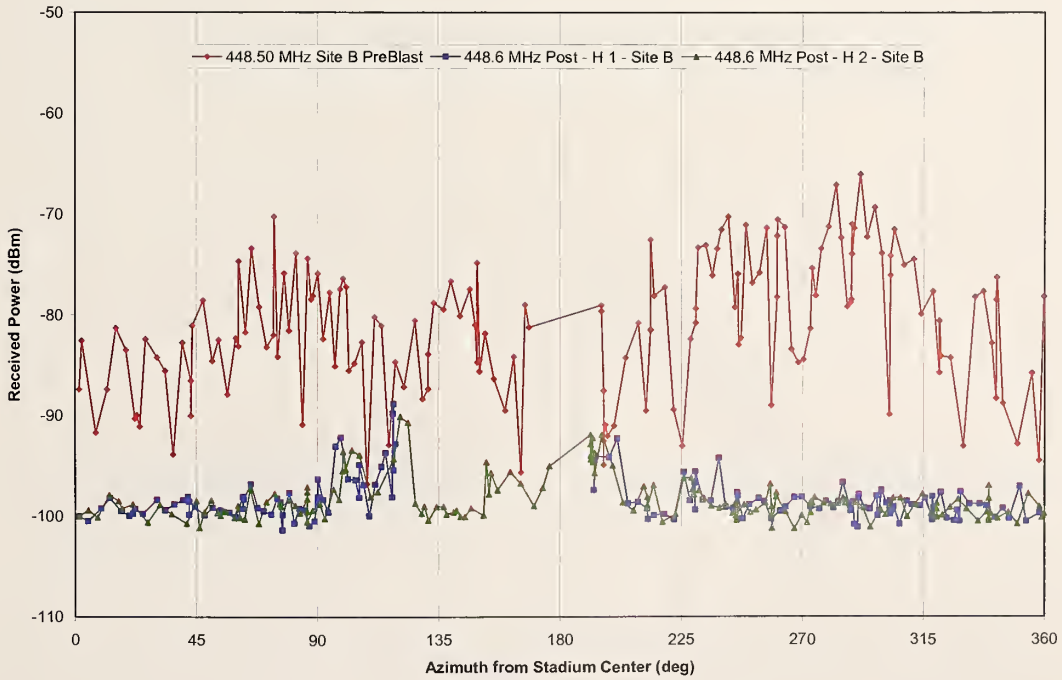

Figure 92. Comparison of pre- and post-implosion mobile cart perimeter measurements for the transmitters at transmitter Site B for horizontally polarized receiving antennas: 450 MHz band.

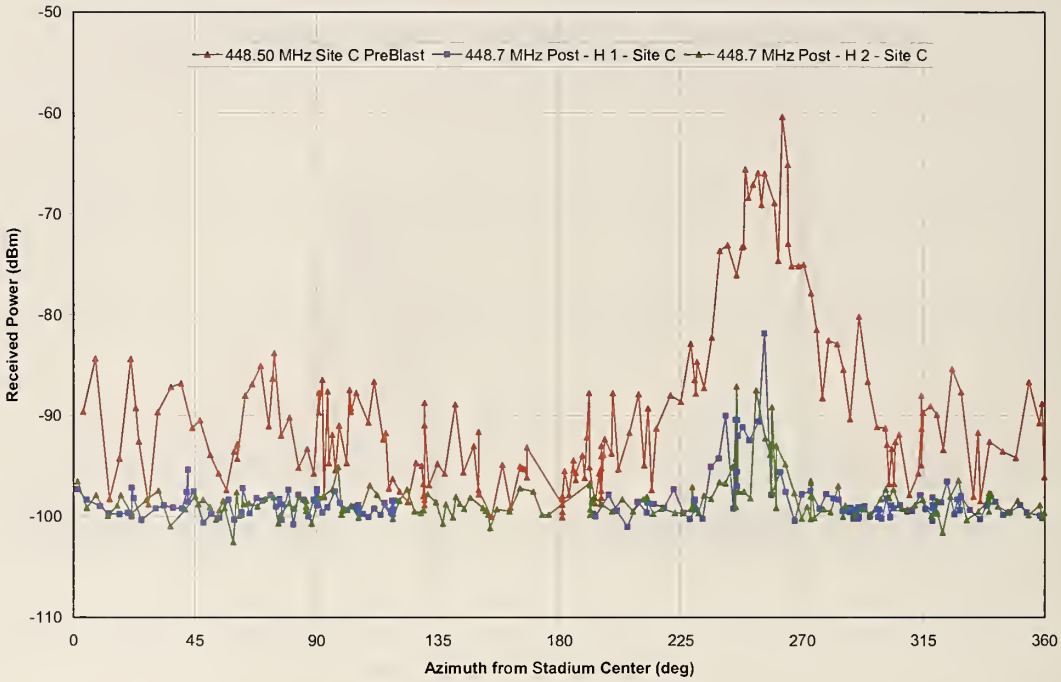

Figure 93. Comparison of pre- and post-implosion mobile cart perimeter measurements for the transmitters at transmitter Site C for horizontally polarized receiving antennas: 450 MHz band.

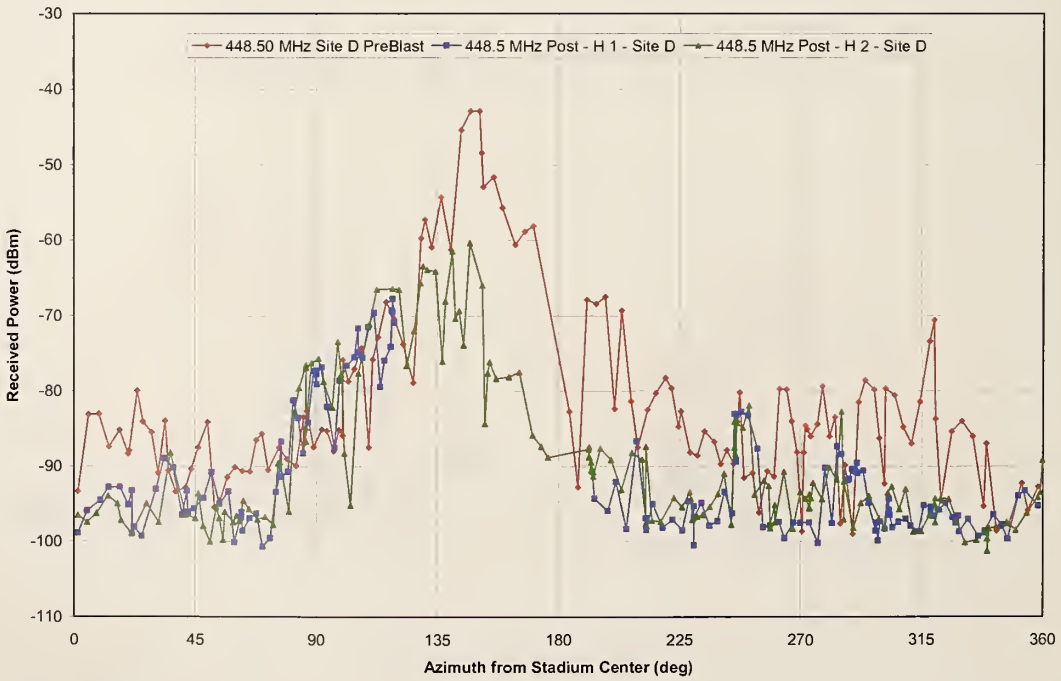

Figure 94. Comparison of pre- and post-implosion mobile cart perimeter measurements for the transmitters at transmitter Site D for horizontally polarized receiving antennas: 450 MHz band.

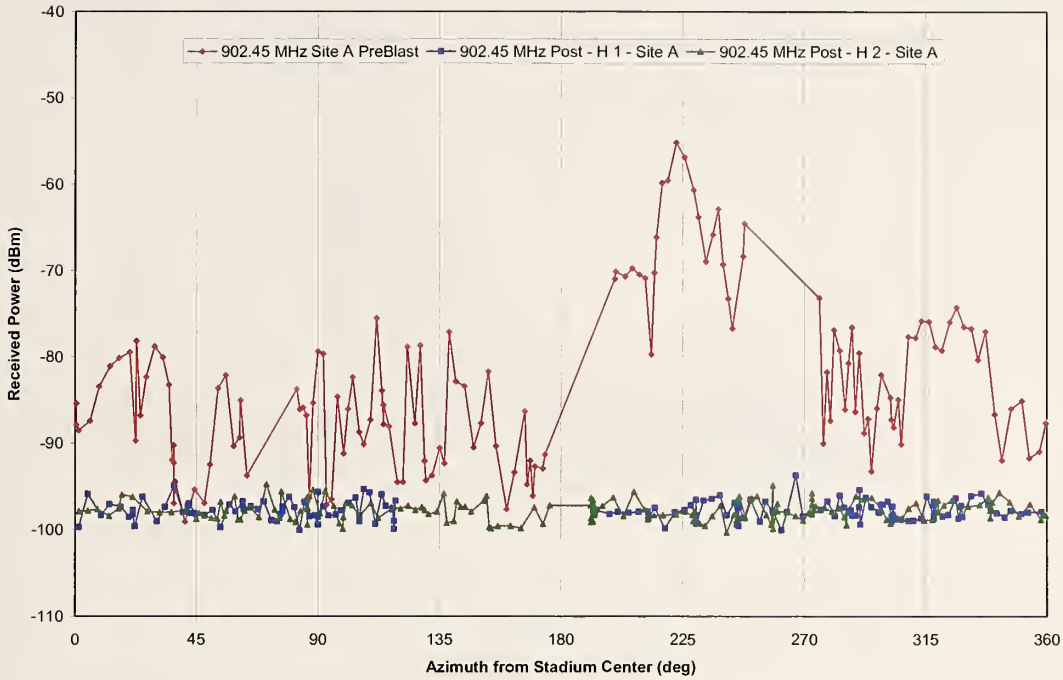

Figure 95. Comparison of pre- and post-implosion mobile cart perimeter measurements for the transmitters at transmitter Site A for horizontally polarized receiving antennas: 900 MHz band.

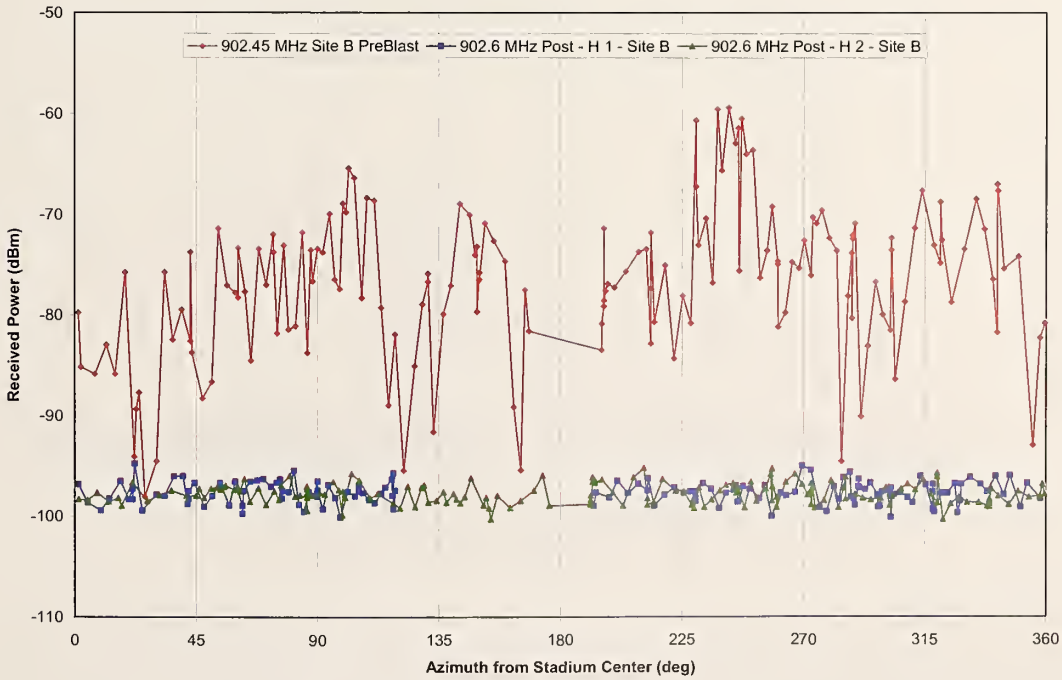

Figure 96. Comparison of pre- and post-implosion mobile cart perimeter measurements for the transmitters at transmitter Site B for horizontally polarized receiving antennas: 900 MHz band.

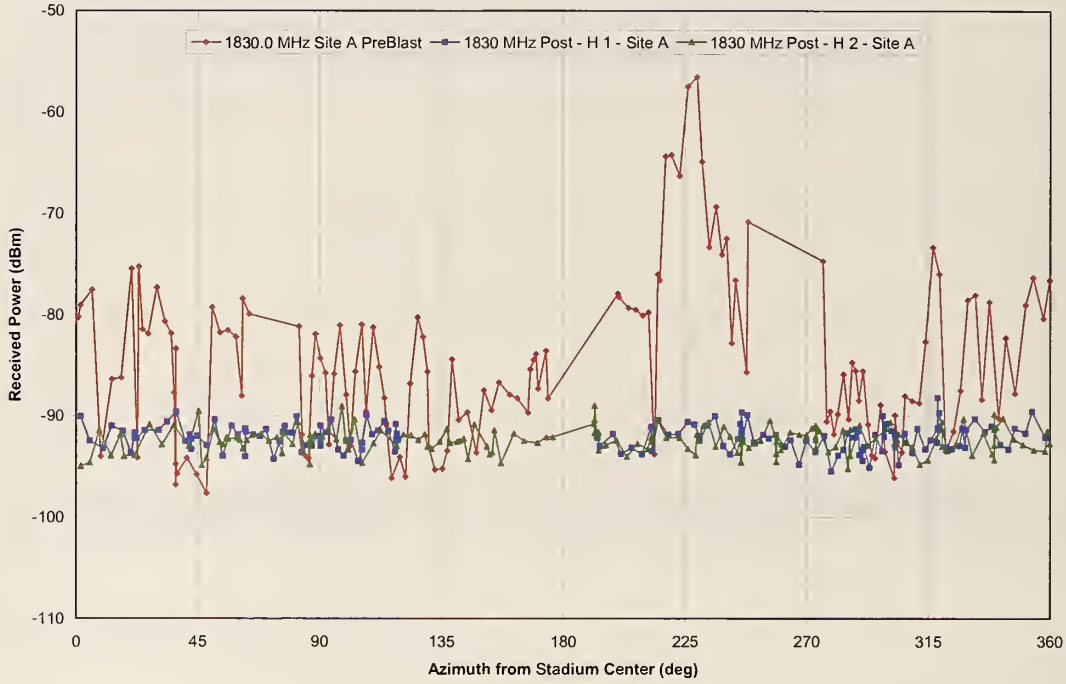

Figure 97. Comparison of pre- and post-implosion mobile cart perimeter measurements for the transmitters at transmitter Site A for horizontally polarized receiving antennas: 1800 MHz band.

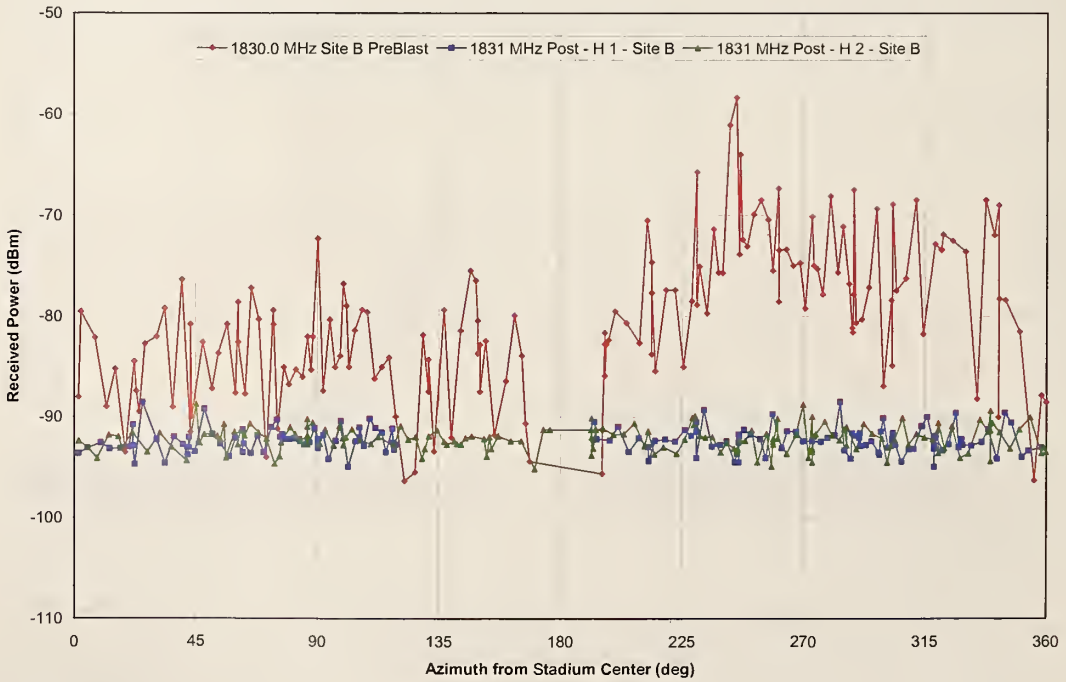

Figure 98. Comparison of pre- and post-implosion mobile cart perimeter measurements for the transmitters at transmitter Site A for horizontally polarized receiving antennas: 1800 MHz band.

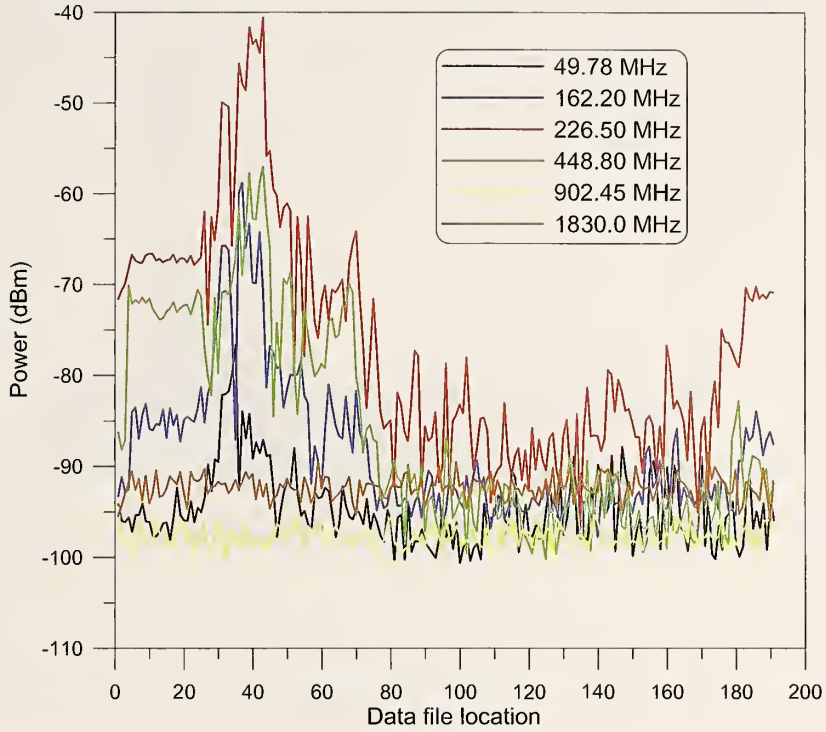

Figure 99. Post-implosion mobile cart perimeter measurements for the transmitters at transmitter Site A for vertical polarized receiving antennas: perimeter walk 1.

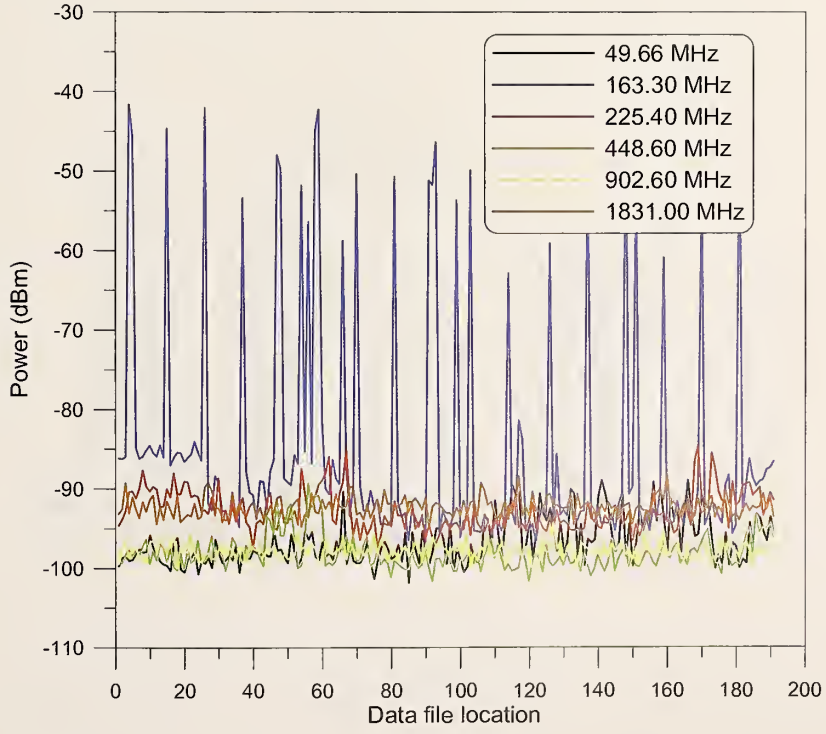

Figure 100. Post-implosion mobile cart perimeter measurements for the transmitters at transmitter Site B for vertical polarized receiving antennas: perimeter walk 1.

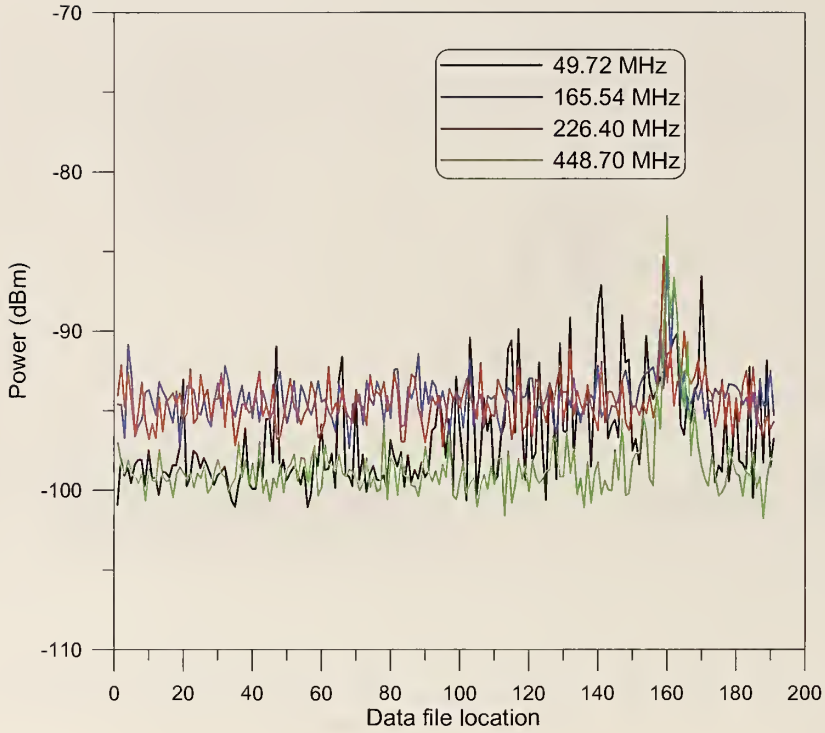

Figure 101. Post-implosion mobile cart perimeter measurements for the transmitters at transmitter Site C for vertical polarized receiving antennas: perimeter walk 1.

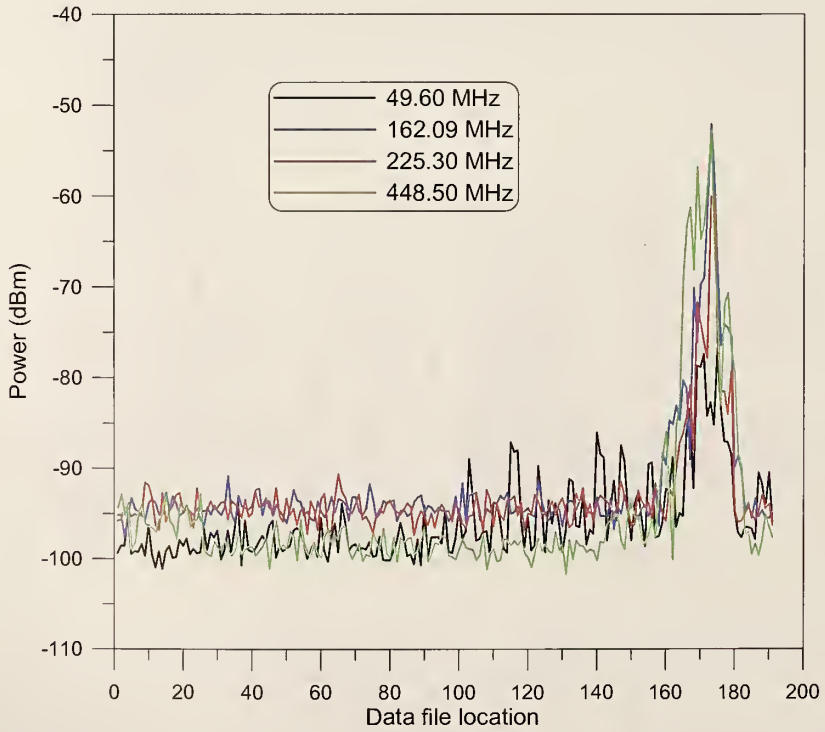

Figure 102. Post-implosion mobile cart perimeter measurements for the transmitters at transmitter Site D for vertical polarized receiving antennas: perimeter walk 1.

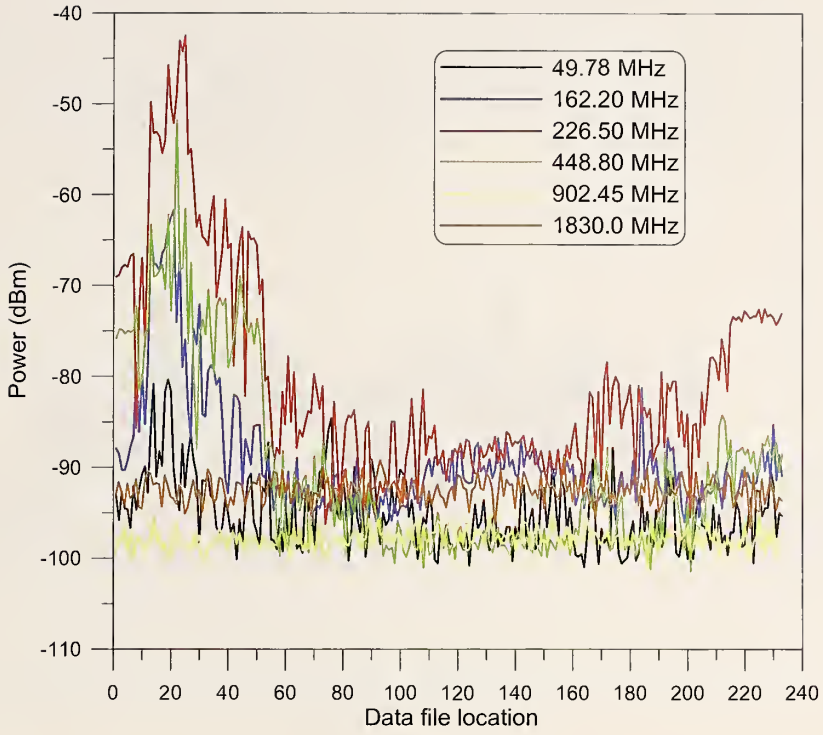

Figure 103. Post-implosion mobile cart perimeter measurements for the transmitters at transmitter Site A for vertical polarized receiving antennas: perimeter walk 2.

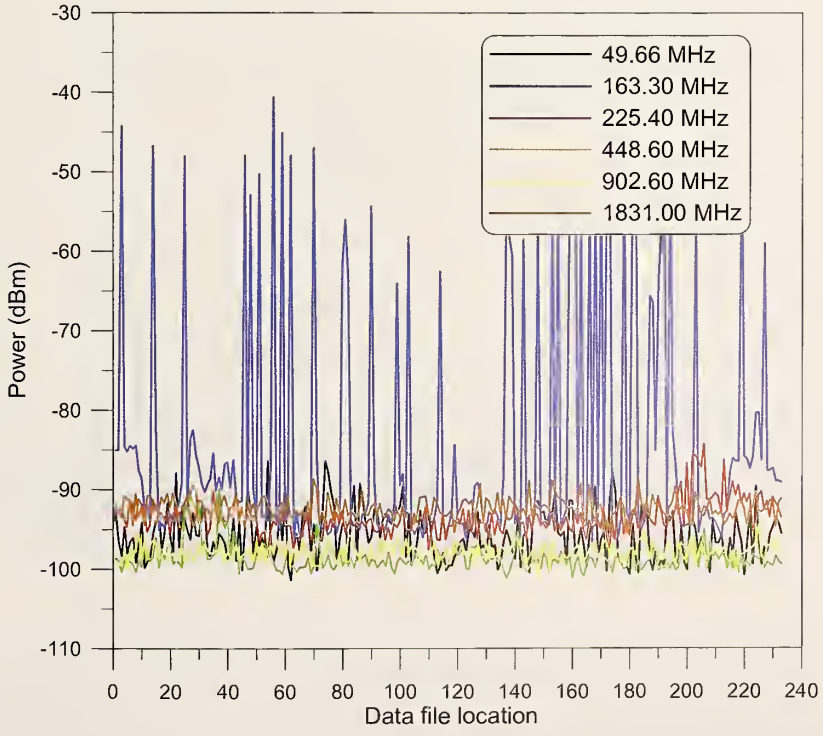

Figure 104. Post-implosion mobile cart perimeter measurements for the transmitters at transmitter Site B for vertical polarized receiving antennas: perimeter walk 2.

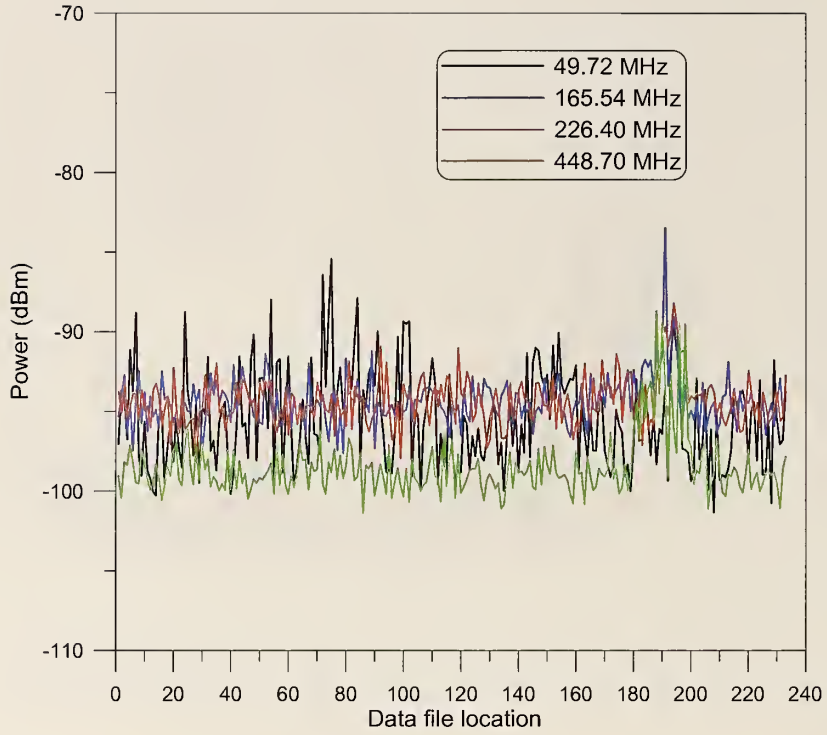

Figure 105. Post-implosion mobile cart perimeter measurements for the transmitters at transmitter Site C for vertical polarized receiving antennas: perimeter walk 2.

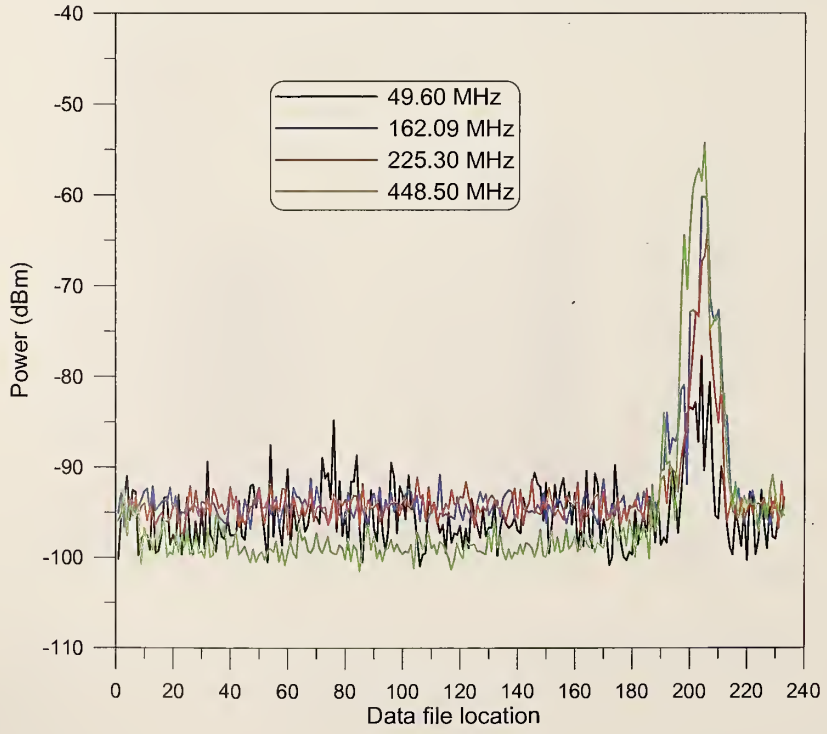

Figure 106. Post-implosion mobile cart perimeter measurements for the transmitters at transmitter Site D for vertical polarized receiving antennas: perimeter walk 2.

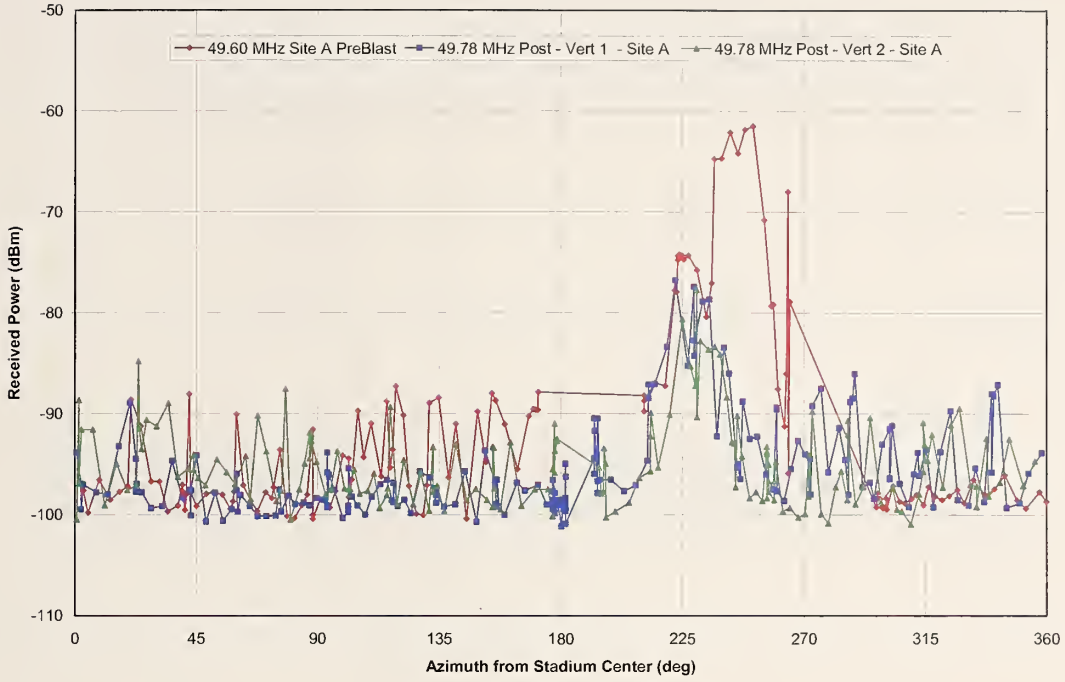

Figure 107. Comparison of pre- and post-implosion mobile cart perimeter measurements for the transmitters at transmitter Site A for horizontally polarized receiving antennas: 49 MHz band.

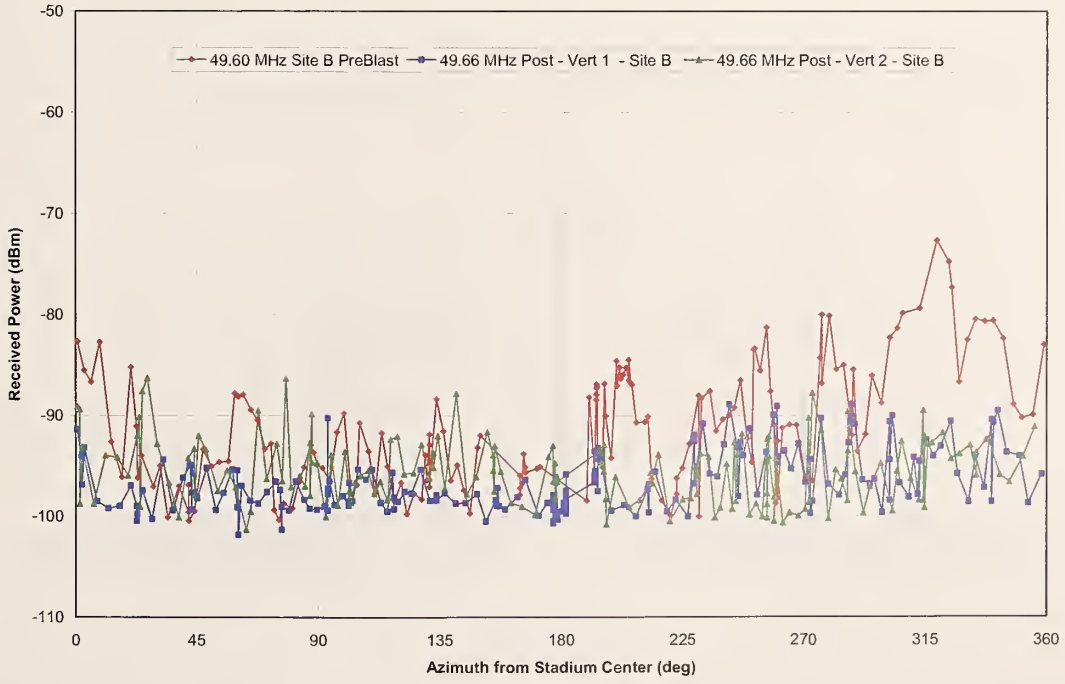

Figure 108. Comparison of pre- and post-implosion mobile cart perimeter measurements for the transmitters at transmitter Site B for horizontally polarized receiving antennas: 49 MHz band.

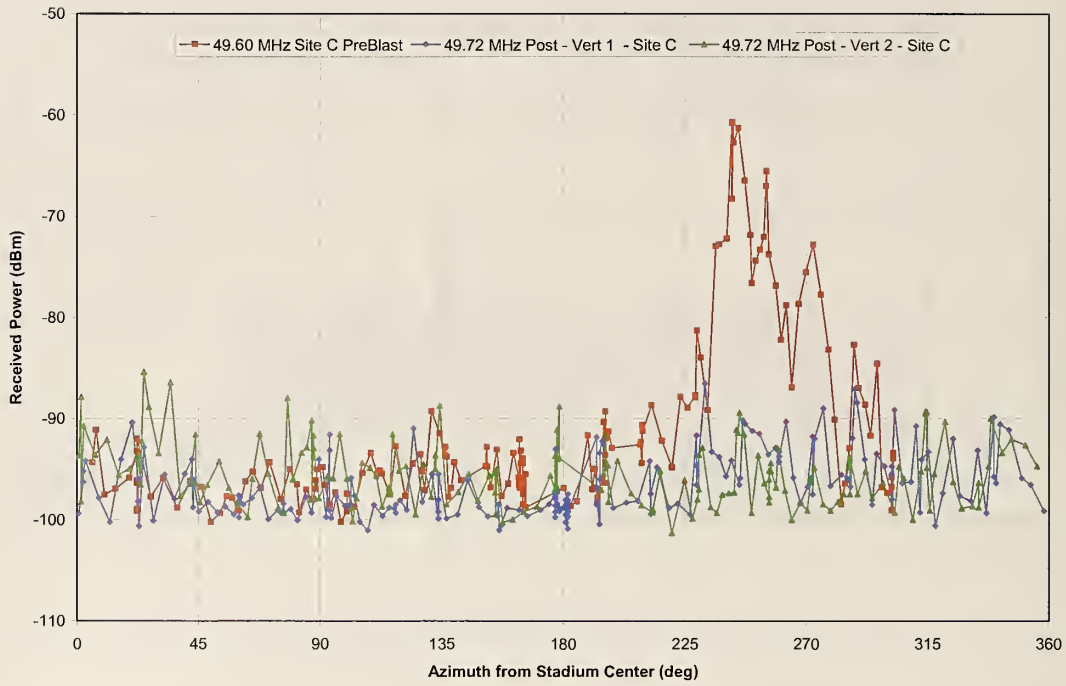

Figure 109. Comparison of pre- and post-implosion mobile cart perimeter measurements for the transmitters at transmitter Site C for horizontally polarized receiving antennas: 49 MHz band.

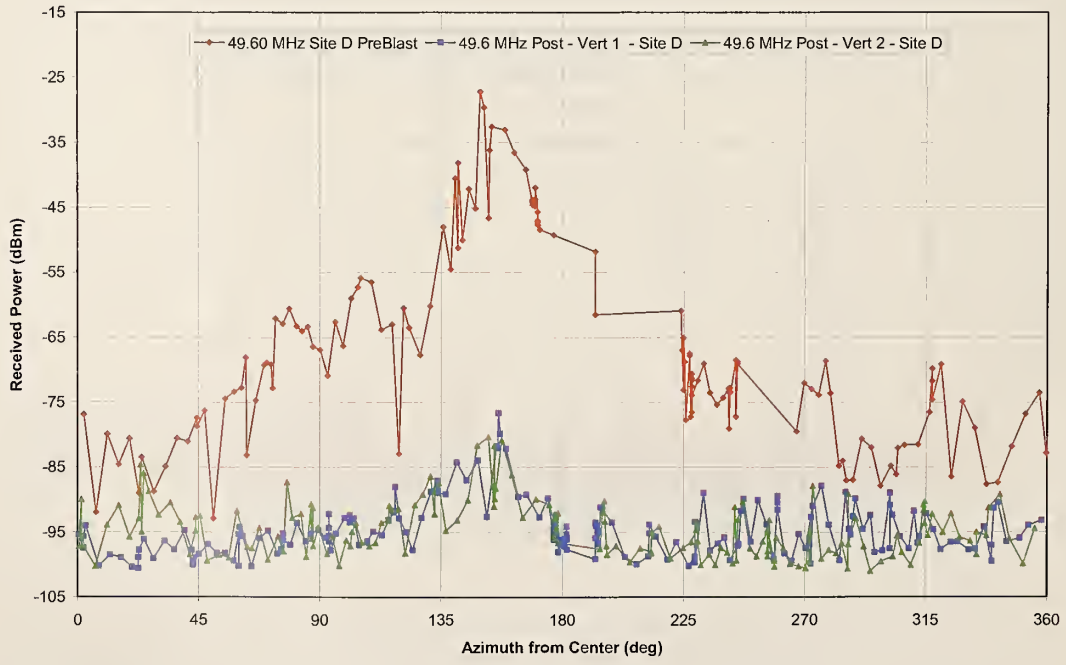

Figure 110. Comparison of pre- and post-implosion mobile cart perimeter measurements for the transmitters at transmitter Site D for horizontally polarized receiving antennas: 49 MHz band.

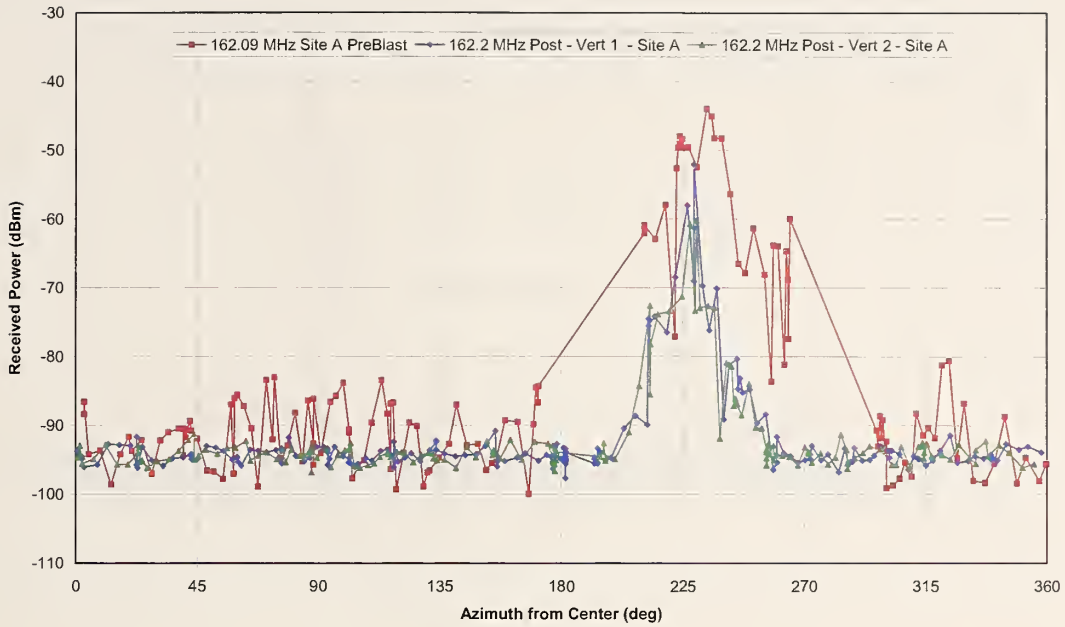

Figure 111. Comparison of pre- and post-implosion mobile cart perimeter measurements for the transmitters at transmitter Site A for horizontally polarized receiving antennas: 160 MHz band.

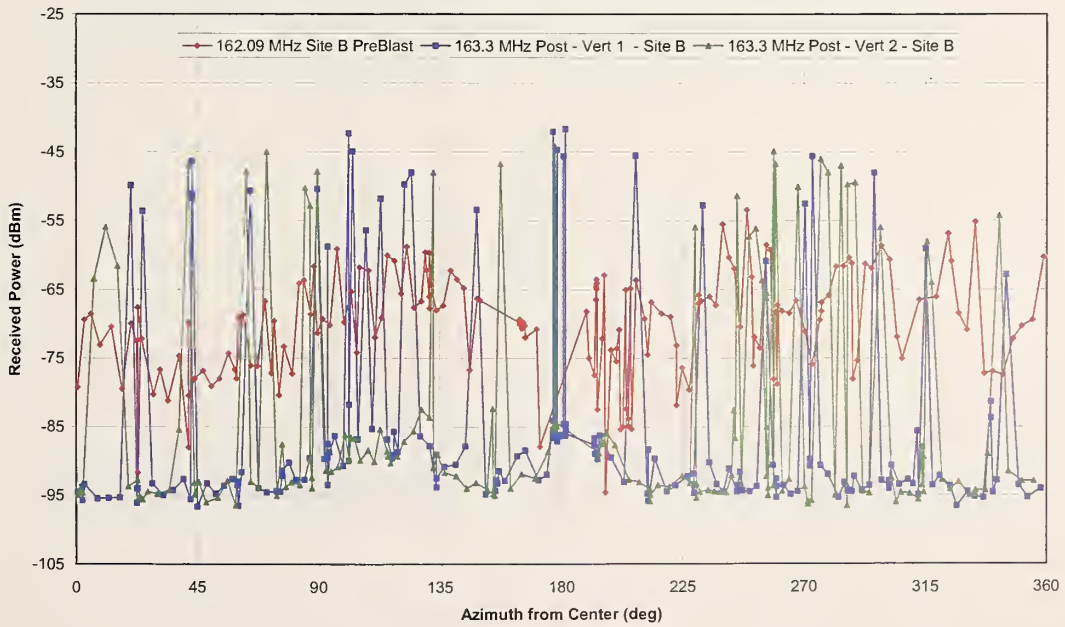

Figure 112. Comparison of pre- and post-implosion mobile cart perimeter measurements for the transmitters at transmitter Site B for horizontally polarized receiving antennas: 160 MHz band.

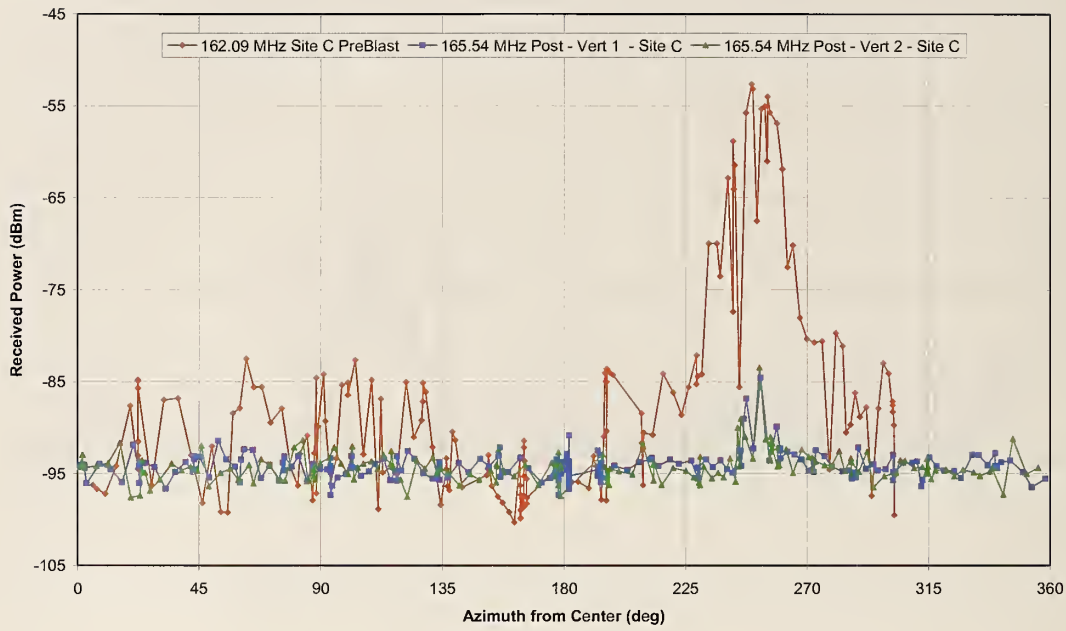

Figure 113. Comparison of pre- and post-implosion mobile cart perimeter measurements for the transmitters at transmitter Site C for horizontally polarized receiving antennas: 160 MHz band.

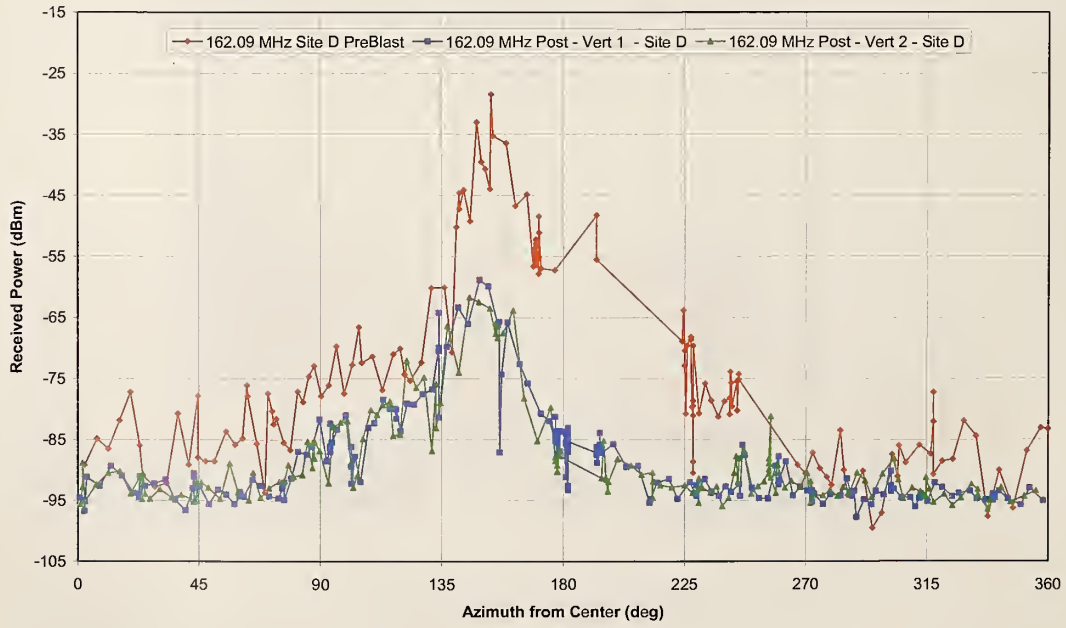

Figure 114. Comparison of pre- and post-implosion mobile cart perimeter measurements for the transmitters at transmitter Site D for horizontally polarized receiving antennas: 160 MHz band.

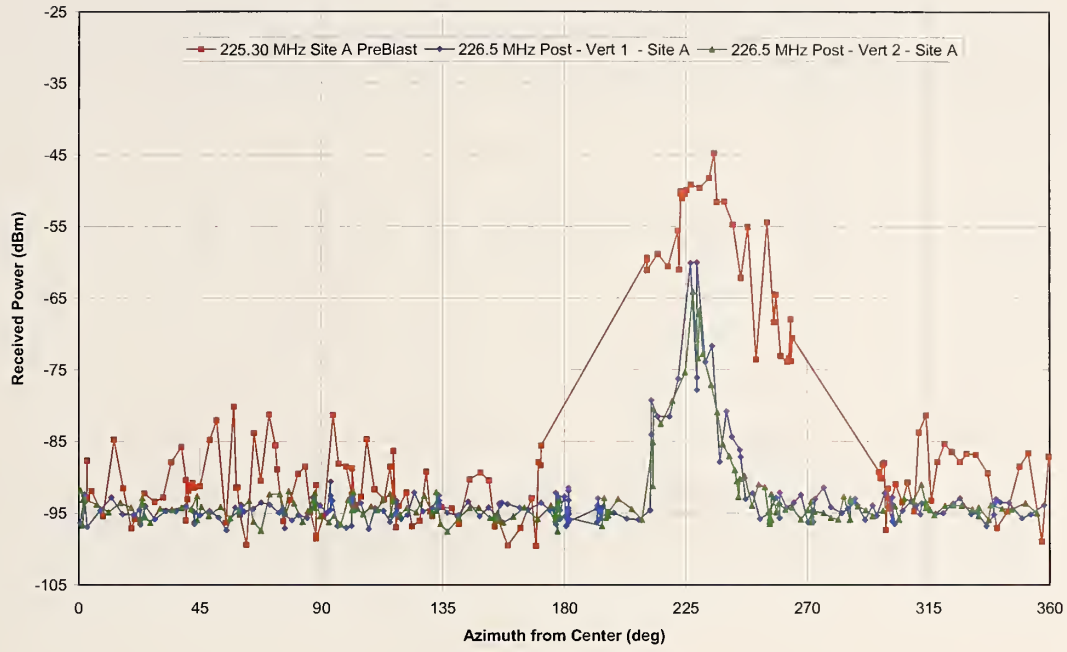

Figure 115. Comparison of pre- and post-implosion mobile cart perimeter measurements for the transmitters at transmitter Site A for horizontally polarized receiving antennas: 225 MHz band.

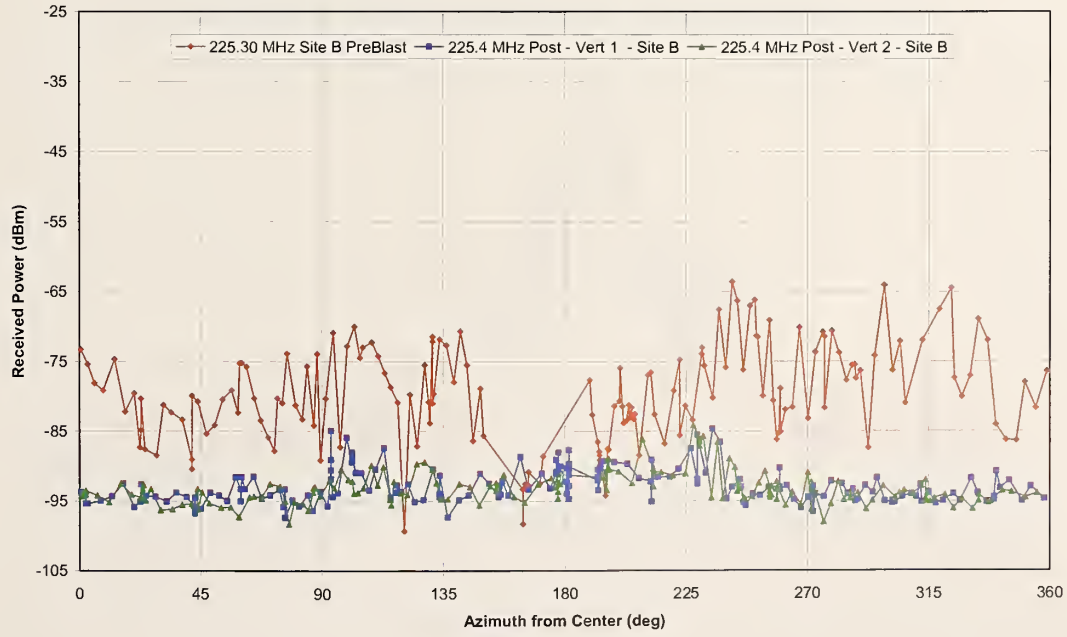

Figure 116. Comparison of pre- and post-implosion mobile cart perimeter measurements for the transmitters at transmitter Site B for horizontally polarized receiving antennas: 225 MHz band.

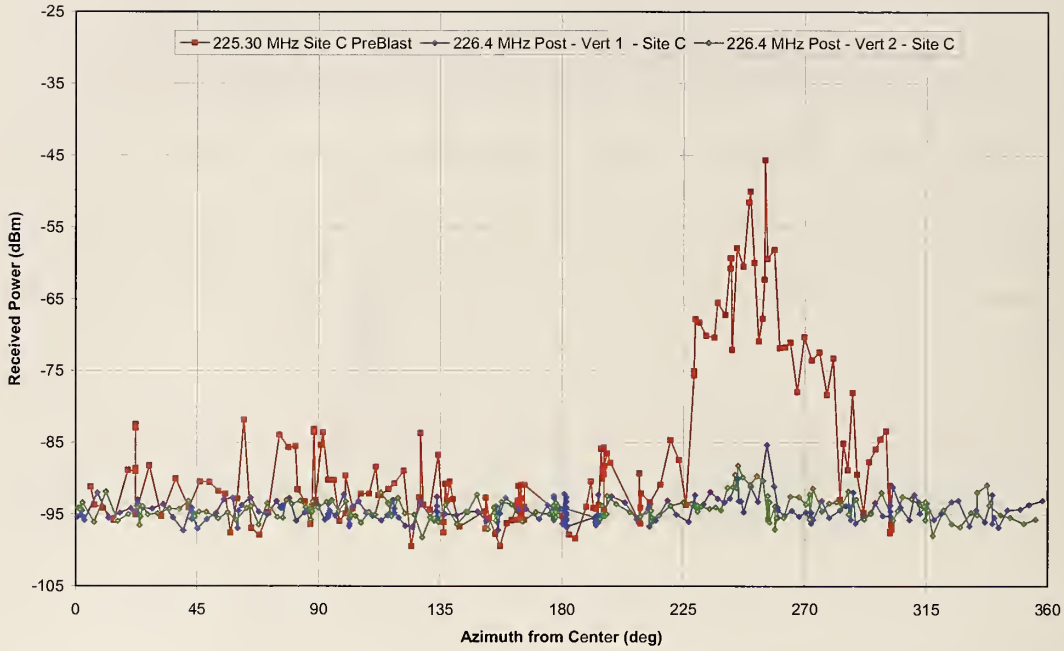

Figure 117. Comparison of pre- and post-implosion mobile cart perimeter measurements for the transmitters at transmitter Site C for horizontally polarized receiving antennas: 225 MHz band.

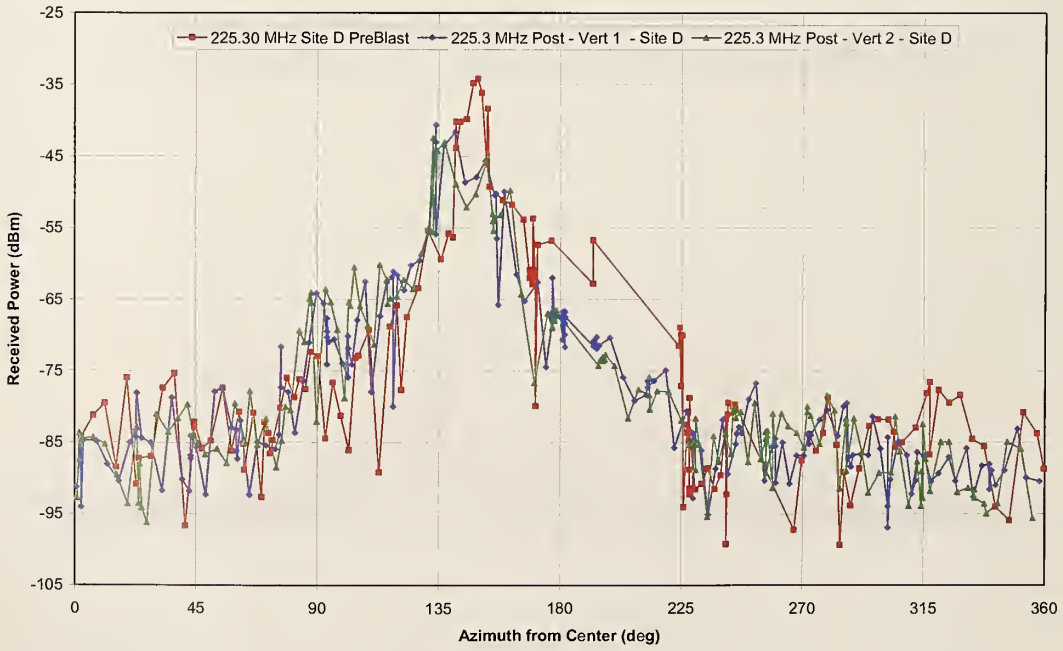

Figure 118. Comparison of pre- and post-implosion mobile cart perimeter measurements for the transmitters at transmitter Site D for horizontally polarized receiving antennas: 225 MHz band.

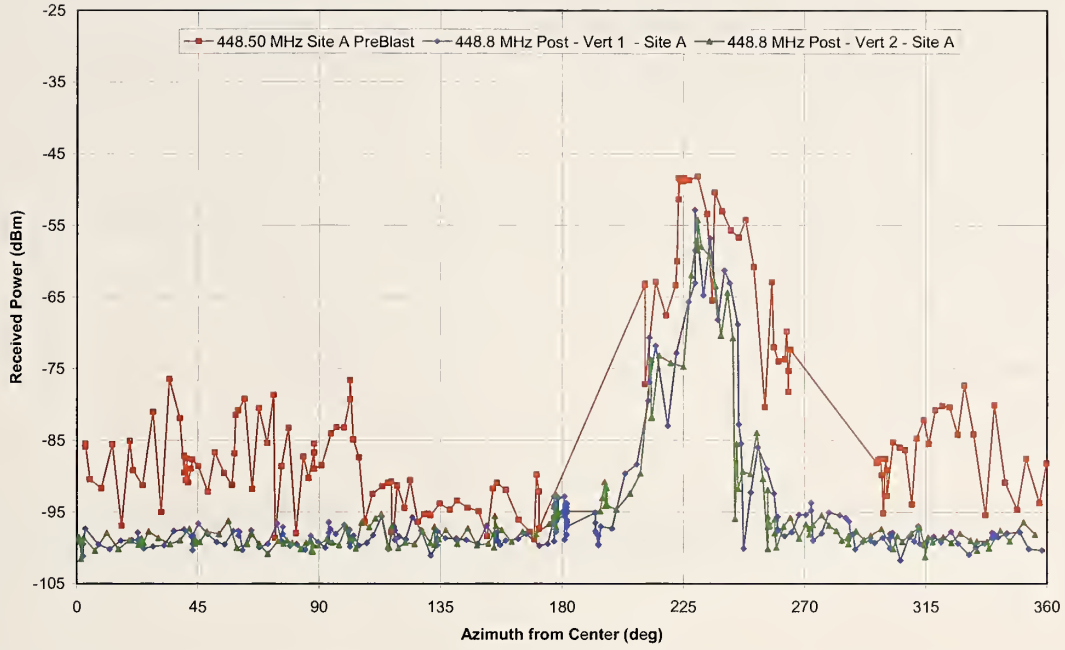

Figure 119. Comparison of pre- and post-implosion mobile cart perimeter measurements for the transmitters at transmitter Site A for horizontally polarized receiving antennas: 450 MHz band.

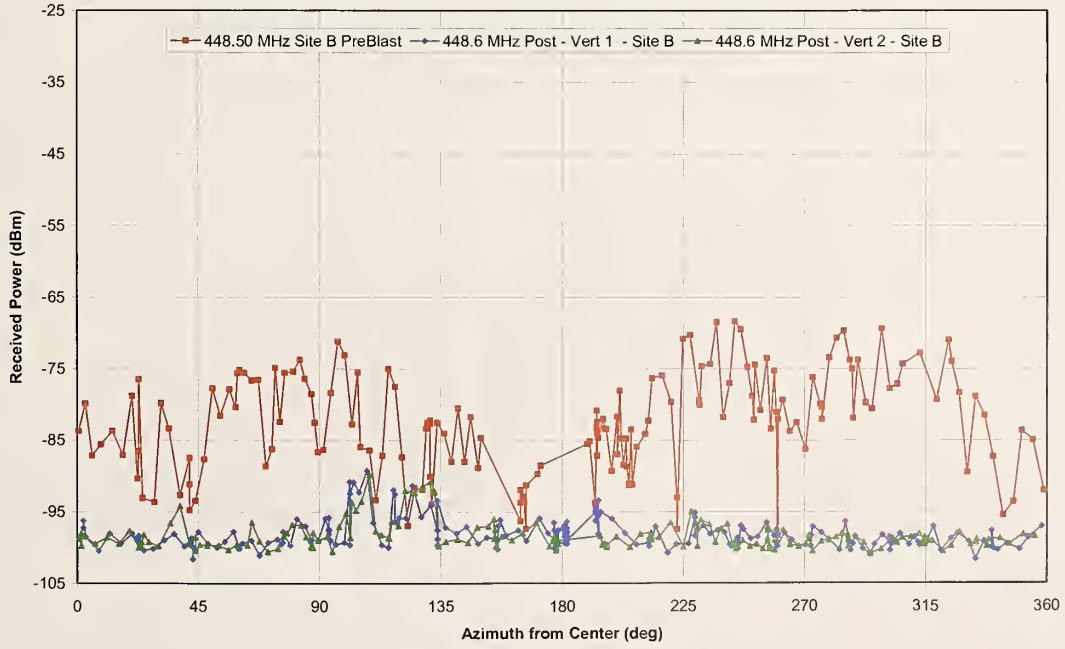

Figure 120. Comparison of pre- and post-implosion mobile cart perimeter measurements for the transmitters at transmitter Site B for horizontally polarized receiving antennas: 450 MHz band.

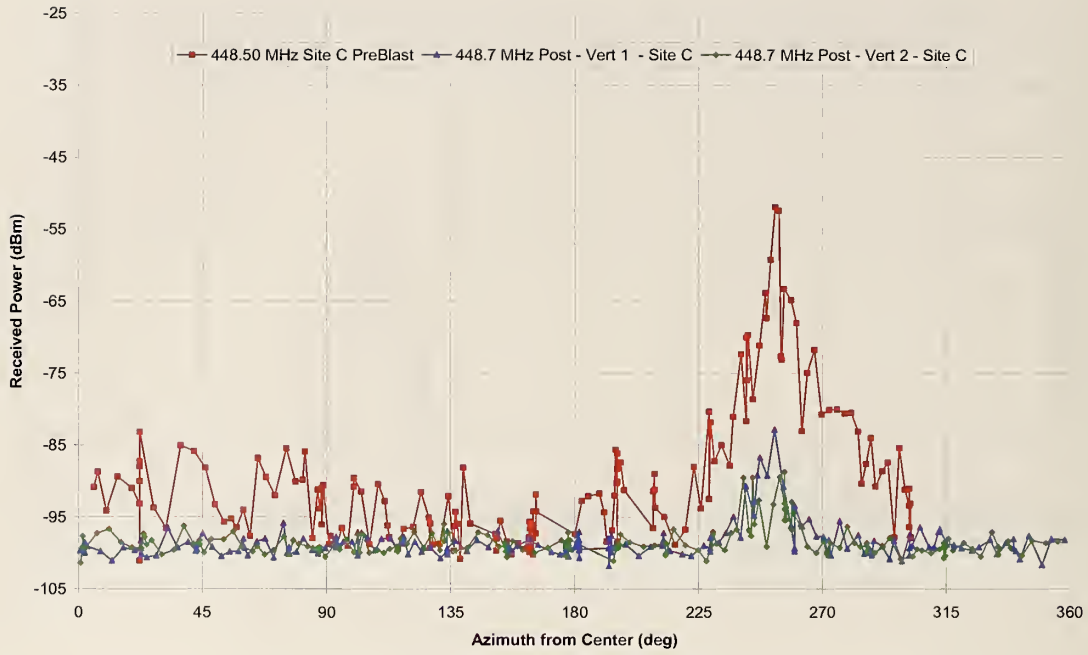

Figure 121. Comparison of pre- and post-implosion mobile cart perimeter measurements for the transmitters at transmitter Site C for horizontally polarized receiving antennas: 450 MHz band.

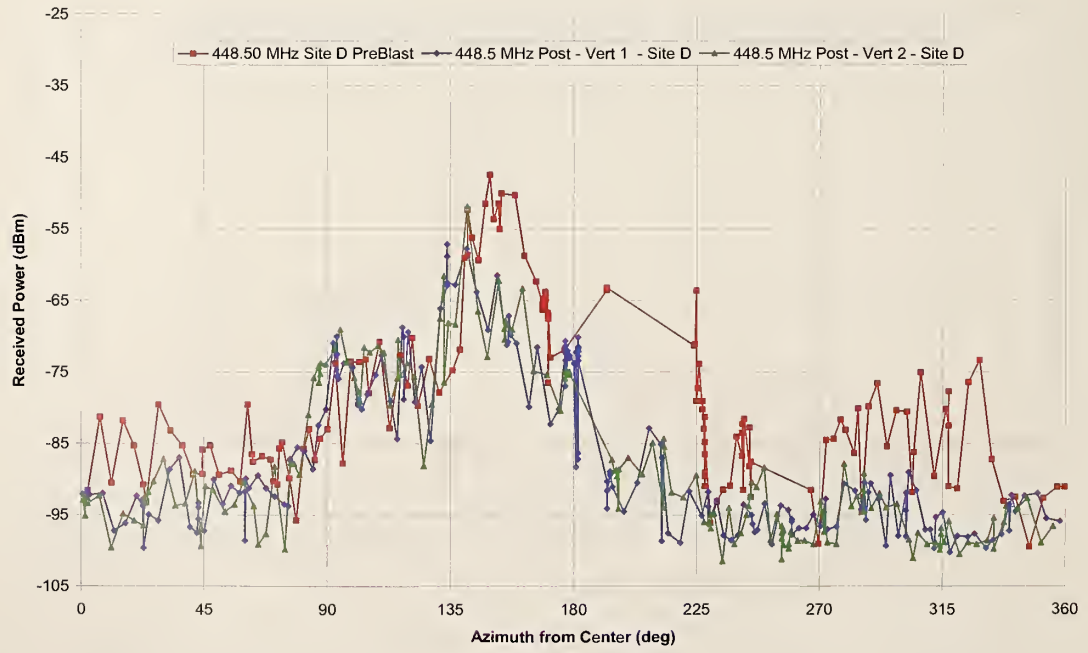

Figure 122. Comparison of pre- and post-implosion mobile cart perimeter measurements for the transmitters at transmitter Site D for horizontally polarized receiving antennas: 450 MHz band.

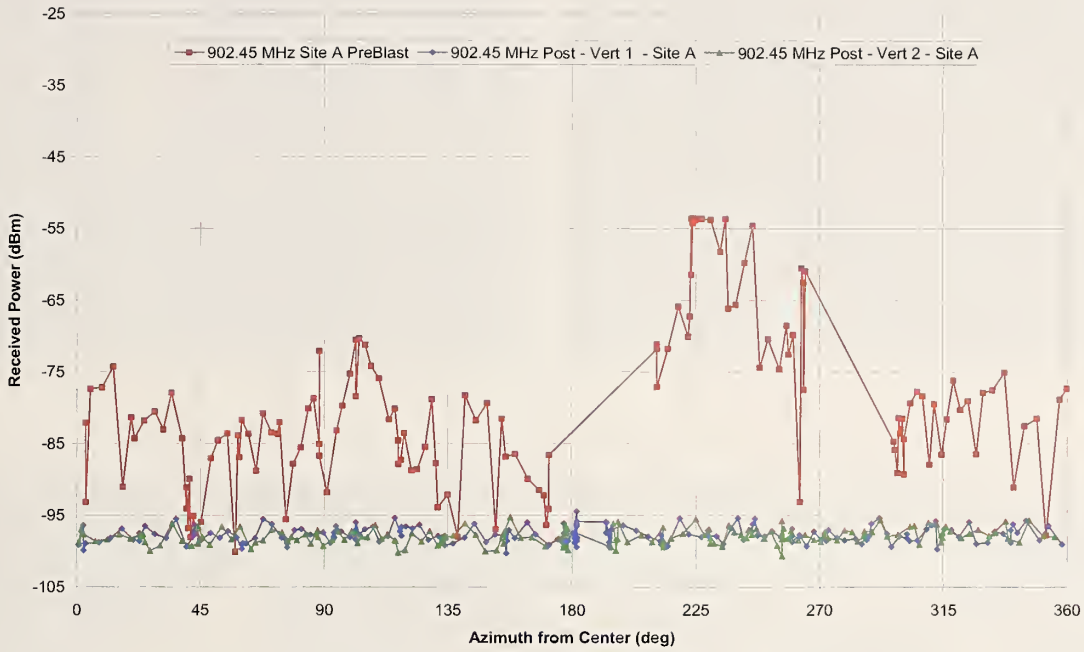

Figure 123. Comparison of pre- and post-implosion mobile cart perimeter measurements for the transmitters at transmitter Site A for horizontally polarized receiving antennas: 900 MHz band.

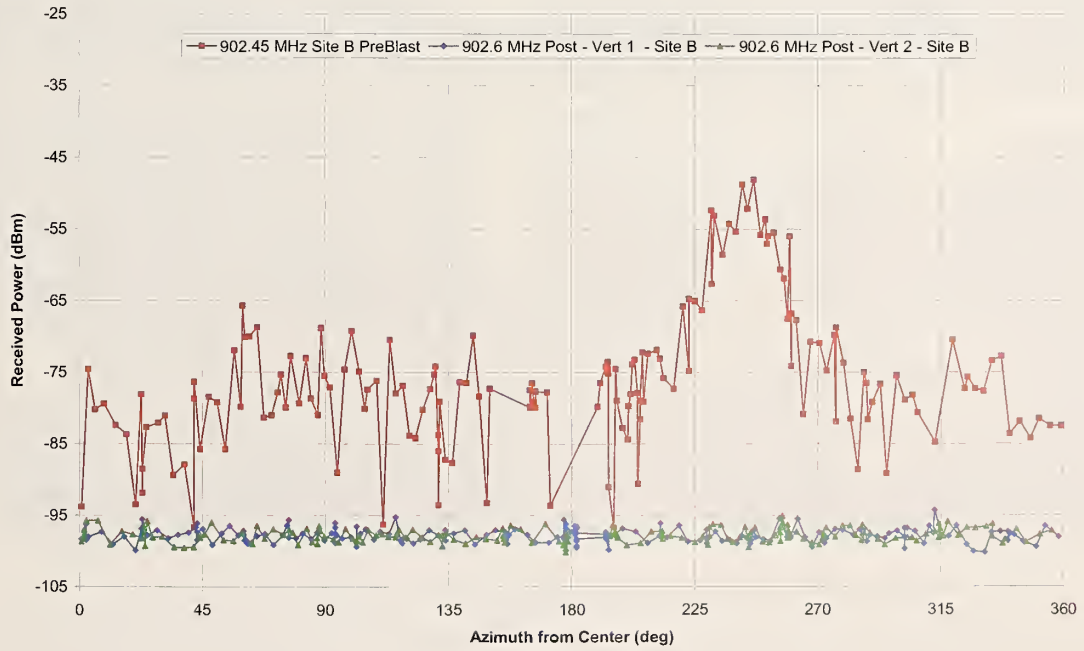

Figure 124. Comparison of pre- and post-implosion mobile cart perimeter measurements for the transmitters at transmitter Site B for horizontally polarized receiving antennas: 900 MHz band.

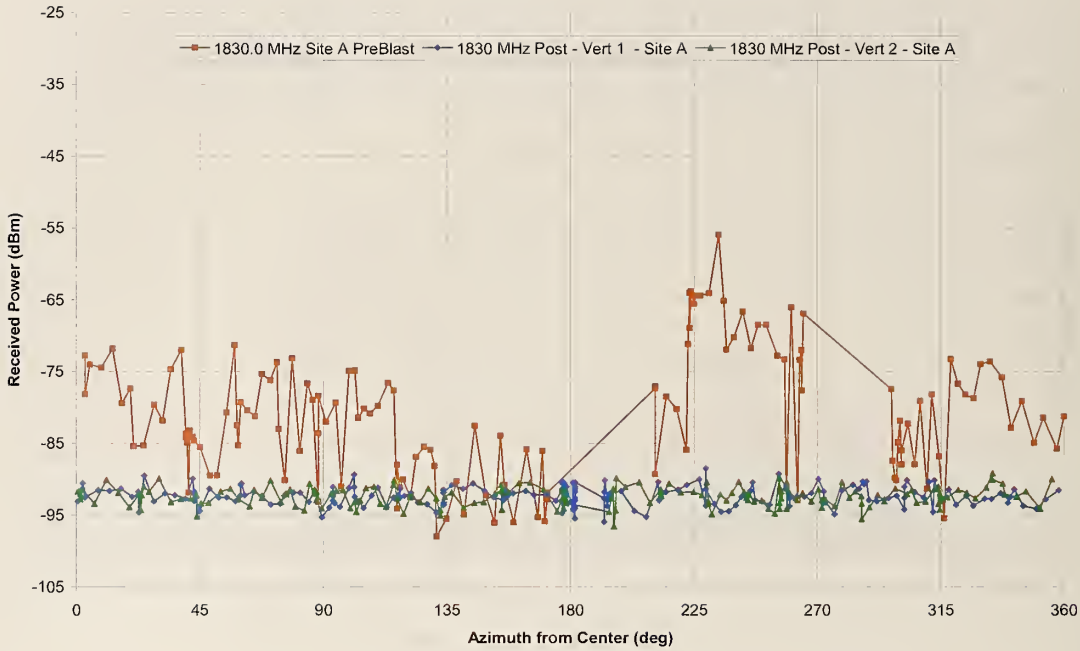

Figure 125. Comparison of pre- and post-implosion mobile cart perimeter measurements for the transmitters at transmitter Site A for horizontally polarized receiving antennas: 1800 MHz band.

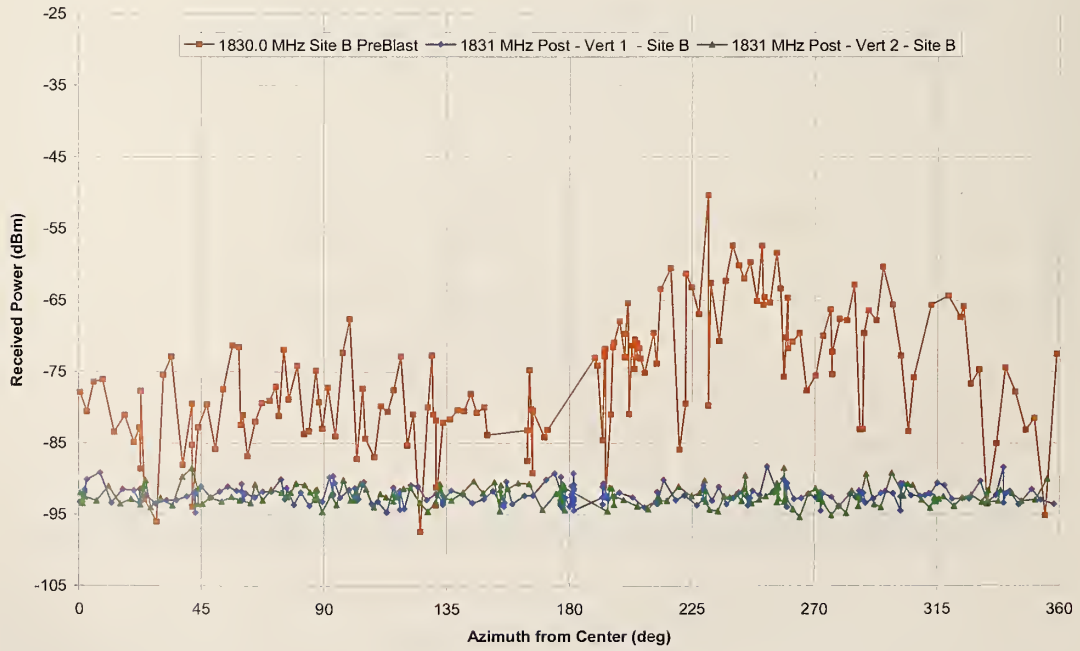

Figure 126. Comparison of pre- and post-implosion mobile cart perimeter measurements for the transmitters at transmitter Site B for horizontally polarized receiving antennas: 1800 MHz band.

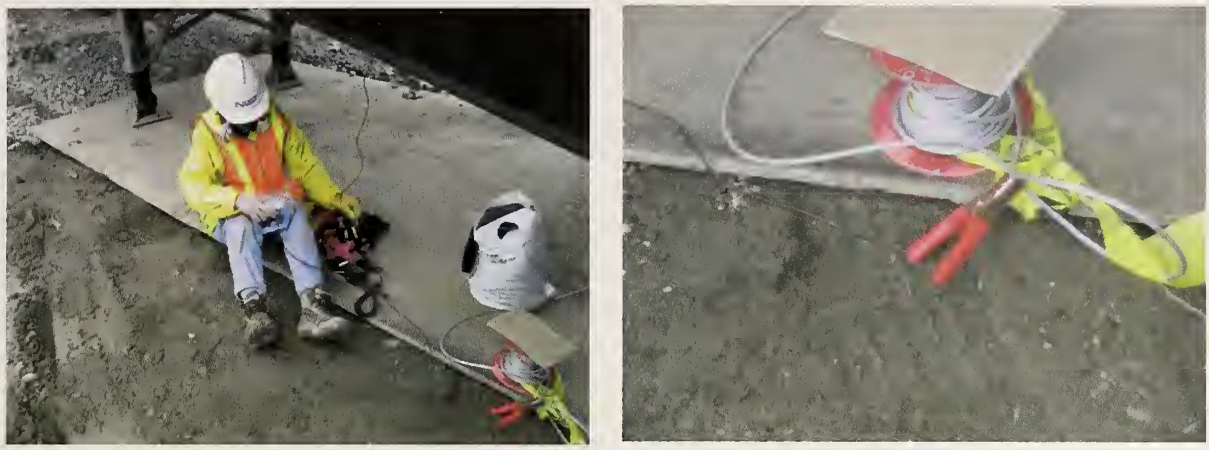

(a)

(b)

Figure 127. Illustration of debris radiator measurements: (a) on Cable 1 on south side of stadium, (b) on Cable 2 on north side of stadium.

NIST Technical Publications

Periodical

Journal of Research of the National Institute of Standards and Technology—Reports NIST research and development in metrology and related fields of physical science, engineering, applied mathematics, statistics, biotechnology, and information technology. Papers cover a broad range of subjects, with major emphasis on measurement methodology and the basic technology underlying standardization. Also included from time to time are survey articles on topics closely related to the Institute's technical and scientific programs. Issued six times a year.

Nonperiodicals

Monographs—Major contributions to the technical literature on various subjects related to the Institute's scientific and technical activities.
Handbooks—Recommended codes of engineering and industrial practice (including safety codes) developed in cooperation with interested industries, professional organizations, and regulatory bodies.
Special Publications—Include proceedings of conferences sponsored by NIST, NIST annual reports, and other special publications appropriate to this grouping such as wall charts, pocket cards, and bibliographies.
National Standard Reference Data Series—Provides quantitative data on the physical and chemical properties of materials, compiled from the world's literature and critically evaluated. Developed under a worldwide program coordinated by NIST under the authority of the National Standard Data Act (Public Law 90-396). NOTE: The Journal of Physical and Chemical Reference Data (JPCRD) is published bimonthly for NIST by the American Institute of Physics (AIP). Subscription orders and renewals are available from AIP, P.O. Box 503284, St. Louis, MO 63150-3284.
Building Science Series—Disseminates technical information developed at the Institute on building materials, components, systems, and whole structures. The series presents research results, test methods, and performance criteria related to the structural and environmental functions and the durability and safety characteristics of building elements and systems.
Technical Notes—Studies or reports which are complete in themselves but restrictive in their treatment of a subject. Analogous to monographs but not so comprehensive in scope or definitive in treatment of the subject area. Often serve as a vehicle for final reports of work performed at NIST under the sponsorship of other government agencies.
Voluntary Product Standards—Developed under procedures published by the Department of Commerce in Part 10, Title 15, of the Code of Federal Regulations. The standards establish nationally recognized requirements for products, and provide all concerned interests with a basis for common understanding of the characteristics of the products. NIST administers this program in support of the efforts of private-sector standardizing organizations.

*Order the **following** NIST publications—FIPS and NISTIRs—from the National Technical Information Service, Springfield, VA 22161.*

Federal Information Processing Standards Publications (FIPS PUB)—Publications in this series collectively constitute the Federal Information Processing Standards Register. The Register serves as the official source of information in the Federal Government regarding standards issued by NIST pursuant to the Federal Property and Administrative Services Act of 1949 as amended, Public Law 89-306 (79 Stat. 1127), and as implemented by Executive Order 11717 (38 FR 12315, dated May 11,1973) and Part 6 of Title 15 CFR (Code of Federal Regulations).
NIST Interagency or Internal Reports (NISTIR)—The series includes interim or final reports on work performed by NIST for outside sponsors (both government and nongovernment). In general, initial distribution is handled by the sponsor; public distribution is handled by sales through the National Technical Information Service, Springfield, VA 22161, in hard copy, electronic media, or microfiche form. NISTIRs may also report results of NIST projects of transitory or limited interest, including those that will be published subsequently in more comprehensive form.

U.S. Department of Commerce
National Bureau of Standards and Technology
325 Broadway
Boulder, CO 80305-3328